Fiber-reinforced, Anisotropic Superporous Cryogels for Meniscal Replacement

A Thesis

Submitted to the Faculty

of

Drexel University

by

Samuel James Laurencin

in partial fulfillment of

the requirements for the degree

of

Doctor of Philosophy

May 2015

Office of Graduate Studies
Dissertation/Thesis Approval Form

This form is for use by all doctoral and master's students with a dissertation/thesis requirement. Please print clearly as the library will bind a copy of this form with each copy of the dissertation/thesis. All doctoral dissertations must conform to university format requirements, which is the responsibility of the student and supervising professor. Students should obtain a copy of the Thesis Manual located on the library website.

Dissertation/Thesis Title: Fiber-reinforced, anisotropic superporous cryogels for meniscal replacement

Author: Samuel James Laurencin

This dissertation/thesis is hereby accepted and approved.

Signatures:

Examining Committee

Chair

Members

Academic Advisor

Department Head

Dedications

To the memory of my sister,

Joi Olivia Laurencin

Acknowledgements

My journey through Drexel has spanned 17 years, serving first as a research assistant while in high school in the lab of my uncle, Dr. Cato Laurencin, and culminating in 2015 with completion of my MD and PhD in Chemical Engineering. I have benefited from the support and guidance from countless individuals. It is important for me to acknowledge those individuals that played a particularly vital role in my academic growth.

Dr. Anthony Lowman has served as a great mentor to me since 2005. As my research advisor he provided invaluable support and guidance throughout my time as a member of the Biomaterials and Drug Delivery Laboratory. His success in both academia and in industry are only two examples of why he is a great role model for me for what I hope my future career will resemble. As a member of his lab I was fortunate to work with many bright and talented individuals, all of which supported my research efforts. While a member of the lab, Dr. Kara Spiller, was a great resource, “partna” and friend. Her brilliance is only matched by her kindness and sense of humor. Dr. Erik Brewer, Dr. Valerie Binetti, and Pamela Graney all provided great feedback to my research questions and were a great source of support. I am grateful for the numerous positive interactions I had with other members of the lab including: Dr. Meredith Hans, Dr. Tony Tuesca, Dr. Jennifer Vernengo, Dr. Noelle Comolli, Dr. Garland Fussell, Dr. Jonathan Thomas, Dr. Jason Coleman, Dr. Michael Marks, Dr. Kris Kita, Vanessa Vardon, Line Kouecheu, and Andrew Cheng.

Dr. Giuseppe Palmese was instrumental in my research progress in his role as my research advisor. I am grateful for him accepting me in his lab and for his support of my logistically-challenging combined degree academic track. His expertise in composite science proved to be an extremely valuable as new areas of research interests grew for me. From his lab, Dr. Julianne Holloway, was great source of feedback and support. I am also grateful for my time with other members of the Polymers and Composites Laboratory including: Dr. James Throckmorton, Dr. Arianna Watters, Dr. Majid Sharifi, Dr. Ian McAninch, Dr. Ya Ling, Dr. Santosh Yadav, Fengshuo Hu, Sadella Santos, John Vergara, Emre Kinaci, and Natalie Gogotsi.

I was fortunate to have additional supportive thesis committee members, each of which provided great feedback to help guide my research goals. Dr. Suzanne Maher from the Hospital for Special Surgery (HSS) provided consistent support of my work and as a clinician scientist, I was fortunate to be able to work with her and the many distinguished clinical faculty at HSS. Dr. Richard Cairncross and Dr. Kenneth Lau not only supported my research efforts but also provided great instruction to me in the classroom. I am also grateful for the opportunity to work with and advise many talented high school, BS and MS students, especially Katherine Roelofs and Mary Ziegler.

My uncle, Dr. Cato Laurencin, has been a role model for me in academia and in life. Any small success I have attained thus far in my academic career is in large part due to his early support of my career goals and his continued mentorship. I am also grateful to the many individuals affiliated with his lab that supported me, especially during my time as a

high school student and undergraduate. Thank you to Dr. James Cooper, Dr. Saadiq El-Amin, Dr. Yusuf Khan, Dr. Michelle Kofron, Dr. Mohamed Attawia, Dr. Helen Lu, Dr. Dhirendra Katti, Dr. Eshan Jabbarezesh, Dr. Mark Borden, Dr. Edward Botchwey, and Dr. Swami Sethuranum.

Many members of the Drexel community have also supported my professional and personal development. I am particularly grateful to Stephen Cox for his support and guidance. In addition, thank you to Gregory Ross, Dr. Michele Marcolongo, Veniece Keene, Antoinette Torres, Dr. Fred Allen, Sherita Glenn and the faculty and staff of the Department of Chemical and Biological Engineering and the College of Medicine.

I am forever indebted to my family for their continued support and encouragement. Thank you to my entire family, particularly to my mother, Ester Laurencin, and my cousin, Gayle Watkins, who both served to instill in me an appreciation for life-long learning and for working tirelessly to support my academic pursuits. Thank you to my brother, Scott Laurencin, for being a great source of motivation for me to continue to strive for achievement so I can be a positive role model for him. Thank you to my many friends, especially Dr. David Delaine, Gabe Carryon, Gabriel Burks Amaliris Gonzalez and Virginia Kocieda, for their continued support.

Finally, thank you to my wife, Nicole Laurencin, for without her none of my accomplishments would have been possible. The love and support from her (and Teddy) makes all of the hard work and sacrifice worthwhile.

Table of Contents

List of Tables

List of Figures

Abstract

Fiber-reinforced, Anisotropic Superporous Cryogels for Meniscal Replacement

Samuel James Laurencin

Giuseppe R. Palmese, Ph.D. and Anthony M. Lowman, Ph.D.

Menisci are anisotropic, semicircular fibrocartilaginous tissues that must withstand extensive loads and sustain adequate locomotion in the knee joints. Meniscal tears are the most common intra-articular injury affecting the knee joint and consequently are the most common reason for procedures performed by orthopaedic surgeons. Once damaged, the partially vascular tissue has limited self-regenerative capabilities. Gold standard treatment of meniscal tears involves controlled excision of the damaged area, which exposes more of the underlying cartilage to increased contact pressure and increase the risk of early onset osteoarthritis.

Currently, there is a critical need to develop a biomaterial that is firm enough to resist the high, anisotropic loads the menisci experience and can permit fixation to the rigid underlying bone, yet soft and lubricous enough to protect the cartilage it interfaces and allow for normal joint locomotion. Polyvinyl alcohol (PVA) cryogels are water swollen polymers (hydrogels) that undergo low temperature-induced physical crosslinking and have been proposed as a meniscal replacement due to their biocompatibility, low coefficient of friction and compressive strength, which can be tailored to match native menisci. The hydrogel's mechanical capabilities are limited by its tensile strength being

much lower than the meniscus. Fixation of a water swollen polymer into the joint space is also a challenge that must be addressed for the scaffold to restore normal joint mechanics.

Through this research, it was demonstrated that ultra-high molecular weight polyethylene (UHMWPE) fibers could be introduced into a PVA cryogel in a controlled fashion using a coupon system. The interfacial shear strength between the fibers and cryogel were optimized using a 2-step process utilizing atmospheric pressure dielectric barrier discharge oxygen plasma and a glutaraldehyde covalent linkage. The presence of UHMWPE makes the cryogel anisotropic with respect to the direction of the applied stress, consonant with the native menisci. A liquid-liquid phase separation technique was employed to create a second PVA phase with an interconnected superporous network to aid *in vivo* implant fixation through cellular infiltration along the scaffold periphery. The structural and functional properties of the superporous PVA can be dictated by the synthesis parameters and influenced by post-synthesis osmotic conditioning. Transport properties through the cryogel was also established. Finally, the two-phase, tri-component cryogel was successfully scaled-up from the coupon system to native meniscus dimensions. This work provides great insight into the structural and functional features of fiber-reinforced, superporous cryogels and advances the field of biomaterials closer to a viable nondegradable meniscal replacement.

Chapter 1: Introduction

Meniscal tears are the most common intra-articular injury affecting the knee joint and consequently are the most common reason for procedures performed by orthopaedic surgeons [1]. Menisci are semicircular fibrocartilaginous tissue that must withstand extensive loads and sustain adequate locomotion in the knee joints [2-4]. They are able to convert compressive loads into transverse tensile loads [5, 6]. The hoop stresses that are formed are resisted by the tissue's radially and circumferentially oriented collagen fibers. Once damaged, the partially vascular tissue has limited self-regenerative capabilities. When injury occurs, the shock absorbing and joint stabilizing functions of the meniscus are lost [7, 8]. Gold standard treatment of meniscal tears involves controlled excision of the damaged area, which exposes more of the underlying cartilage to increased contact pressure and increase the risk of early onset osteoarthritis [9, 10]. For large non-repairable tears, meniscal allografts are a treatment option but donor availability and allograft sizing remains a challenge [11-13].

Researchers have proposed a myriad of novel materials, both degradable and nondegradable, to repair, regenerate or replace torn menisci [1, 14, 15]. Polyvinyl alcohol (PVA) cryogels are water swollen polymers (hydrogels) that undergo low temperature-induced physical crosslinking and have been proposed as a meniscal replacement due to their biocompatibility and compressive strength, which can be tailored to match native menisci [16, 17]. Incorporation of an secondary phase during the synthesis can influence the native porous structure and ultimately the function of the cryogel [18]. Biphasic

response to compressive loads, modulus within the range of native cartilage, low surface coefficient of friction, and low wear rates are all key factors of PVA cryogels that make them suitable for cartilaginous tissue repair [19]. The hydrogel's mechanical capabilities are limited by its tensile strength being much lower than the meniscus [20]. Fixation of a water swollen polymer into the joint space is also a challenge that must be addressed for the scaffold to restore normal joint mechanics [12]. While natively biologically inert, tissue engineering techniques, utilizing extracellular matrix proteins [21] or encapsulated cells [22, 23], can further mimic native tissues and aid in successful *in vivo* integration. Preliminary work by Holloway et al. proposed the efficacy of a nondegradable, fiber-reinforced cryogel composite scaffold using ultra high molecular weight polyethylene (UHMWPE) to replace damaged menisci [24]. However, despite the strong interest, tissue engineering-based treatment options for meniscal replacement have shown limited efficacy in the clinical setting [19, 25-27].

Currently, there is a *critical need* to develop a biomaterial that is firm enough to resist the high, anisotropic loads the menisci experience and can permit fixation to the rigid underlying bone, yet soft and lubricous enough to protect the cartilage it interfaces and allow for normal joint locomotion. Without addressing this need, the development of a hydrogel or similar biomaterial with properties suitable for meniscal replacement may remain unfulfilled.

Chapter 2: Background

2.1 Knee Joint Anatomy

Menisci are pairs of wedge-shaped cartilaginous tissues situated between the femoral condyles and tibial plateau. As seen in Figure 2.1, they are in close contact the stabilizing ligaments of the knee joint interact directly with articular cartilage above and below. They are also in close contact with the synovium making up the joint capsule.

Figure 2.1: Knee joint gross anatomy [28].

2.2 Meniscus

2.2.1 Composition

The meniscus has features of both fibrous tissue, with its extracellular matrix structure and composition, as well as cartilage tissue, with its territorial matrix around oval, cartilage-like cells and the presence of collagen type II [2]. Consequently, the meniscus is designated as fibrocartilage. The cells within the meniscus have properties found in both chondrocytes and fibroblasts, thus they are often classified as fibrochondrocytes. The meniscus is composed of 72% water, 22% collagen, and 0.8% proteoglycan. The collagen fibers form a complex interlacing hydroxylpyridinum aldehyde-crosslinked network encompassing the cells with the extracellular matrix of proteoglycans and glycoproteins. Over 90% of the collagen is type I collagen, having increased strength compared to the other types of collagen: II, III and VI.

2.2.2 Ultrastructure

An understanding of the menisci ultrastructure provides great insight into its functional properties. The primary orientation of collagen fibers is circumferential (Figure 2.2). Radially oriented fibers are also present, primarily within the inner two-thirds of the meniscus. The circumferential fibers serve to resist tension in the meniscus, while it is proposed that the radial fibers serve to hold the circumferential fibers together and also transfer axial compressive load from the femur to the tibia. There are randomly orientated collagen bundles at the surface of the meniscus similar to the collagen orientation in articular cartilage. There is also zonal variation of proteoglycan content, with the inner

one one-third having approximately four times the concentration as the peripheral one-third.

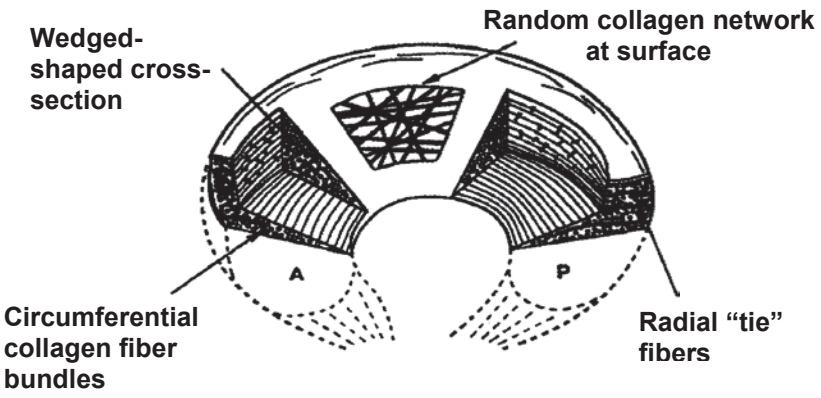

Figure 2.2: Ultrastructure of meniscus [2].

While the cells within the meniscus can generally be classified as fibrochondrocytes, the predominance of the cell properties varies with location in the meniscus. The outer portion contains fibroblast-like cells and the inner and middle portions containing primarily fibrochondrocyte cells. The fibroblast-like cells lack the pericellular matrix found surrounding fibrochondrocytes but they do possess multiple cytoplasmic projections that contact neighboring cells, which has lead researchers to believe that the strong intercellular connections allow the outer portion of the meniscus to respond to mechanical loading and sense the tissue's environment to maintain homeostasis [2]. The superficial zone contains cells with a distinct morphology that are believed to be progenitor cells, possibly arising from the synovium, and may play a role in meniscal wound repair.

A perimeniscal capillary plexus exists around the periphery of the menisci. Radial fibers from this plexus penetrate the meniscus at intervals and generate a rich vascular outer one-third zone known as the red-red zone. The innermost one-third of the meniscus is avascular, thus referred to as the white-white zone, with a middle one-third transition area referred to as the red-white zone. Axons are found throughout the meniscus in a paravascular, likely supporting vasomotor action, and non-paravascular location. The additional presence of mechanoreceptors has suggested that the non-paravascular axons may support knee-joint afferent nerve transmission and joint proprioception. Vascularization of the medial meniscus is approximately 10-30% of the total width and is key factor of healthy tissue and impacts the self-repair capabilities of the meniscus.

2.2.3 Gross Anatomy

The menisci are pairs of fibrocartilage tissue found in both knee joints. They remain secured within the knee joint between the femoral condyles and the tibial plateau by fibers connecting the peripheral rim throughout its length to the joint capsule with the midpoint having firmer attachment via connection to the deep portion of the medial collateral ligament. There is also attachment to the inferior tibia by insertional ligaments connecting the circumferential fibers of the meniscus at the tapered ends anteriorly and posteriorly. These represent essential fixation points for the menisci although additional attachments with varying degrees of prevalence in the population and less defined clinical value exists, such as the anterior intermeniscal ligament connecting the menisci to each other at their anterior horns, the meniscofemoral ligaments connecting the menisci to the

femoral condyles superiorly, and the patella-tibial ligaments connecting the patella to the anterior horns of the menisci. The meniscal ligaments control the mobility and motion of the meniscus and thus sufficient meniscal attachment is essential for adequate functionality.

2.3 Meniscus Biomechanics

The primary role of the meniscus is to transmit loads from the femur to the tibia. Supporting the role of various ligaments within the knee, the menisci also serve as secondary stabilizers and restraints to tibial internal-external rotation. Their role as stabilizers is to resist tensile forces, which is accomplished by the collection of circumferential and radial tie-fibers that transmit compressive loads to radial and circumferential tensile loads. This allows the meniscus to redistribute contact force across the tibiofemoral area. The meniscus has been shown to have average tensile strength of 110 MPa and 10 MPa in the circumferential and radial directions respectively. The elastic modulus ranges from 2 MPa to 23 MPa and is tissue location-dependent. The viscoelastic nature of the meniscus allows it to serve as a shock absorber of the knee. In menisectomized knees, the shock absorbing capacity is decreased by 20%. The compressive force placed on the meniscus is distributed over a portion of the articulating contact area. This creates a contact stress, which is proportional to the load and inversely proportional to the contacted surface area. The inner one-third experiences primarily compressive loads, which is supported by the higher concentration of glycosaminoglycans in this zone which serve to resist compression in a similar fashion to their role in articular cartilage. The high water content within a complex, interconnected

scaffold allows for water to act as an incompressible fluid under high rate loads where hydrostatic pressure resists the load and frictional drag created by the fluid attempting to escape is used to absorb the shock. Due to the impact of fluid flow, the instantaneous compressive strength has been shown to increase exponentially with level of strain, whereas higher strain rates limit the ability for fluid to escape and thus contribute to load resistance. The aggregate compressive modulus, representing an equilibrium state between fluid and solid tissue components, has been reported as 0.15 MPa with a corresponding permeability of 1.9×10^{-15} m^4/Ns.

Under load, the menisci have tendency to displace radially but this displacement is minimized primarily by the insertional ligaments, which creates hoop stress within the tissue. This allows the meniscus to deform by increasing its circumference to conform to the geometry of the femoral condyles during joint motion instead of being displaced and allows for distribution of the load. The menisci, however, do not perfectly distribute the load over the entire contact surface area. Under no load the contact within the knee is primarily over the meniscus but with large loads, such as 1470 N, the menisci cover only 59 to 71% of joint contact surface area. MRI studies during knee flexion have shown that there is posterior excursion of the medial and lateral meniscus of 3.9 mm and 5.6 mm respectively and peripheral movement of the medial and lateral meniscal bodies of 3.6 mm and 3.7 mm respectively during full extension to full flexion of a load-bearing knee. The lateral meniscus has greater mobility primarily due to less capsular attachment. The normal meniscal mobility is important criteria for developing replacements where fixation without implant movement hindrance is an important balance.

2.4 Meniscal Lesions

Meniscal lesions can be classified as traumatic, degenerative or a combination of both. Primary degenerative lesions typically occur in the fourth or fifth decade of life but can been seen earlier in certain demographics such as athletes. Despite the natural aging process of the meniscus, the possibilities of primary traumatic lesions or combined degenerative and traumatic lesions are possible in older individuals. The menisci can also be damaged as a result of injury to other structures within the knee. For example, damage to the anterior cruciate ligament causes increased stress on the meniscus as subsequent progressive meniscal destruction.

Medial meniscus tears outnumber lateral meniscal tears by 2:1. This is likely due to the increased attachment sites and flatter surface of the tibial plateau over the medial meniscus causing the meniscus to bear more load with deep flexion while the lateral meniscus has greater posterior displacement under the same degree of flexion. The medial meniscus is often torn due to rotational forces experienced in a partially flexed knee. Circumferential splitting occurs more common than radial tears, possibly due to the higher load on the meniscus in circumferential orientation. However, radial tears disrupt the continuity of the circumferential fibers and are thus more detrimental to meniscal function.

2.4.1 Meniscal Damage and Osteoarthritis

The menisci combined occupy up to 71% of the intra-articular contact area within the knee joint, thus highlighting their importance as load bearing structures and their intimate

relationship with articular cartilage. Englund et al. reports a complex relationship between meniscal damage and osteoarthritis in the knee [29]. A meniscal lesion in a healthy knee can lead to osteoarthritis and, conversely, osteoarthritis may lead to meniscal tears that further accelerate the osteoarthritis in the knee. Degenerative meniscal tears seen in middle-aged and elderly, as opposed to traumatic tears seen in the young, are often associated with preexisting structural articular cartilage changes, which may represent early stage osteoarthritis. The pathologic process causing early- stage osteoarthritis is also expected to affect meniscal and ligament integrity in a similar fashion. Shear stress and early proteolytic degradation of the meniscal matrix may result in decreased tensile strength.

It is also common for middle-aged and elderly to experience meniscal extrusion, which is often a sign of meniscal degradation and existing osteoarthritis with moderate to large osteophytes or cartilage loss [2]. Meniscal extrusion may also contribute to increased joint-space narrowing seen on radiographs, which combined with meniscal tears and displacement are strong determinants of the rate of cartilage loss. Also, it is suggested that MRI-visible meniscal damage predates visible cartilage damage. There is a weak association between meniscal tears and knee symptoms in this age group, yet meniscal subluxation is highly associated with symptomatic knee osteoarthritis.

A study of 154 patients with osteoarthritis (mean age 53 years), found the prevalence of meniscal tears to be 76% in asymptomatic patients and 91% in symptomatic patients with osteoarthritis grade correlating with a higher frequency of meniscal tears [30]. Patients

with a degenerative meniscal tear on MRI had increased severity of cartilaginous lesions compared to the control group. This relationship was most prominent on the medial femorotibial side.

2.5 Treatments

2.5.1 Indication

The most common indication for surgery is repair of the main substance of the meniscus [2]. By comparison, tears of the periphery of the meniscus at the meniscosynovial junction are less frequent. Young age and recent injury are common indications to treat meniscal lesions. It is ideal to preserve the meniscus as much as possible when treating a meniscus tear. Of particular importance is the meniscal wall which serves to reduce the loading stress between femur and tibia by over 50%.

2.5.2 Repairable Meniscal Tears

Peripheral, longitudinal tears often have good functional results. This is due to the rich vascular network in this zone that utilizes a fibrin clot as a scaffold for vessel formation and mesenchymal stem cell proliferation with remodeling months later yielding meniscus tissue shape and mechanical properties. The avascular region has a less propensity for self-repair. Research has shown that meniscal cells do radially migrate to damaged avascular areas and attempt self-repair. This was shown by a canine meniscal injury plug model where a portion of tissue was taken from the avascular region, repeatedly frozen and thawed to destroy the contained cells and then re-implanted [31]. After one year the plug region was repopulated with cells, which demonstrates the meniscal cell migration

ability in response to injury despite overall poor haling and limited functional tissue restoration in the avascular zone.

More novel approaches are often an extension of traditional techniques. Mechanical trephination is a method to create vascular access channels to aid in healing meniscal lesions. The method involves abrasion or rasping of the adjacent synovium and the meniscal surface to stimulate bleeding and the release of growth factors to the healing area. Flaps are used, either free or pedicle type, to cover the meniscus or specifically over the tear. Wrapping the meniscus in a collagen matrix is a similar concept to using a free flap or fascia sheath coverage with the idea that the collagen will create a bioreactor environment guiding cell in-growth and improved suture stability. However this technique is technically demanding and time-consuming.

Various options exist to aid repair of the avascular zone. These include connecting the inner portion to the outer via vascular access channels, creating a synovial flap to cover the lesion, or using a fibrin clot with or without growth factors at the lesion. While each option improves the healing capabilities of the avascular region, their results are limited by the formation of meniscal tissue that is incapable of normal meniscal function, as shown in canine studies where a fibrin clot filled a meniscal defect but the resulting tissue had higher aggregate modulus and lower permeability [32].

2.5.3 Non-repairable Meniscal Tears

Menisectomy is often the first-line treatment for meniscal tears, with arthroscopic menisectomy considered the gold standard. However this often causes accelerated cartilage degradation and progressive osteoarthritis [2]. Following meniscectomy, patients are 14 times more likely to develop signs of osteoarthritis within 21 years on radiographs. Furthermore, medial meniscectomy has been shown to cause altered gait patterns. Therefore, meniscal substitution following a partial or total meniscectomy is a more favorable treatment option. Substitution is essential to prevent subsequent cartilage damage, restore biomechanical function and relieve pain. Multiple risk factors are correlated to a poor surgical prognosis when treating meniscal tears including: younger age at operation, presence of ligament injury, instability of the knee joint, presurgical presence of varus or valgus deformity and long preoperative duration of symptoms.

Meniscal allografts are an option for non-repairable meniscal tears [33]. Allograft transplantation provide pain relief and improved stability. They are indicated primarily for young patients with stable, minimally varus or valgus knee joints, and limited signs of osteoarthritis. Accurate meniscal allograft sizing is extremely important when performing meniscal transplantation using bony bridge fixation technique. Given the specific demographic indicated for allografts, they are not routinely performed.

2.5 Tissue Engineering of the Meniscus

The field of tissue engineering has seen much growth in recent years with the ability to engineer a wide variety of synthetic and natural scaffolds [34]. Tissue engineering

approaches employ either natural or synthetic scaffolds and/or tissue-generating cell populations introduced to the defect site [35]. Numerous synthetic and natural scaffolds have been investigated to provide a 3-D environment for *in vitro* cell culture and introduction of cells to a defect site [36, 37]. Medical imaging and computer aided technology can be utilized to fabricate scaffolds with complex geometries and assess implant integration *in situ* [38, 39]. Scaffolds can support the culturing and transplantation of both mature chondrocytes and mesenchymal stem cells (MSCs) to treat defects. The use of MSCs is often preferred due to limitations in a donor source of autologous mature chondrocytes in some patients [38]. However, the use of stem cells requires increased control over the microenvironment during cell culture to regulate *in vitro* and *in vivo* differentiation [40].

There are basic requirements for scaffolds to be applicable for biomedical use including biocompatibility, structural stability, and adequate tissue integration [35]. For cartilaginous tissue applications, it is also important that the scaffold provide a low frictional index at the surface and restore mechanical integrity at the native site. The mechanical properties for a scaffold used in meniscal defect repair or replacement must exhibit the same ability to resist forces in compression, tension, and shear. Furthermore, the avascular nature of inner two-thirds of the meniscus requires consideration of the diffusive and transport properties within a scaffold to ensure proper nutrient delivery to the internal cells [41]. The diffusive and transport capabilities are a function of the scaffold's porosity and permeability and water content. The porosity is a measure of the void volume of the material but other characteristics including pore size, pore geometry,

pore interconnectivity, and pore channel tortuosity must also be considered when describing the porosity of a scaffold. It is generally accepted that a high porosity, around 90%, high interconnectivity, and high surface area-to-mass ratio is needed for uniform tissue ingrowth [41, 42]. However, this high porosity may compromise the integrity of certain materials for applications involving large physiological loads, thus optimization in porosity and mechanical properties must often be obtained.

2.5.1 Novel Engineered Replacements

Actifit™ is a degradable aliphatic polycaprolactone-polyurethane-based scaffold developed to promote meniscal tissue ingrowth for treatment of partial meniscal tears. The Menaflex™ collagen meniscal implant was developed to serve as a porous biodegradable scaffold consisting of crosslinked type 1 collagen with glycosaminoglycan. It was reported to provide immediate restoration biomechanical function while allowing for cellular ingrowth and tissue regeneration during the scaffold degradative phase. Menaflex™ successfully completed clinical human trials and was FDA approved for marketing in the US. However, the FDA rescinded their approval in part due to concerns regarding the proven safety of the device. This demonstrates the importance of key understanding of the translational and clinical potential challenges in developing a tissue engineered meniscal replacement. Both implants require intact meniscal rim for tissue ingrowth [43]. NuSurface ® meniscal implant is a nondegradable polycarbonate-urethane and UHMWPE implant for total meniscal replacement. It replicates the discoid meniscus shape and thus does not require attachment in the knee joint. Clinical trials are currently ongoing in the US.

2.5.2 Hydrogels

Hydrogels are swellable polymer materials that can be degradable or nondegradable and have high concentrations of water, often up to 90% (w/w) [44]. Numerous research groups have been involved in extensive investigation in the use of hydrogels for various tissue engineering applications [45-48]. A common hydrogel used in biomedical applications is PVA [49]. The biocompatibility and mechanical properties of PVA has prompted investigation in its use to treat articular cartilage defects [50]. PVA has shown to display reduced wear behavior when chemically stabilized with PVP [51]. Blends of PVA-PVP have shown potential in the repair of various musculoskeletal tissues due to its nondegradable nature, mechanical strength, and low surface frictional index [52-55]. The synthesis method is an important consideration since the use of some polymer crosslinking agents and other synthesis materials can be harmful to cells. Freezing and thawing cycles can form physical crosslinks of adjacent polymer chains through hydrogen bonding, resulting in a 3-D cryogel with tunable material properties [49]. The designation of cryogel, as opposed to hydrogel, is reserved for freezing-temperature induced crosslinking.

2.5.3 Hydrogels for Meniscal Repair

Researchers have explored synthetic hydrogels for meniscal replacement applications. Kobayashi et al. investigated physically crosslinked PVA hydrogels [16]. The scaffold was compressive reinforced to permit suturing of the scaffold to the joint capsule in a rabbit model. After two years *in vivo*, the scaffold showed no breakage, shrinkage, dislocation or wear and demonstrated less cartilage wear than control groups. Following

that study, Kelly et al. investigated a fiber reinforced hydrogel in a large (*ovine*) animal model [56]. The fibers were used to secure the implant at the posterior and anterior horns. At 2 and 4 months the implant showed good chondroprotective ability. However, by one year follow up, the scaffolds failed due to propagation of a radial tear. Most recently, Holloway et al. further explored the potential for a fiber-reinforced PVA hydrogel as a meniscal replacement [24, 57]. This work focused in characterizing the functional capabilities of the hydrogel and improving the interface between the hydrogel and the fibers for better composite performance. These studies have demonstrated that PVA hydrogel with fiber-reinforcement has great potential as a meniscal replacement.

Chapter 3: Research Goals

The *long-term goal* of this project is to develop a nondegradable biomaterial that is clinically translatable and a viable treatment for non-repairable meniscal tears. The *overall objective* of this research, working towards the long-term goal, is to fabricate a cryogel that has material properties equivalent to menisci and also permits adequate nutrient transport and cellular proliferation and migration along the scaffold periphery for enhanced integration. *To achieve this objective, the central hypothesis is that high-tensile strength fibers can be incorporated into a cryogel to make the, otherwise isotropic, cryogel mechanical properties anisotropic with respect to compressive and tensile strength, consonant with the native menisci. An interconnected porous network can be introduced into the cryogel through a novel liquid-liquid phase separation technique that has pore network features sufficient for cellular proliferation and migration in vivo to aid implant attachment and integration. The cryogel can be secured to the bone at natural fixation points through the embedded fibers and allow for contact pressures on interfacial cartilage remain at levels seen in the presence of fully functional native menisci.* The *rationale* for the proposed research is that it will provide significant insight into (i) the relationship between scaffold synthesis, structure, and function and (ii) the cryogel's potential as a biomaterial for meniscal replacement.

To explore the validity of the central hypothesis, the following four *specific aims* are proposed:

Specific Aim 1: Synthesize and characterize cryogels reinforced with chemically grafted UHMWPE fibers. *Hypothesis:* Isotropic cryogels can be made anisotropic based on the rule-of-mixture where the tensile moduli of a composite fiber-cryogel will be significantly higher than that of a non-fiber reinforced cryogel due to the large tensile strength of UHMWPE. The compressive moduli will also increase due to the presence of fibers but to a much lesser degree. The effect of fibers on cryogel properties will be dependent on fiber volume, fiber spacing and orientation of fibers within the composite.

Specific Aim 2: Synthesize and characterize physically crosslinked, superporous cryogels. *Hypothesis:* PVA chemically stabilized with PVP can be synthesized using a novel liquid-liquid phase separation technique and form a scaffold containing an interconnected pore network that is dependent on the type of organic solvent used, solvent concentration, and mixing speed. The synthesis parameters will ultimately dictate the material properties such as compressive moduli and porosity. Swelling in conditions matching the knee joint will cause deswelling of the cryogel and changes in both structural and functional properties.

Specific Aim 3: Characterize the transport properties of superporous and non-superporous cryogels. *Hypothesis:* The diffusion of proteins can be determined through permeation

chamber measurements. The rate of diffusion will be dependent on synthesis parameters and ultimately cryogel compositional and structural features.

Specific Aim 4: Synthesize a meniscus dimension-matched fiber braid-reinforced cryogel with integrated superporous rim. *Hypothesis:* A complex fiber arrangement replicated the complex arrangement of collagen in native menisci can be introduced to the cryogel in a reproducible fashion. The cryogel with optimized material properties can be fashioned into the dimensions of the meniscus. A superporous cryogel periphery can be introduced to the bulk cryogel to form a stable tri-composite scaffold.

Chapter 4: Synthesize and characterize cryogels reinforced with chemically grafted UHMWPE fibers

4.1 Introduction

PVA cryogels have been proposed as a cartilaginous tissue replacement due to their biocompatibility and compressive strength, which can be tailored to match tissue-specific applications [16, 17]. Biphasic response to compressive loads, modulus within the range of native cartilage, low surface coefficient of friction, and low wear rates are all key factors of PVA cryogels that make them suitable for cartilaginous tissue repair [19, 57-59]. For certain applications, the isotropic nature of cryogel's mechanical strength would be advantageous. However, meniscus replacement requires anisotropic material functional properties. PVA-based hydrogels have a synthesis-structure-function relationship and can be tailored to have modulus values on par with menisci compressive and radial tensile moduli [60]. The hydrogel's mechanical capabilities are limited by its tensile strength being much lower than the circumferential tensile modulus of the meniscus [20, 61, 62].

Holloway et al. proposed the use of a nondegradable, fiber-reinforced cryogel composite scaffold to replace damaged menisci [24]. The composite designed was proposed to take advantage of the beneficial features of the cryogel, while utilizing the high tensile strength of the embedded fibers. The study explored the use of both polypropylene and UHMWPE fiber mats that were added to PVA using a wet lay-up process leading to a multiple fiber mats contained within a cryogel without control over inter-fiber mat spacing or linearity of the mats. Tensile tests demonstrated a proportional relationship

between fiber volume and tensile modulus, with UHMWPE formulations reaching 258.1 MPa with 29% fiber volume. This value is well within the circumferential tensile modulus range of 100-300 MPa reported for native menisci [1]. Scanning electron micrograph of the cross-section of embedded fibers demonstrated PVA-rich regions defining holes surrounding the fibers with the hole size proportional to the fiber size. These holes were much larger than the fibers themselves and highlights the poor interface between the chemically inert fibers and PVA. To improve the interface, Holloway et al. developed a process to create reactive oxygen species on the fiber surface and covalently link to the PVA hydroxyl groups use glutaraldehyde as a linking agent [63]. The benefit of glutaraldehyde treatment was evident by the improved interfacial shear strength (IFSS) between the fiber and matrix. Despite the significant insight gained in the potential for covalently linked fiber-reinforced cryogels for meniscal replacement, more insight is needed into the impact of fiber type and fiber spacing within the matrix and the ability to incorporate fibers in a controlled and reproducible manner.

This works explores the influence of UHMWPE braids on the tensile properties of PVA-based cryogels. The use of glutaraldehyde to improve interfacial properties of the composite with fibers of different diameters will also be assessed. Finally, the impact of fiber dispersion within the matrix on interfacial strength and resistance of tear propagation will be evaluated. An establishment of the tensile modulus, interfacial strength and tear strength will be essential in the development of a fiber-reinforced cryogel for meniscal replacement.

4.2 Materials and Methods

4.2.1 Materials

PVA (>99% hydrolyzed) with molecular weight 89,000 to 98,000 g mol^{-1} and polyvinyl pyrrolidone (PVP) with molecular weight of 58,000 g mol^{-1} were obtained from Sigma Aldrich (St. Louis, MO). Glutaraldehyde was also obtained from Sigma Aldrich. Dyneema® brand UHMWPE as braided fiber bundles (BFB) with 10 lb break strength was obtained from Lee Fisher International, Inc. (Tampa, Fl). The UHMWPE fibers were commercially available with intended use as a fishing line. They were received as a BFB and reduced to three single fiber braid (SFB) and further reduced to approximately 200 single fibers (SF) using a custom designed mechanical separation process (Figure 4.1). Due to the fragility of the SFs, they were tested as a collection of 200 separated SFs, or fiber tow (FT).

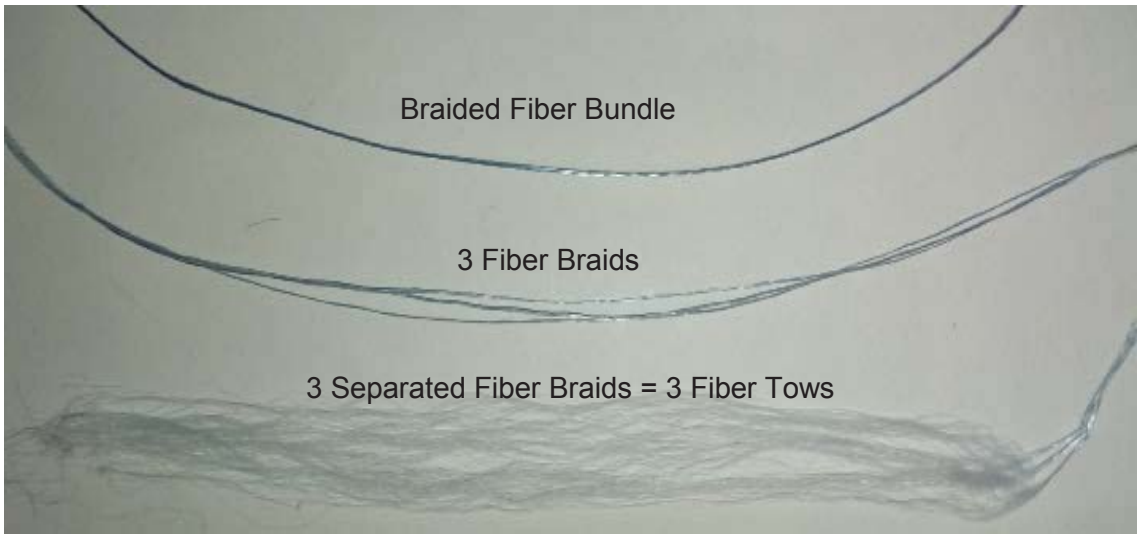

Figure 4.1: Hierarchy of fibers used for composite synthesis

4.2.2 Scanning Electron Microscopy

Fiber diameter was determined from scanning electron micrographs. Fiber were coated with platinum and imaged in a high vacuum scanning electron microscopy (SEM) model FEI/Phillips XL30 (Hillsboro, OR).

4.2.3 Cryogel Synthesis

PVA was made as a 10, 20, or 30 w% solution in deionized H_2O. PVP was added to the PVA solution as a network stabilizing agent at a PVA to PVP ratio of 99:1 (w/w) [52]. The PVA-PVP solution was autoclaved at 121 ^oC for one hour with additional heating, if necessary, in a 90 ^oC oven until the polymer was completely dissolved. The solution was poured into 24-well polystyrene tissue culture trays to form cylindrical samples of 15 mm diameter and approximately 6 mm in height for compression testing or into dog-bone

shaped specimens using custom fabricated Teflon spacers secured between glass slides for tensile testing. The solution was subjected to six cycles of freezing at -21 ^{o}C for 21 hours and thawing at room temperature for three hours to form a crosslinked cryogel.

4.2.4 Fiber-reinforced cryogel synthesis

A coupon system was designed and fabricated to control the spacing and orientation of fibers (Figure 4.2). The coupon system was used to scale-down from typical cryogel and fiber volumes needed for *in vivo* meniscal dimensions. BFBs or SFBs were thread through the coupon frame and spaced a minimum of 0.5 mm apart. Multiple rows were obtainable without control for spacing with respect to height within the cryogel. The fibers were held taught in the coupon system and encased between to dog-bone shaped Teflon spacers that were contained within two glass slides. PVA was added through an entry port with effort taken to prevent incorporation of air bubbles in the specimen. Tensile and tear testing samples were made into the dog-bone shape with a gauge length of 28 mm, width of 10 mm, and thickness of 2 mm. Fiber-reinforced samples for compression testing were made with 4 mm thickness and a single dog-bone shaped sample was cut into squares of 10 x10 mm.

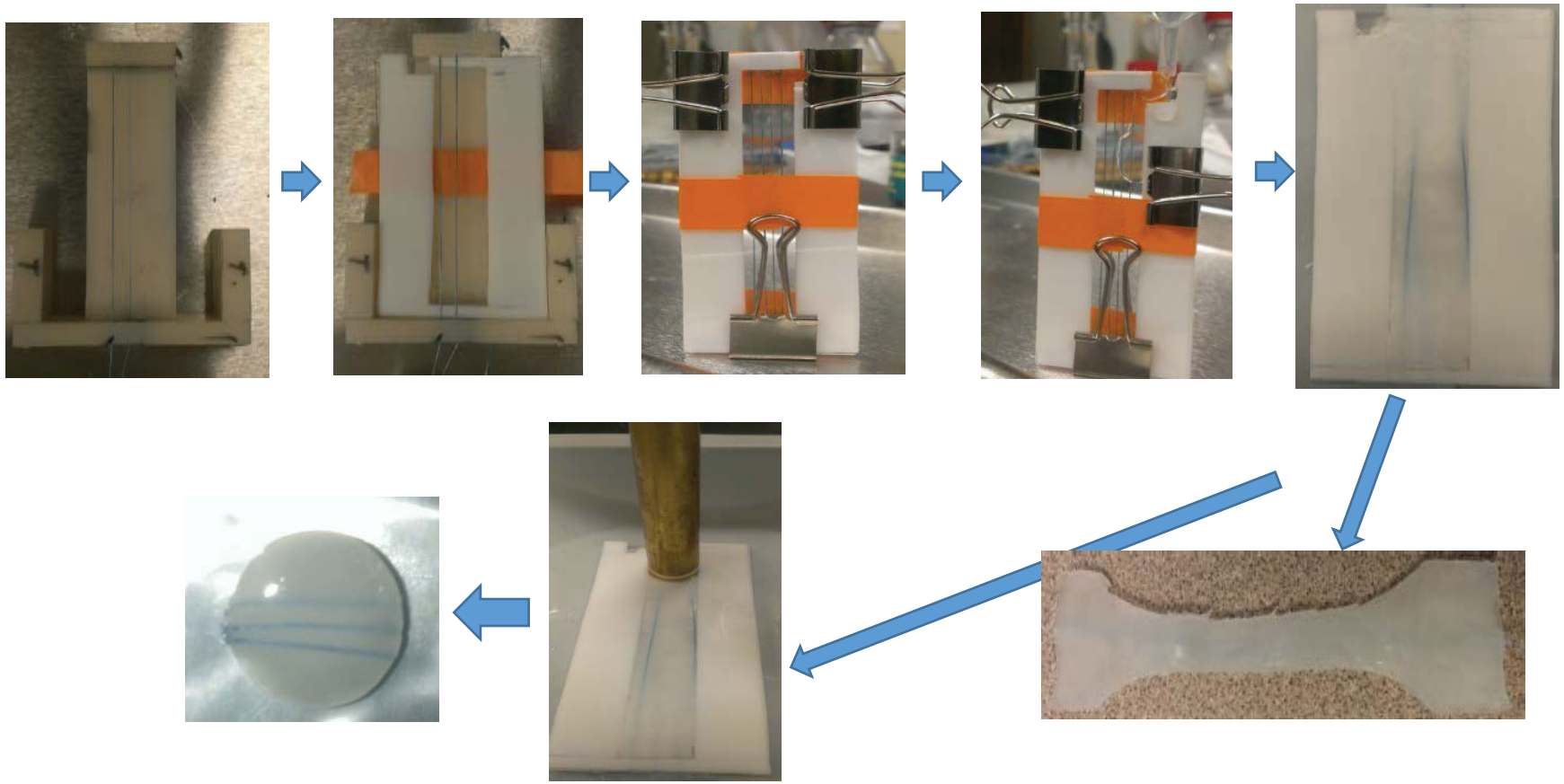

Figure 4.2: Coupon system for controlled addition of fibers to PVA showing synthesis steps for tensile and compression specimen synthesis.

4.2.5 Theoretical Composite Modulus Calculation

The upper bound of obtainable tensile modulus can be predicted by the rule-of-mixtures. This theoretical value is based on an external tensile load being applied in-line with the orientation of the parallel, continuous fibers within the matrix. The upper bound modulus, E_{UB}, can be calculated from the equation for the longitudinal tensile modulus:

$$E_{UB} = E_f V_f + E_m(1 - V_f)$$

where E_f is the modulus of the fiber, V_f is the volume fraction of fiber, and E_m is the modulus of the matrix. Conversely, the low bound tensile modulus, E_{LB}, can be predicted by the equation for the transverse tensile modulus:

$$E_{LB} = \frac{E_f E_m}{E_m V_f + E_f(1 - V_f)}$$

These equations provide a framework for what can be obtained in the fiber-reinforced system. The value of E_f $(17\ \text{GPa})$ was determined from experimental tensile testing due to BFB modulus values not being available from the manufacturer.

4.2.6 Chemical Grafting

Glutaraldehyde was used to create a covalent linkage between PVA and UHMWPE using previously described methods [63]. Briefly, a custom designed plasma reactor was used to produce reactive oxygen species on the fiber surface (Figure 4.3) [64]. Dielectric barrier discharge oxygen plasma using two charged plates at 1 W cm^{-2} under room

temperature and atmospheric pressure was employed. O_2 was supplied at 1 L min^{-1} flow rate over the fiber surface for 6 minutes for optimal reactive group formation.[63]

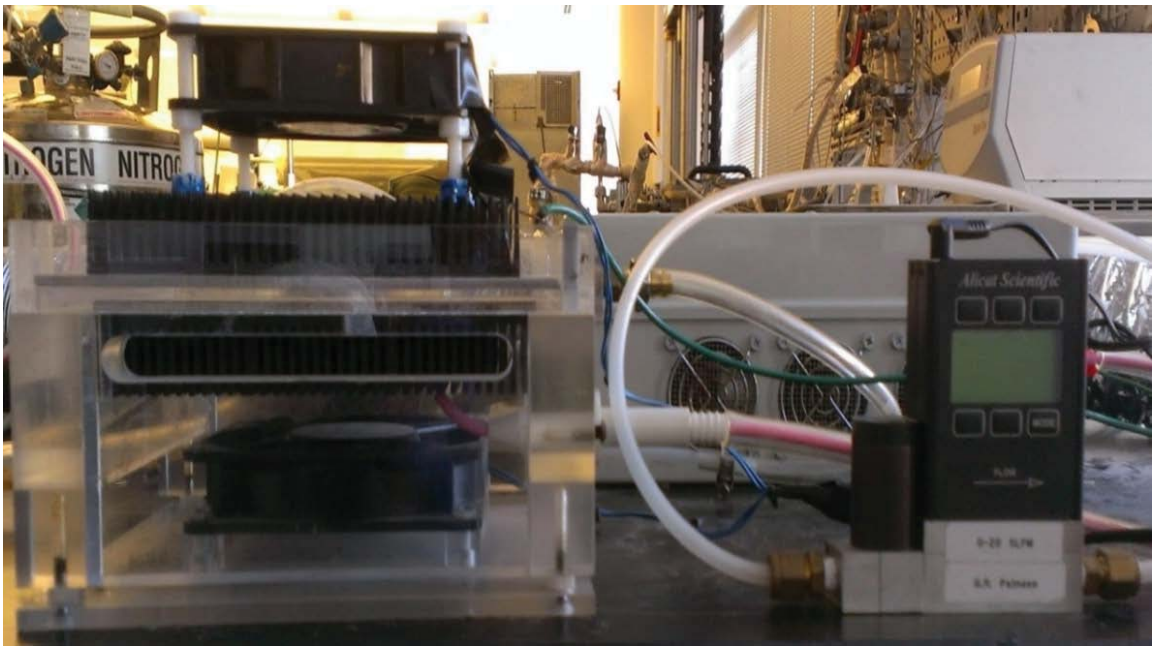

Figure 4.3: Atmospheric pressure dielectric barrier discharge system with flow-controlled oxygen delivery

Reactive UHMWPE fibers were submerged in 10 w% glutaraldehyde for 4 hours in the presence of an acid catalyst followed by suspension in 10 w% PVA with an acid catalyst overnight. The aldehyde-based crosslinking agent creates an acetyl bridge with subsequent covalent bonding. The glutaraldehyde-linked fibers are immersed in 10 w% PVA in the presence of an acid catalyst overnight to create a covalent link between the fiber surface and PVA polymer hydroxyl groups. The proposed reaction scheme is shown in Figure 4.4.

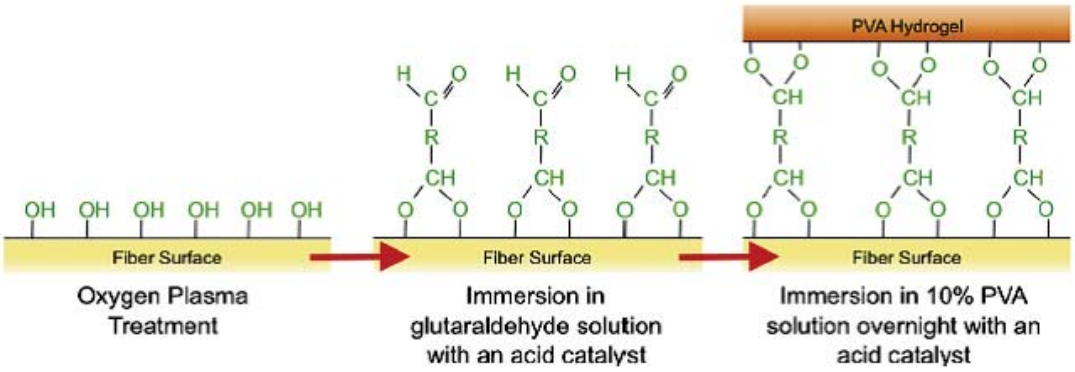

Figure 4.4: Proposed reaction scheme for glutaraldehyde linkage between fiber surface and PVA hydroxyl groups [63].

4.2.7 X-ray Photoelectron Spectroscopy

The presence of reactive groups on fiber surface was confirmed with X-ray photoelectron spectroscopy (XPS) using a Physical Electronics PHI VersaProbe 5000 (Chanhassen, MN). An Al anode provided a scanning monochromatic x-ray source with a dual beam charge neutralization system used to prevent charging of samples. Survey spectra was acquired at 100 W from a pass energy of 117.4 eV, 0 to 1000 eV range, step size of 0.5 eV and 20 ms dwell time. High resolution elemental C1 peaks were acquired at 100 W from a pass energy of 23.5 eV, 278 to 292 eV, step size of 0.2 eV and 50 ms dwell time. CasaXPS processing software was used for deconvolution of the high resolution C1s peak. Binding energy values for functional groups expected after oxygen plasma treatment are: 286.5 eV for hydroxyl (C-O) and 288.0 eV for carbonyl (C=O) and they were used to guide deconvolution peak fitting [64]. The area under each deconvoluted peak was used to calculate surface coverage of each functional group.

4.2.8 Mechanical Testing

Mechanical performance and suitability as a cartilaginous tissue replacement was determined through unconfined compressive loading [65]. Compression testing was conducted using a bench-top Instron loading machine model 4442 (Norwood, MA) with a 500 N load cell. Cylindrical cryogel specimens were subjected to a 0.1 N preload and compressed at 100 % min^{-1} to 50% strain. The compressive modulus was determined from the slope of the initial linear region of the stress-strain curve taken as 0 to 6% strain. Tensile testing was conducted using the same testing equipment and performed at 50 % min^{-1} to failure with an initial 0.01 N preload. Tensile modulus was calculated as the initial linear region for non-reinforced specimens. For fiber-reinforced specimens, the initial strain range where the fibers were fully engaged as determined by the linearity of the curve's slope was used to obtain the modulus.

Pullout tests were conducted with a modified tensile testing set-up. Specimens were prepared as dog-bone shaped samples and half of the cryogel was cut away from the fiber after the first freeze-thaw cycle. This provided an embedded length of 30 mm. The exposed fiber was secured to the upper portion of the Instron stage through a metal attachment and the bottom embedded portion was held between sandpaper within the stationary tensile grips. The tests were conducted at a strain rate of 10 % min^{-1} to failure. The IFSS per fiber, $\tau_{max,interface}$, can be determined from the max force obtained during a fiber pullout test using the equation:

$$\tau_{max,interface} = \frac{F_{max}}{\pi DLn}$$

where F_{max} is the maximum force needed to separate the fiber from the cryogel, D is the fiber diameter, L is the embedded fiber length and n is the number of fibers surrounded by the matrix. The shear strength of the cryogel represents the upper limit of the IFSS and was determined from previous studies to be 1.42 ± 0.20 MPa for 20 w% PVA [63].

Tear tests were conducted with a tensile test set-up. Specimens were subjected to a 5 mm notch and the max force required to propagate the notch was taken as the tear strength of the material. All tests were conducted with minimum replication of $n = 4$.

4.2.9 Statistical Analysis

One way analysis of variance (ANOVA) tests were conducted at a 95% confidence interval using GraphPad Prism software. Tukey's multiple comparisons test at a 5% error rate was performed to compare multiple groups simultaneously when differences were found through ANOVA. In all figures, error bars represent ±1 SD and statistical significance is defined as $p < .05$. A significant change with respect to a previous concentration, volume or distance (independent variables) is denoted by #. A statistically significant difference between multiple formulations at a specific concentration, volume or distance (independent variables) is denoted by *.

4.3 Results

To evaluate the potential of a fiber-reinforced cryogel for meniscal replacement, the isotropic mechanical features of non-reinforced cryogels was first established. These results were contrasted to the composite mechanical properties using UHMWPE fiber-reinforcement with and without the use of a covalent fiber-polymer linkage. For meniscal replacement applications, the tensile modulus and tear strength are of particular importance.

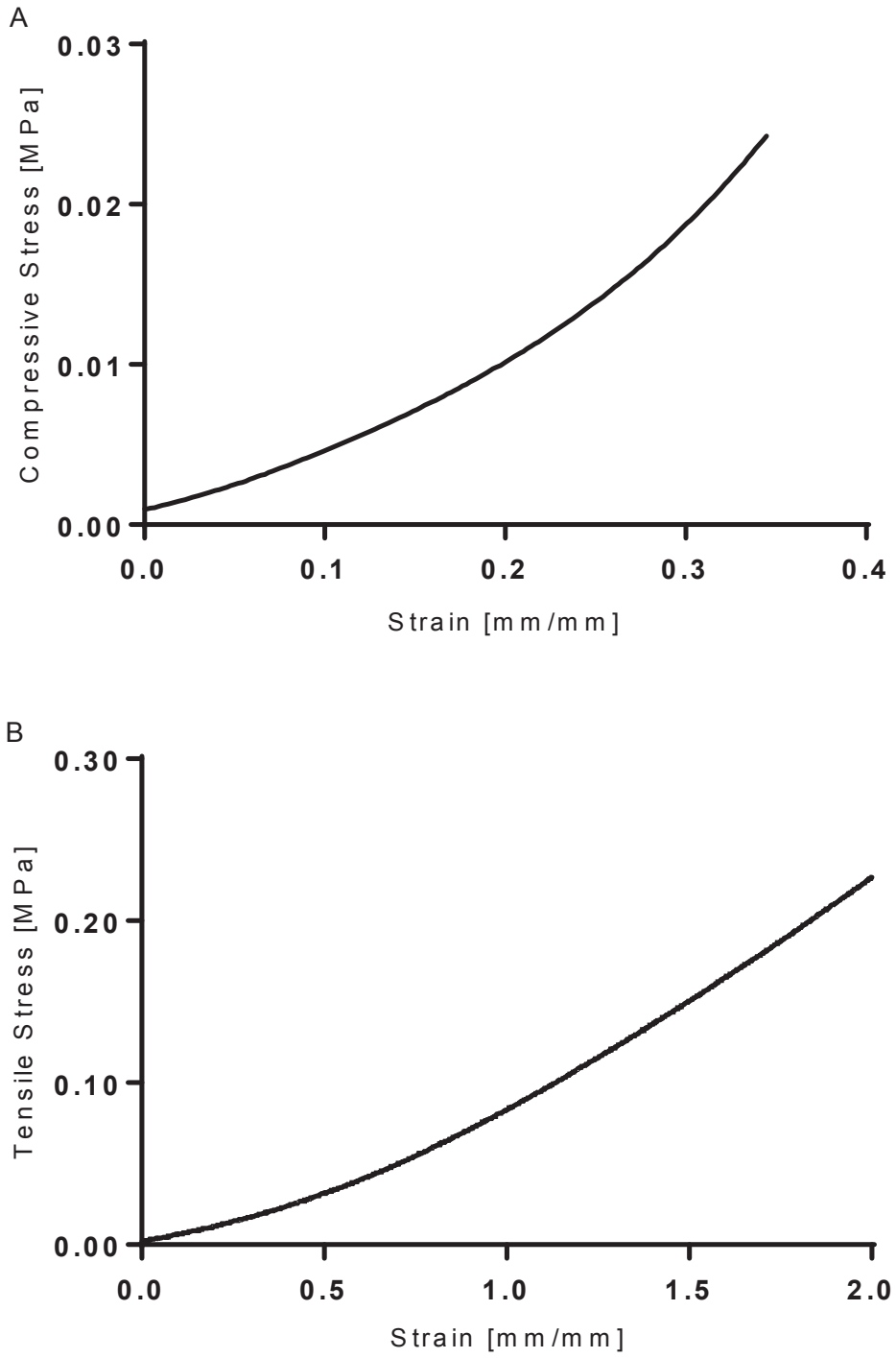

Figure 4.5: Representative stress versus strain behavior for a typical cryogel in compression (A) and in tension (B).

Figure 4.5 shows the typical mechanical behavior of PVA cryogels in compression (Figure 4.5-a) and tension (Figure 4.5-b). PVA in compression exhibited a hyperplastic behavior. However, in tension, it was considered to behave linearly over the strain ranges of interest. Due to the irregularities at the surface of compression samples, a 0.1 N preload was applied, which is evident by the slight compressive stress at zero strain. The compressive modulus was taken as the slope of the best fit line through the 0 to 6% strain range. Tensile modulus was taken as the initial linear portion of the tensile stress-strain curve, in which the strain range varied based on the presence or absence of fiber reinforcement.

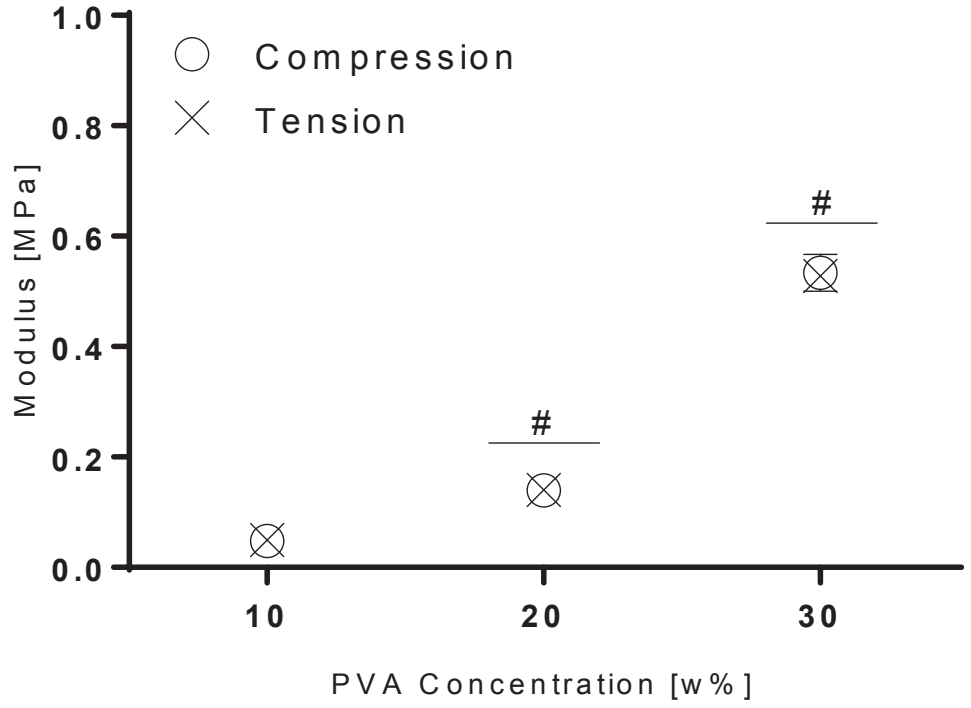

Figure 4.6: Cryogel modulus in tension and compression for 10, 20 and 30 w% PVA.

Figure 4.6 highlights the functional properties of PVA cryogels. At each PVA concentration the cryogel exhibits similar modulus when tested in either compression or tension. The amount of PVA used in synthesis has a clear proportional relationship with modulus ($p<.05$). 30 w% was chosen as the limit for cryogel synthesis due to the high viscosity of 30 w% PVA, which can pose difficulty in the incorporation of UHMWPE fibers and thus affect sample reproducibility.

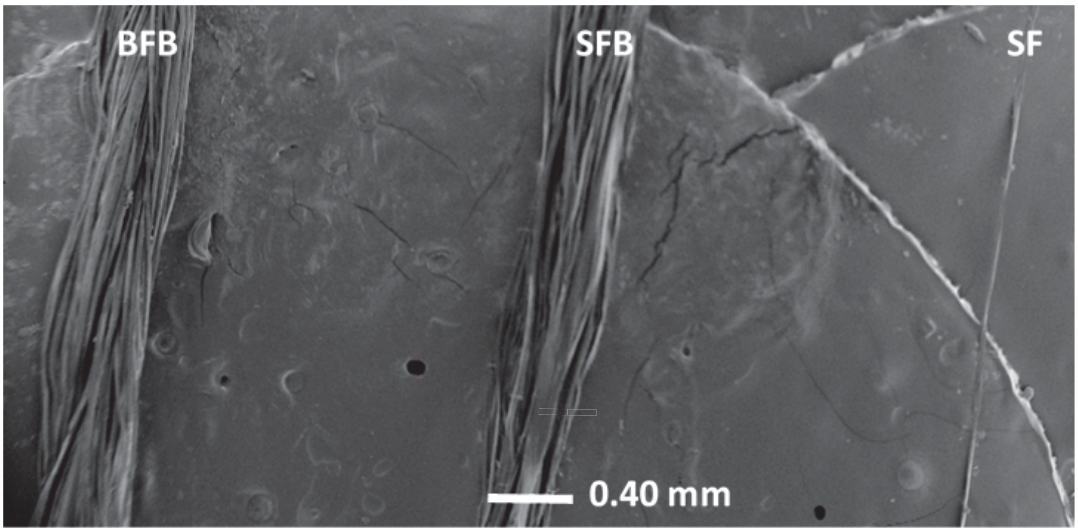

Figure 4.7: Scanning electron micrograph displaying fiber hierarchy for a braided fiber bundle (BFB), single fiber bundle (SB) and single fiber (SF).

Scanning electron microscopy (SEM) micrograph in Figure 4.7 shows the hierarchy of fibers used for composite synthesis: braided fiber bundle (BFB), single fiber bundle (SFB) and single fiber (SF). Approximately 200 SFs are contained within a SFB with three SFBs braided to form a BFB. The average diameters for BFB, SFB and SF are 0.45 mm, 0.30 mm and 0.02 mm respectively. Fibers were incorporated into cryogels in a

controlled fashion as: i) BFB, ii) SFB or iii) fiber tows (FT) representing a collection of approximately 200 separated SFs per FT.

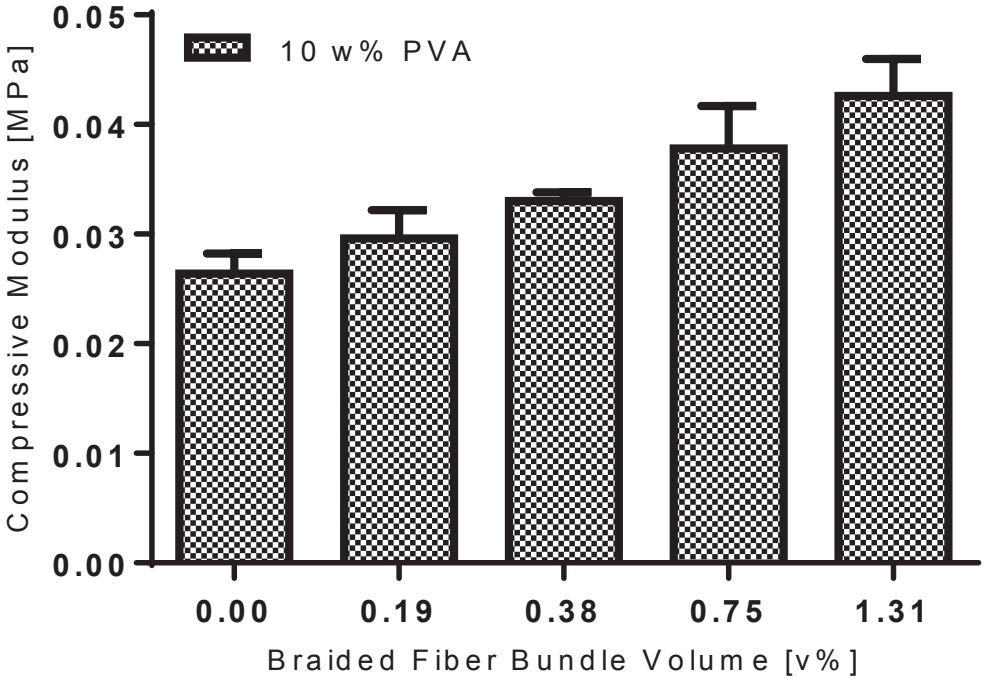

Figure 4.8: Fiber volume versus compressive modulus.

While the main goal of introducing UHMWPE fibers is to increase the tensile modulus of PVA cryogels and match the circumferential tensile modulus of menisci, Figure 4.8 demonstrates that the presence of BFB also influences the compressive modulus. There is a slight increase in modulus over the control with increases in fiber volume. The increase in modulus from BFB in 10 w% PVA does not reach a level on par with the native menisci compressive modulus of approximately 0.16 MPa (at 6% strain) [5], it does

provide insight into the interaction between the cryogel matrix and UHMWPE fibers. In unconfined compression, the PVA is able to deform radially under the compressive load. The presence of the BFB appears to inhibit the complete deformation and allows the matrix to increase its resistance to the applied load.

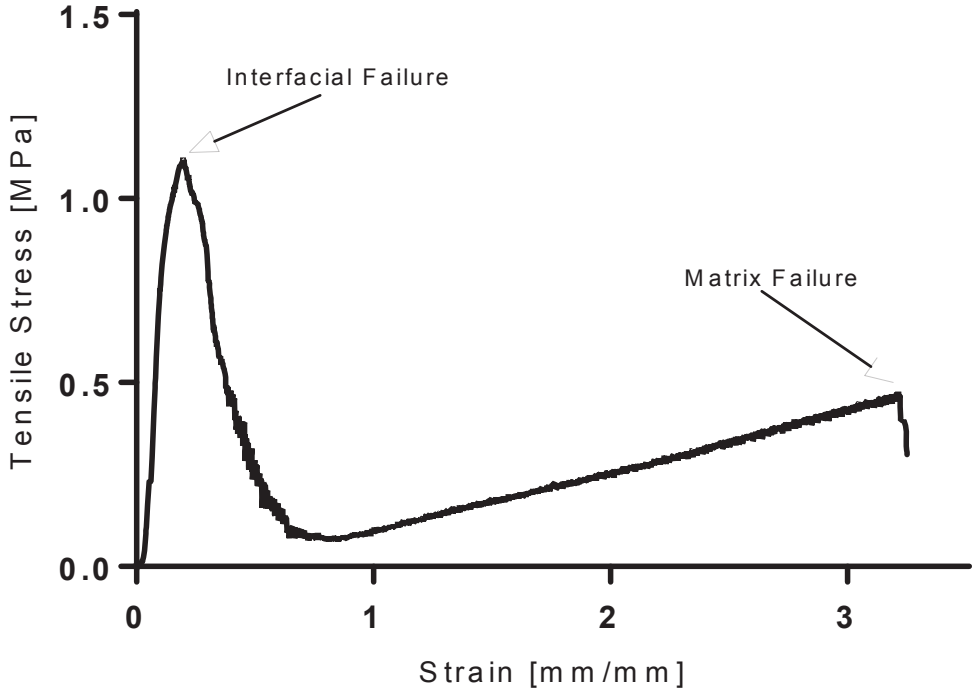

Figure 4.9: Stress versus strain behavior for a typical cryogel in tension with fiber reinforcement. Profile depicted is for 10 w% PVA with 0.12 v% BFB.

Figures 4.9 shows the typical stress-train profile of composite formulations. The maximum stress obtained can differ greatly within each formulation tested. The maximum stress obtained represents the point at which failure occurs within the fiber-composite interface followed by a reduction in stress due to reduced impact of fibers

resisting the external force. For samples that maintained good contact within the Instron tensile grips, a second increase is seen which is due to resistance of external load by the matrix until failure of the cryogel is reached.

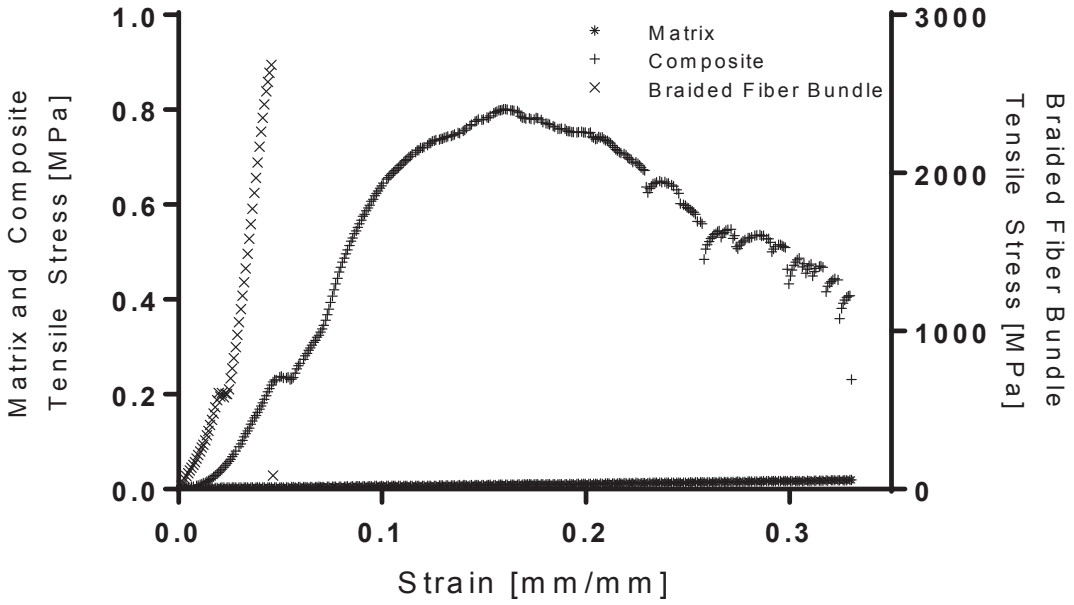

Figure 4.10: Tensile stress-strain profile of 10 w% PVA cryogel and single BFB and a 10 w% PVA single BFB-reinforced composite.

The typical stress-strain profile for: i) plain cryogel, ii) plain fiber bundle, and iii) cryogel reinforced with single BFB (0.04 v%) is seen in Figure 4.10. The difference in slopes for plain cryogel and plain fiber indicates the drastic difference in modulus of the two materials. The composite slope shows the influence of both components on the overall composite profile. The maximum stress on the composite is the point of interfacial failure followed by movement of the fiber within the matrix. There is a brief period of increased strain with constant stress for both the composite and plain BFB. This is due to

experimental error of the Instron system and reflects straightening and full engagement of the fibers followed by movement of the upper specimen clamp. It does not reflect a true behavior of the sample.

The coupon system permits multiple BFBs to be added in parallel within one plane and equally spaced. It is important to determine how the spacing of the fibers may affect the stress-transfer ability of the composite and consequently the effect on modulus.

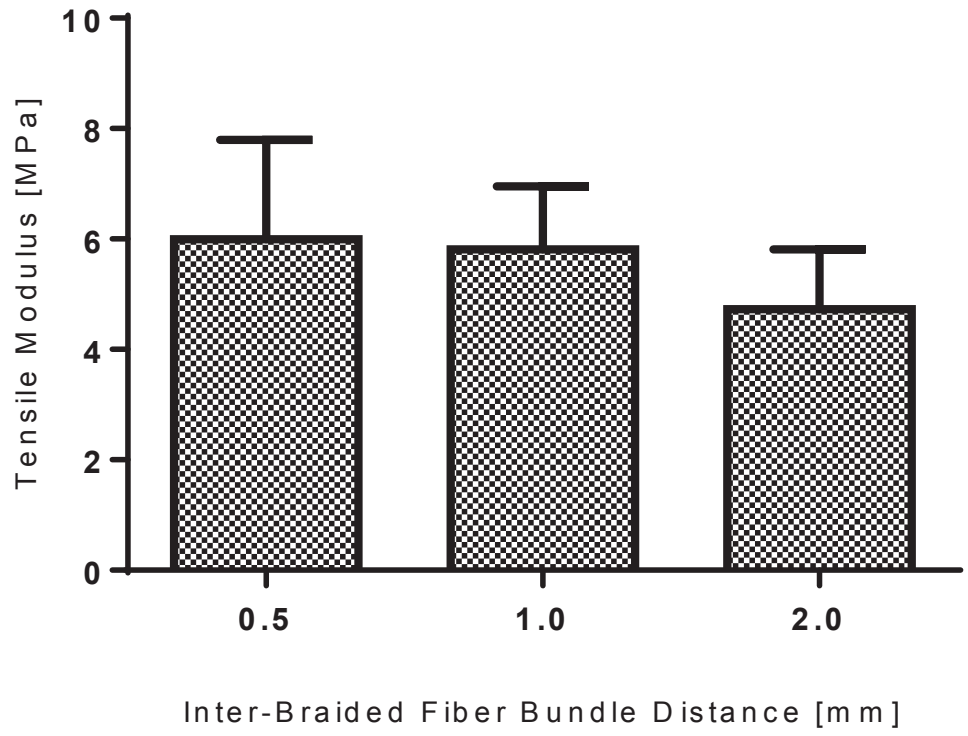

Figure 4.11: Tensile modulus with respect to interfiber distance for 0.43 v% BFB 10 w% PVA cryogel.

The coupon system permits multiple BFBs or SFBs to be added in parallel and equally spaced within the horizontal plane. It is important to determine how the spacing of the fibers may affect the stress-transfer ability of the composite and consequently the effect on modulus. It can be seen from Figure 4.11 that there while there appears to be a trend toward decreasing tensile modulus with increasing BFB distance in 10 w% PVA, there is no statistical difference between the values ($p>.05$). The coupon system was limited to a minimum interfiber distance of 0.5 mm and maximum distance of 2.0 mm. Despite the lack of difference due to spacing within the limited range evaluated, subsequent formulations were synthesized with a fiber spacing of 0.5 mm unless otherwise noted to control for the potential effect of fiber spacing on composite properties.

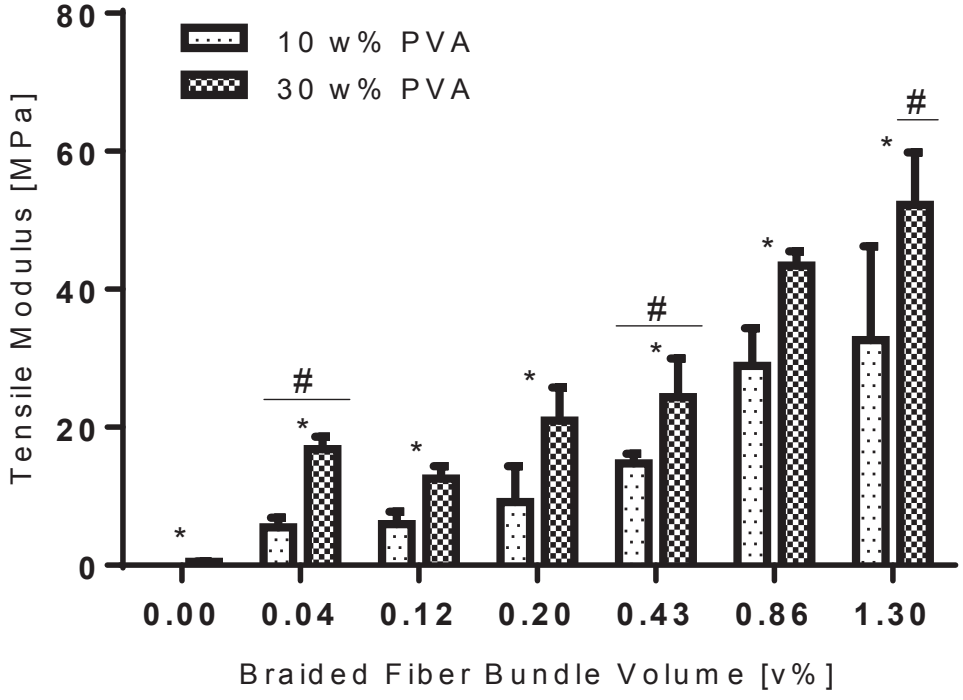

Figure 4.12: Tensile moduli of various BFB volumes for 10 and 30 w% PVA.

Figure 4.12 shows the tensile modulus with respect to fiber bundle volume for 10 and 30 w% PVA. The addition of 0.04 v% has a large impact over 0.00 v% (control) formulations at both PVA concentrations. For both 10 and 30 w% PVA there is a significant increase in tensile modulus for 0.04 to 0.43 v%, with further increases in modulus at 0.86 and 1.30 v%. 1.30 v% represents the upper limit of BFBs and SFBs that can be introduced into the cryogel in a reproducible fashion using the coupon system designed. The use of 30 w% PVA over 10 w% PVA produces a significant increase in modulus at each fiber bundle volume fraction except 1.30 v%. The maximum modulus at 30 w% PVA with 1.30 v% BFB approaches 60 MPa.

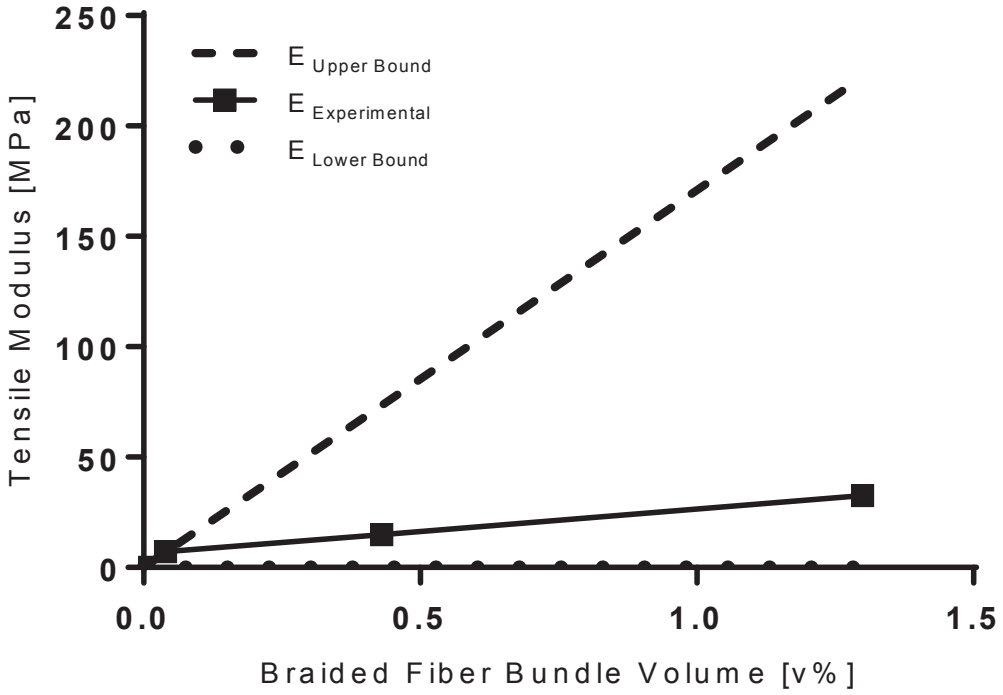

Figure 4.13: Upper and lower bound tensile moduli based on rule of mixtures versus the experimental tensile moduli at various BFB volumes.

Figure 4.13 compares the predicted upper and lower bounds of the composite tensile modulus based on the rule-of-mixtures. While there is very good agreement with the upper bound and the experimental modulus at low BFB volumes, the upper bound is an order of magnitude higher with increased BFB volume. With force applied along the direction of fiber orientation, it is expected that the experimental values would closely match the upper bound. An understanding of the cause of the discrepancy between theoretical and experimental tensile modulus can be gained by evaluating the interfacial properties of the composite. Tensile modulus is a bulk material property and does not provide insight into the strength of the composite interface, which can be a potential source of failure *in vivo* if not adequate to resist external loads. Fiber pullout tests are used to assess the strength of the interface between the fiber and matrix. It is expected that the IFSS will be relatively poor since both PVA cryogel and UHMWPE are relatively inert. Thus atmospheric pressure dielectric barrier discharge oxygen plasma deposition followed by glutaraldehyde covalent linking was used to strengthen the composite interface. Confirmation that reactive oxygen species were created on the surface was made through XPS as shown in Figure 4.14.

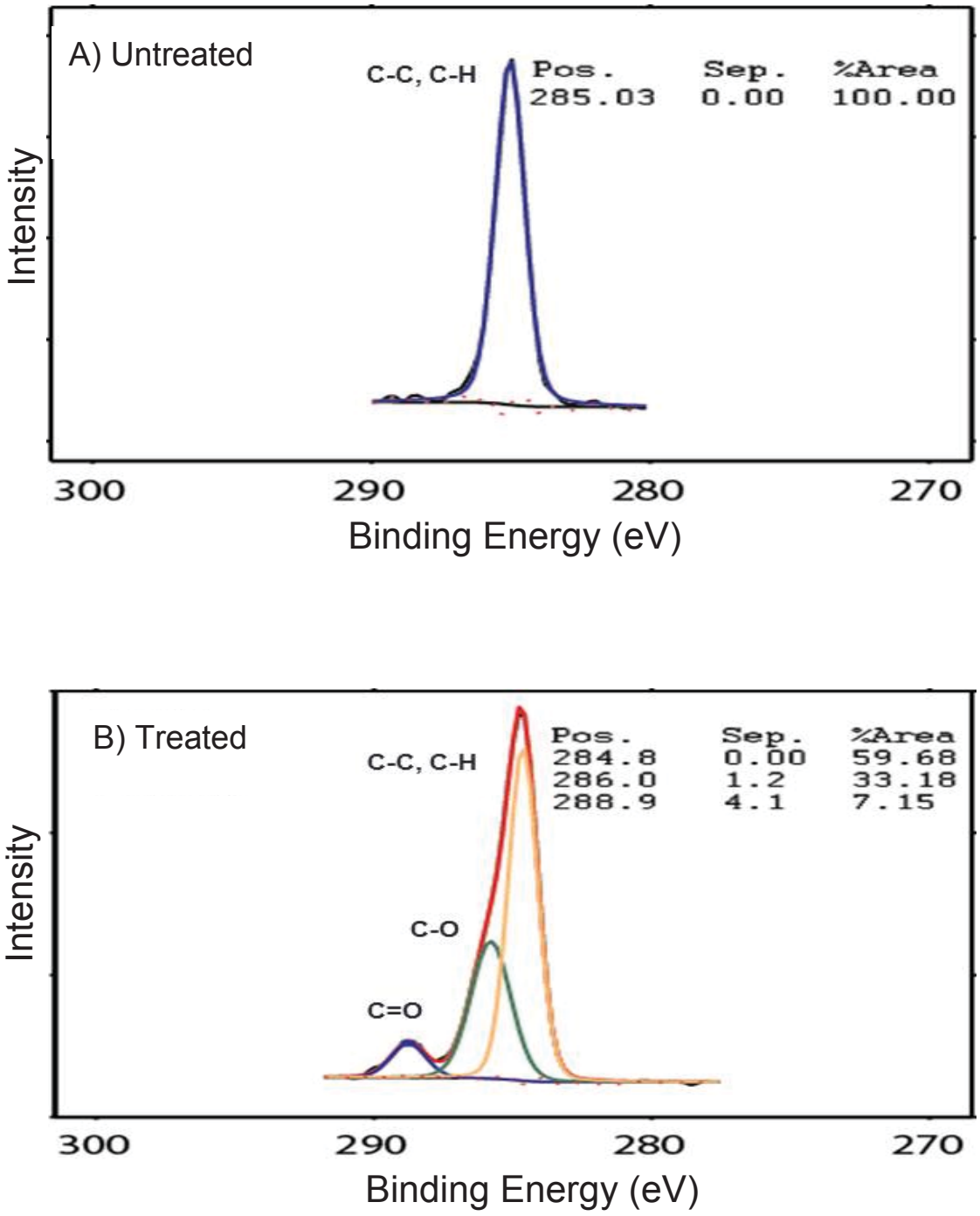

Figure 4.14: X-ray photoelectron spectroscopy spectra for both (A) untreated and (B) treated fiber surfaces.

Fiber 4.14-a shows the presence of C-C and C-H on the untreated fiber surface. After plasma oxygen treatment, as shown in Figure 4.14-b, the formation of C-O and C=O groups is evident, with an estimated surface area coverage of 33.18% and 7.15% respectively. Through chemical treatment of the UHMWPE surface, improvements in the fiber-matrix interface are expected.

As shown in Figure 4.11, there is a trend toward inversely proportional relationship between inter-fiber distance and modulus although the affect is not apparent given the limited range of distances capable with the coupon system. In addition to evaluating the impact on glutaraldehyde treatment, pullout studies were conducted evaluating the impact of small fiber diameter, low interfiber distance on the IFSS using FTs. The coupon system was not equipped to incorporate FTs into the cryogel, thus less control was retained over the orientation and dispersion of FTs within the cryogels. Figure 4.15 provides optical images showing the cross-section of cryogels with BFBs and FTs.

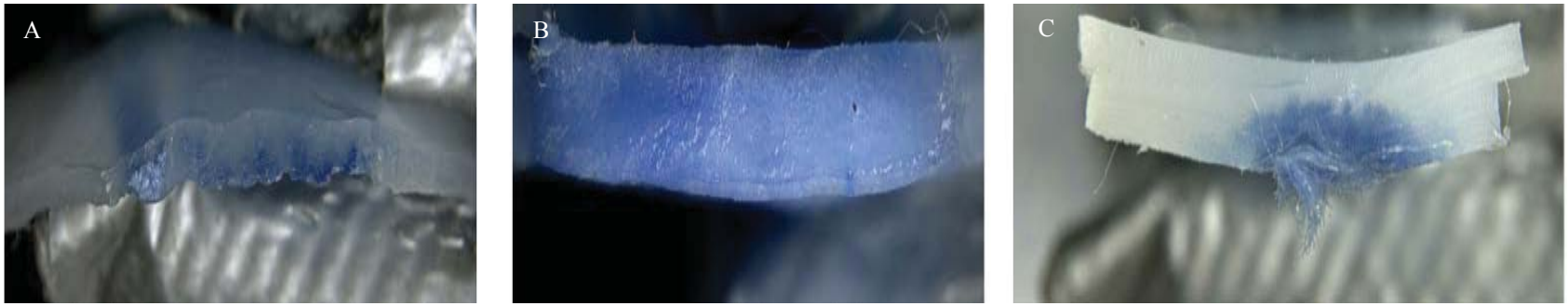

Figure 4.15: Optical micrographs of cryogel cross-section with (A) dispersed 1 v% BFB in 10 w% PVA, (B) 1 v% FT in 10 w% PVA and (C) 1 v% FT in 30 w% PVA.

Figures 4.15 shows the cross-section of reinforced cryogels. Incorporation of BFB and FT as shown in 4.15-a and 4.15-b respectively, highlights the minimization of interfiber matrix volume for FT reinforcements. Figure 4.15-c shows the effect of PVA w%, and thus polymer viscosity during cryogel synthesis, on the ability to incorporate FTs. The high viscosity of 30 w% PVA causes agglomeration of fiber tows compared to low viscosity 10 w% PVA that permits good dispersion of the fibers throughout the cryogel. The use of glutaraldehyde and the dispersion of fibers was evaluated in fiber pullout tests. A typical force versus extension curve for a pullout test using a 30 mm SFB or FT embedded length is shown in Figure 4.16.

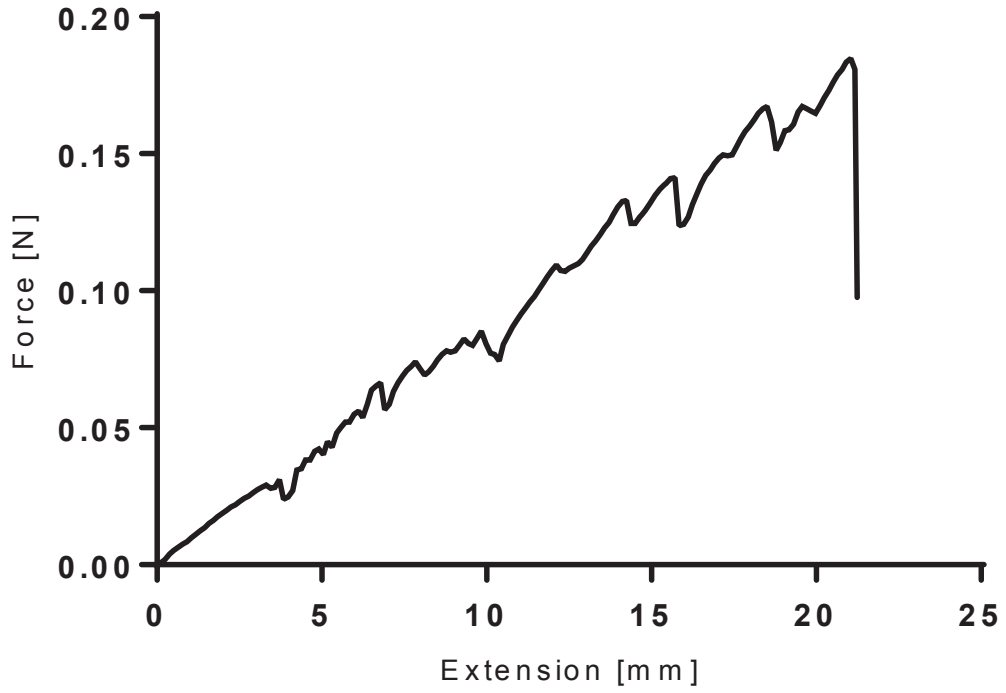

Figure 4.16: Representative force versus extension curve obtained from a fiber pullout test.

Figure 4.16 shows that there is a linear relationship between force and extension during the pullout test. The maximum force represents the point at which the applied force exceeds the interactive forces between the SFB and matrix. The oscillating nature of the curve can be attributed to stretching and elastic recoil of the matrix during pulling of the exposed fiber. The impact of glutaraldehyde treatment, fiber dispersion and PVA w% on IFSS is summarized in Table 1.

Table 4.1: IFSS for SFB and FT reinforced cryogels with (+) and without (-) glutaraldehyde treatment.

PVA [w%]	Fiber Type	± Glutaraldehyde	τ [kPa/Fiber]	SD	Mode of Failure
10	SFB	-	93.32	70.26	Interface/Matrix
10	SFB	+	214.30	114.01	Interface/Matrix
10	FT	-	89.98	28.09	Fiber; Interface/Matrix
10	FT	+	194.15	30.39	Fiber; Interface/Matrix
30	SFB	-	198.60	40.68	Interface/Matrix
30	SFB	+	796.70	94.59	Interface/Matrix

Table 1 displays the IFSS at 10 and 30 w% PVA for SFB and FT cryogels with and without glutaraldehyde surface treatment. Non-treated cryogels have a relatively poor fiber-cryogel interface as evident by the IFSS in Table 1. The use of glutaraldehyde drastically improves the IFSS at both 10 and 30 w% PVA ($p<.05$). Comparing FT to SFB formulations at 10 w% PVA, there does not appear to be a significant difference in IFSS ($p>.05$). However, when using the FT, the samples were more likely to fail within the fiber instead of consistently failing at the interface or within the matrix. It is not possible to differentiate between the interfacial failure and failure within the cryogel immediately

surrounding the fiber without high resolution imaging or surface analysis. This serves to under-report the true IFSS for FT formulations. Increasing the PVA w% had a significant impact on IFSS ($p<.05$), with the strongest interface contained within the SFB, 30 w% PVA +glutaraldehyde formulation.

Meniscal damage typically involves the propagation of tears within the tissue, thus a potential biomaterial replacement must exhibit adequate tear strength *in vitro*. PVA alone cannot resist propagation of a tear under loads likely to be experienced *in vivo.* Composite tear tests were conducted for both SFBs and FTs at various fiber volumes. The tear strength of the material is taken as the peak force required to propagate the initial notch as shown in Figure 4.17.

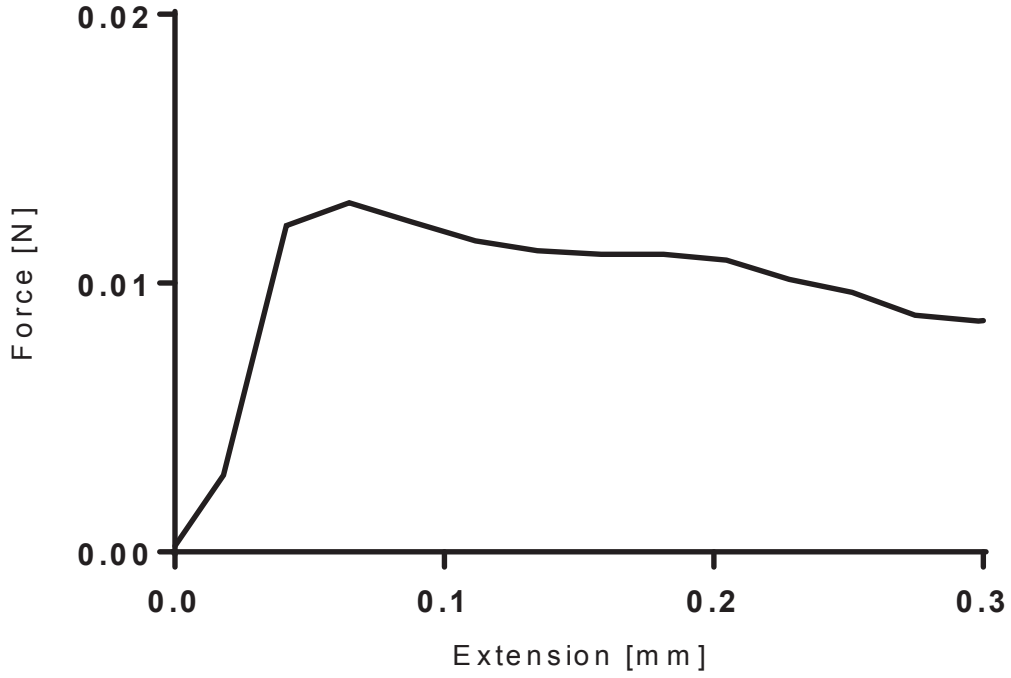

Figure 4.17: Representative force versus extension curve from a tear strength test.

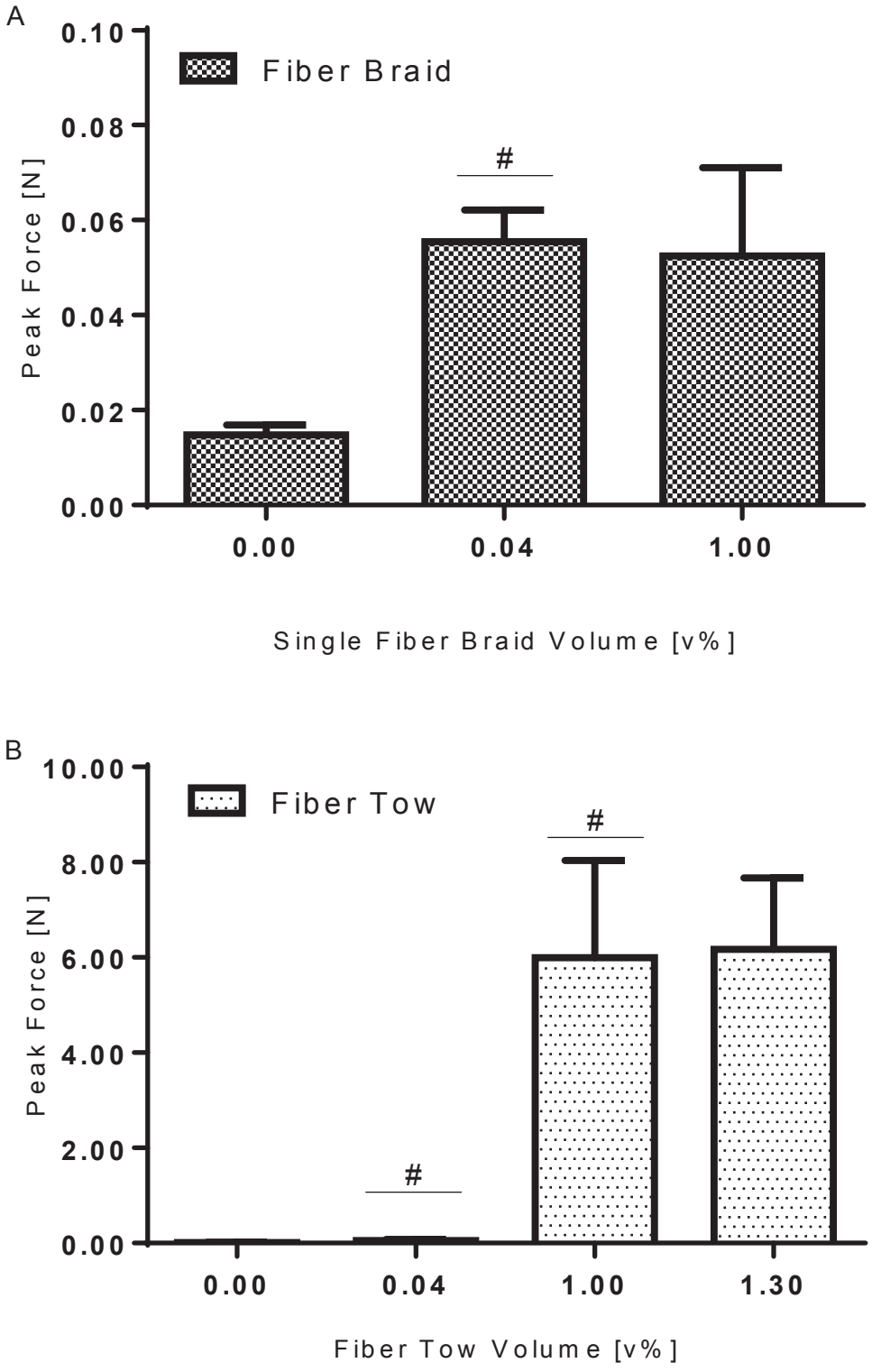

Figure 4.18: Peak load versus (a) SFB volume and (b) FT volume in 10 w% cryogel during tear strength testing.

Figure 4.18-a shows the force required to tear the cryogel matrix when reinforced with fiber braids. The presence of braids interspersed amongst cryogel matrix causes a slight increase in peak load, thus increasing tear strength ($p<.05$). This is likely due to SFB entanglement resisting tear propagation. Figure 4.18-b shows the force required to tear the cryogel matrix when reinforced with separated FT. The presence 0.04 v% of individual fibers of the FT interspersed amongst the cryogel matrix significantly improves cryogel tear strength over control strength ($p<.05$). Increasing the fiber volume to 1.00 v% leads to a drastic increase in force required to tear the cryogel ($p<.05$). Further increase of fiber volume to 1.30 v% does not significantly increase the tear strength beyond the 1.00 v% ($p>.05$).

4.4 Discussion

In this study, the impact of fiber-reinforcement on the mechanical performance of isotropic PVA cryogels was established. The presence of 1.30 v% BFB produces a modulus increase from 0.05 MPa to 33.61 MPa for 10 w% PVA and 0.53 to 52.26 MPa for 30 w% PVA. This proportional relationship between fiber volume and modulus is advantageous from a meniscal replacement standpoint since an optimal fiber volume can be determined to produce modulus values equivalent to native tissue. For the meniscus, the circumferential and radial tensile moduli are on the order of 100-300 MPa and 10-100 MPa respectively. Despite the large increase in modulus for a relatively small volume of fibers, the modulus approached 60 MPa, which is below the range of 100-300 MPa.

Increasing the fiber volume beyond the currently designed coupon system limitation of 1.30 v% is expected to further increase the modulus.

In addition to modifying the coupon system to permit incorporation of larger fiber volumes, the expected tensile modulus for fiber volumes tested can be predicted by the rule-of-mixtures. This theoretical value is based on volume of the composite components with an upper and lower bound value determined by the orientation of fibers with respect to the external tensile load. The maximum predicated modulus is found with the load being applied in-line with the orientation of the parallel, continuous fibers within the matrix. E_{UB} predicts a 10 w% PVA tensile modulus of 6.88 MPa at 0.04 v% BFB and 222.15 at 1.30 v% BFB. While, the low fiber volume predicted modulus is in close agreement with the experimental modulus, there is an order of magnitude difference at 1.30 v% BFB.

The difference between predicted and experimental moduli at high fiber volumes can be explained by the various assumptions used to develop the rule-of-mixtures. The theory assumes the composite has: i) perfect bond between matrix and fibers, ii) fibers are continuous and parallel and iii) the composite is free of voids, among other assumptions. Failure to satisfy all of these assumptions can cause disassociation between the experimental and predicted moduli. The coupon system was used to incorporate BFBs in a controlled fashion to maintain parallel alignment of the fibers. Repeated freezing and thawing of the cryogel causes slight deformation of the fiber alignment. In addition, fiber braids, such as the BFB used in tensile testing, contain void space between the SFs and

represents significant area where there is SF-SF interface and no stress transfer between fiber and matrix. Furthermore, repeated cryogel freezing and thawing expels water during the condensation of PVA polymer chains. The expelled water has been shown previously to condense around embedded the chemically inert UHMWPE fibers. This also leads to failure to produce a perfect bond between matrix and fibers. All of these factors contribute to the inability to fully satisfy the assumptions of the rule-of-mixtures and explain why the experimental results are lower than the predicted values.

The use of glutaraldehyde has been shown to be successful in improving the bond between fibers and the cryogel matrix, which helps satisfy the rule-of-mixtures. To eliminate the void space between SF within the BFB and SFB, the full separation of fibers to FTs was done, which serves to maximize the number of fibers interfacing with the PVA matrix. The impact of both steps was demonstrated by comparing the IFSS. As shown in Table 1, covalent linkage between UHMWPE and PVA improves the IFSS over non-glutaraldehyde treated formulations. The improved interface yields greater stress transfer between the composite components. Evaluating the influence of PVA w% shows that increasing PVA from 10 to 30 w% greatly increases the moduli. This is also a result of improved stress transfer, but in this case due to the increased density of matrix polymer chains. The increase in the number of embedded fibers surrounded by matrix through the use of FT instead of SFB did not have a significant impact on the IFSS. Contributing to the limited influence of increased fiber dispersion was the increased fragility of the exposed fibers during pullout testing. Specimens with greater separation of exposed fibers were more likely to fail within the fiber prior to reaching a force needed

for interfacial failure. This served to reduce the true IFSS for FT formulations and represents a limitation of the research conducted.

Despite the lack of influence on IFSS, increased dispersion of SFs had a drastic impact on composite tear strength. The use of SFB or any composite designs where there is large areas of cryogel interspersed between the fibers poses a great risk for tear propagation through the matrix. The increase in tear strength using 0.04 v% SFB and maintained at 1.00 v% is likely due to nonlinearity of the embedded fibers and slight fiber entanglement within the matrix. For a perfectly linear and parallel SFB arrangement with 0.5 mm interfiber spacing, the tear strength would be equivalent the tear strength of plain PVA, which is nearly the case with SFB formulations. The use of FT provides increased fiber dispersion within the matrix with significantly reduced mean interfiber matrix volume and greater fiber entanglement. This arrangement of fibers can drastically increase the tear strength over the cryogel tear strength when a sufficient concentration of fibers is used, in this case being between 0.04 and 1.00 v% FT. The correlation between fiber dispersion and tear strength has great implications for the design of fiber-reinforced composites for meniscal replacement since failure of native menisci is typically due to the propagation of tears.

A significant limitation of the work presented is in the experimental set up of both tensile tests and fiber pull-out tests. There is currently no gold standard method to secure soft, hydrated biomaterials to tensile clamps. This is particularly challenging for fiber-reinforced cryogels. For tensile modulus testing, sufficient grip must be maintained on

the embedded fibers to reflect to composite moduli. Conversely, for fiber pullout tests, gripping must be sufficient to secure the cryogel, but not prevent the movement of the embedded fibers. The use of large surface area tensile clamps with adjustable grip strength and sandpaper interfacing the cryogel and smooth clamp surface was shown to improve testing conditions. However, slipping of the samples during testing remained problematic and potentially led to lower modulus and pullout strength values that would be seen with better specimen gripping.

4.5 Conclusion

This work explored the potential for a fiber-reinforced cryogel to serve as a nondegradable meniscal replacement and focused on the UHMWPE fibers' ability to make a PVA cryogel anisotropic with respect to tensile modulus. Furthermore, the improvement of IFSS using a glutaraldehyde linkage was demonstrated. Finally, the benefit of highly dispersed fibers to resist tear propagation was demonstrated.

Chapter 5.0: Synthesize and characterize physically crosslinked, superporous cryogels

5.1 Introduction

For the replacement of tissues in the knee joint, such as articular cartilage or menisci, the mechanical performance must be suitable to withstand the high loads experienced. Of other great importance is the ability for a biomaterial to integrate with the surrounding tissue [19]. The native meniscus is secured in the joint space by multiple attachment sites including fibers connecting the peripheral rim to the joint capsule [2]. Previous hydrogel-based meniscal replacement small and large animal model studies have indicated the importance to recreate these peripheral attachments to minimize implant migration during loading and excessive wear in tibial cartilage [16, 56]. While most biomaterials utilize suturing through the material to surrounding structures, hydrogels are limited by low pullout forces due to their hydrated nature. Even in the case of fiber reinforcement of hydrogels, the interaction between embedded fibers and suture can create local shear forces under joint loading and be a potential source of failure. In addition to direct attachment of the implant to the periphery during implantation, cellular ingrowth *in vivo* has been shown to aid implant integration and viability [66, 67]. The native meniscus is in close contact with the synovial membrane [2]. This membrane serves to provide nutrients to the cartilaginous tissue in addition to being a source of MSCs [68]. Meniscal replacements that support tissue ingrowth have demonstrated improved performance *in vivo* [67].

While natively biologically inert, tissue engineering techniques, utilizing extracellular matrix proteins [21] or encapsulated cells [22, 23], can further mimic native tissues and aid in successful *in vivo* integration. This would be advantageous for tissue engineering approaches using autologous MSCs seeded on a conditioned cryogel *in vivo* to expedite cartilaginous tissue formation and integration *in vivo* [69]. Of utmost importance for cellular infiltration of the biomaterial *in vitro* and *in vivo* is the characteristics of the pore network [70, 71]. While physically crosslinked PVA-based cryogels have inherent porosity, the size of the pore network can limit the migration ability of seeded cells [57]. Cryogels have functional properties that can be tailored through the synthesis parameters employed, providing the developer significant controllability for a range of applications [72]. PVA cryogels can be synthesized through chemical or physical methods [44, 73]. Physical approaches are often preferred over chemical approaches for tissue engineering applications due to their lack of potentially cytotoxic crosslinking agents that can be difficult to remove post-synthesis. PVA-based cryogels can be synthesized through successive freeze-thaw cycling to form a nondegradable scaffold. Superporous cryogels for cartilaginous tissue applications were developed to enhance the degree of porosity and potential for native tissue integration and ultimately successful restoration of joint locomotion. Incorporation of an secondary phase during the synthesis can influence the porous structure and ultimately the function of the cryogel [18]. It is essential to demonstrate that a superporous cryogel does not sacrifice mechanical integrity for the sake of porosity and has compressive load-resisting properties on par with the cartilaginous tissue of interest [60].

For fiber-reinforced composites, the presence of large pores would significantly reduce the stress-transfer capability of the composite. Consequently a superporous cryogel would not be advantageous as the bulk construct for a fiber-reinforced meniscal replacement. Due to the control provided over crosslinking rate by the freeze-thaw process, hydrogels with different properties through alternate synthesis methods can be combined to form two-phase cryogel composites. This would permit the combination of a superporous cryogel peripheral rim to a bulk, fiber-reinforced cryogel.

A liquid-liquid phase separation technique was explored by Spiller et al. for the treatment of articular cartilage focal defects [17]. This early investigation into superporous cryogels utilized a degradable poly (lactic-co-glycolic) (PLAGA) phase incorporated through a double emulsion process resulting in a PVA-PLGA composite solid matrix with PLGA microparticles contained in the pore network for potential drug or chemotactic delivery applications. Through confined compression testing, the aggregate modulus, permeability and time constant demonstrated cryogel behavior on par with cartilaginous tissue. The microspheres can release cell-stimulating growth factors *in vivo* to support cell migration and proliferation. Studies including a degradable phase within porous cryogels have shown a statistically significant impact on cryogel porosity but not always an effect on the functional properties of the cryogel to the same degree [74, 75]. The degradation of the microspheres can leave void areas within the cryogel matrix, thus their presence makes it difficult to directly study the synthesis-structure relationship of PVA superporous cryogels formed through the liquid-liquid phase separation technique and to

isolate the mechanisms by which the material changes in response to external stimuli such as osmotic pressure.

An important feature of cryogels is their ability to swell or deswell in response to the osmotic pressure of their environment. This is critical for knee joint tissue applications, where the intra-articular osmotic pressure can drastically influence the *in vitro* equilibrium water content of cryogels. Traditionally, phosphate buffered saline (PBS) was used for *in vitro* swelling studies for cryogels for cartilaginous tissue applications, which does not impart the expected external pressures on the scaffolds that would be seen *in vivo*. Recent studies investigating the swelling behavior of cryogels have used more appropriate swelling mediums imparting knee joint osmotic pressure [58, 59]. For meniscal replacement, the change in implant volume that can occur in response to the osmotic pressure of the environment can lead to poor scaffold-native tissue interface and ultimately premature implant failure [59]. For a two-phase cryogel system, a large discrepancy in swelling properties may cause interfacial stress and be a potential source of implant failure. Furthermore, the internal pore network generated for *in vivo* cellular migration to promote implant incorporation may be negatively affect by swelling or deswelling behavior imparted by the osmotic pressure. The temporal factor of pore network change versus cellular migration rate would be important in this case. Thus a clear understating of the swelling behavior through *in vitro* swelling studies with appropriate osmotic pressures are needed to provide a context for the synthesis-structure-function relationship of the scaffold and can also be useful in *in vitro* conditioning of cryogels prior to implantation.

This work expands on previous studies that have demonstrated the use of liquid-liquid phase separation synthesis technique to generate an internal pore network via cyclic freezing-thawing cryogel formation [18]. The goal of the work presented is to explore the synthesis-structure-function relationship of fully nondegradable superporous cryogels through characterization of the pore network and the mechanical response to compressive loading. Various solvents- organic or lipid-based- were explored. By evaluating different synthesis parameters and organic solvent types, it is expected to provide insight into the controllability of the synthesis parameters for the development of a superporous cryogel suitable for use as part of a two-phase cryogel meniscal replacement.

5.2 Materials and Methods

5.2.1 Materials

Phosphate buffered saline (PBS), dichloromethane (DCM) and ethyl acetate (EA) were purchased from Sigma Aldrich (St. Louis, MO). Polyethylene glycol (PEG) of molecular weight 20,000 g mol^{-1} was purchased from Crescent Chemical Co (Islandia, NY). Dialysis tubing with molecular weight cut off of 3,500 g mol^{-1} was purchased from Fisher (Pittsburgh, PA).

5.2.2. Superporous Cryogel Synthesis

Cryogels with a porous network were formed through a liquid-liquid phase separation technique modified from previously described methods [17]. Briefly, organic solvents- DCM, EA, Oil, or ESBO- were added at various volume concentrations to PVA in

solution and mixed using an IKA RW 20 digital overhead mixer (Wilmington, NC) at 300 or 1000 rpm for 10 minutes. The emulsion then followed the same cryogel synthesis procedure described in Aim 1. ESBO was mixed with and without the presence of an acid catalyst used to create a covalent linkage between ESBO and some PVA hydroxyl groups utilizing an epoxide ring-opening reaction.

5.2.3 Osmotic Conditioning

Menisci are subjected to an osmotic pressure of approximately 0.95 atm. To assess the influence of the *in vivo* environment on cryogels for cartilaginous tissue replacement applications, an *in vitro* swelling study was performed in a fashion similar to previous studies [59]. Briefly, PEG was dissolved in a PBS solution to generate a solution with osmotic pressure of 0.95 atm. The amount of PEG needed was approximately 92.3 g per L of PBS as determined from the following equation for osmotic pressure, $\prod$:

$$\prod = RT\left(\frac{c_2}{M_2} + Bc_2^2 + Cc_2^2 + \cdots\right)$$

where R is the universal gas constant, T is the absolute temperature and M_2 is the polymer molecular weight. B and C are the second and third viral coefficients for 20,000 g mol^{-1} PEG, which is 2.59 $\times$ 10^{-3} and 13.50 $\times$ 10^{-3} respectively [76]. Crosslinked cryogels were placed in a dialysis membrane and secured at both ends with clips to ensure no PEG adsorption onto the cryogel. The dialysis tubing containing cryogels was placed in the 0.95 atm PEG solution in a temperature-controlled water bath set to 37 ^{o}C. The volume of PEG solution was 100 times that of the total volume of submerged

cryogels to prevent alteration of the osmotic pressure from the flux of fluid into or out of the cryogels. Cryogels not subjected to osmotic conditioning served as controls for the effect of osmotic pressure on cryogels with respect to fluid content, compressive modulus and porous microstructure. Cryogels were assessed between 1 and 28-day time points.

5.2.4 Swelling Behavior

The fluid content of crosslinked cryogels before and after osmotic conditioning was determined through multiple weight measurements. At the pre-determined osmotic conditioning time points, cryogels were weighed then dried in an oven at 90 ^{o}C and re-weighed to determine the fluid content, FC, as calculated from the following equation:

$$FC = \frac{W_w - W_D}{W_w} \times 100$$

where W_w is hydrated cryogel mass and W_D is the dried cryogel mass. FC is an equivalent parameter to swelling ratio, which is commonly reported for hydrogels.

5.2.5 Mechanical Testing

Mechanical performance was determined through unconfined compressive loading in the same fashion as described in Aim 1 [65]. Cylindrical cryogel specimens ($n = 4$) were subjected to a 0.1 N preload and compressed at 100 % min^{-1} to 50% strain. The compressive modulus was determined from the slope of the initial linear region of the stress-strain curve taken as 10 to 16% strain for organic solvent formulations for better comparison with published data.

5.2.5 Microstructure

The average pore diameter of cryogels after osmotic conditioning was determined from environmental scanning electron microscopy (ESEM) use a FEI/Phillips XL30 (Hillsboro, OR) or optical microscope images using a Zeiss Pascal 510 Confocal Imaging System (Oberkochen, Germany). Cross-sections for optical images were made through sectioning the bulk cryogel with a Vibratome Ultra Pro 5000 cryostat producing 20 μm sections. Optical images were Environmental mode using ESEM, as opposed to traditional high vacuum mode, allows the cryogel to be imaged in its native hydrated state without the use of metal coating [17].

Images were taken at seven locations on the cross-section of the cryogel ($n = 7$) and the mean pore diameter (MPD) was determined using the US National Institutes of Health ImageJ software [77]. The same images were used to estimate overall cryogel porosity. The porosity was calculated from the ratio of the total porous area to the total surface area imaged.

5.2.6 Statistical Analysis

One way analysis of variance (ANOVA) tests were conducted at a 95% confidence interval using GraphPad Prism software. Tukey's multiple comparisons test at a 5% error rate was performed to compare multiple groups simultaneously when differences were found through ANOVA. In all figures, error bars represent ±1 SD and statistical significance is defined as $p<.05$. A significant change with respect to swelling time point or solvent volume from the previous value is denoted by #. A statistically significant

difference between multiple formulations at a specific swelling time point or solvent volume is denoted by *.

5.3 Results

Through the liquid-liquid phase separation cryogel synthesis technique, a porous network is able to be formed throughout the cryogel that is dependent on the synthesis parameters. Of these parameters, the organic solvent concentration is of particular interest. For musculoskeletal replacement or repair applications it is of great importance to determine how the concentration of solvent used during the synthesis affects the crosslinked cryogel mechanical performance. Initial superporous cryogel studies utilized organic solvents- DCM and EA- in the liquid-liquid phase separation to better compare with established literature. The formulations chosen for initial studies use a range of DCM or EA volume to establish the impact of solvent volume on structure and functional properties.

Table 5.1: Synthesis parameters for organic solvent formulations evaluated

Porogen Type	Porogen v%	PVA w%	Mix Speed [rpm]
EA	10	10	1000
EA	25	10	1000
DCM	10	10	1000
DCM	25	10	1000

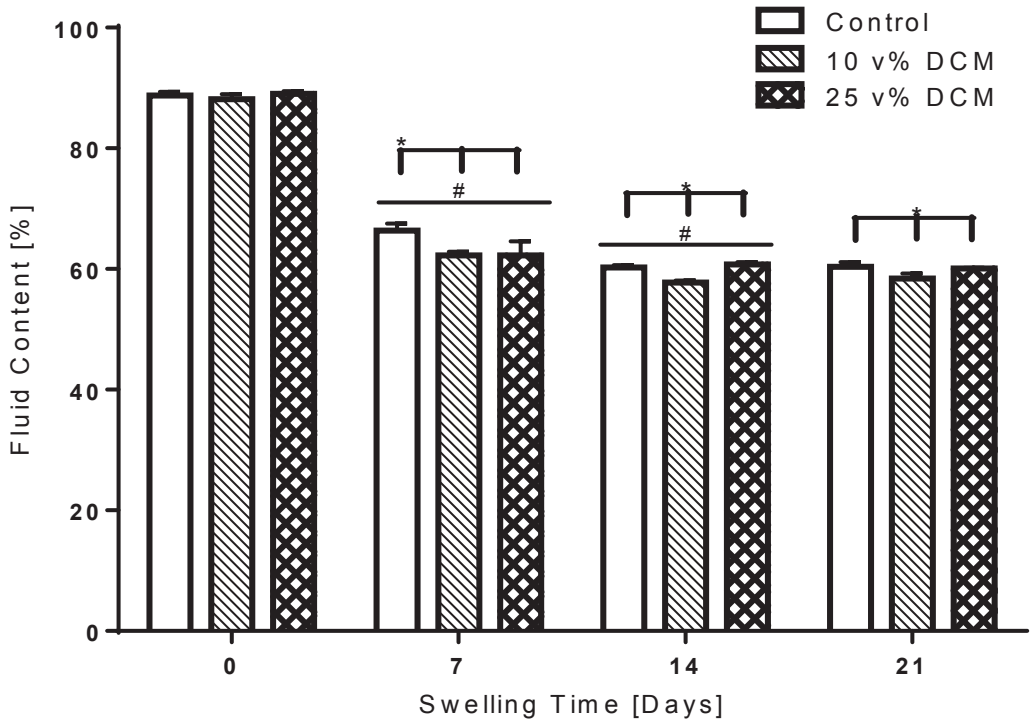

Figure 5.1: FC versus swelling time for 0 (control), 10 and 25 v% DCM formulations.

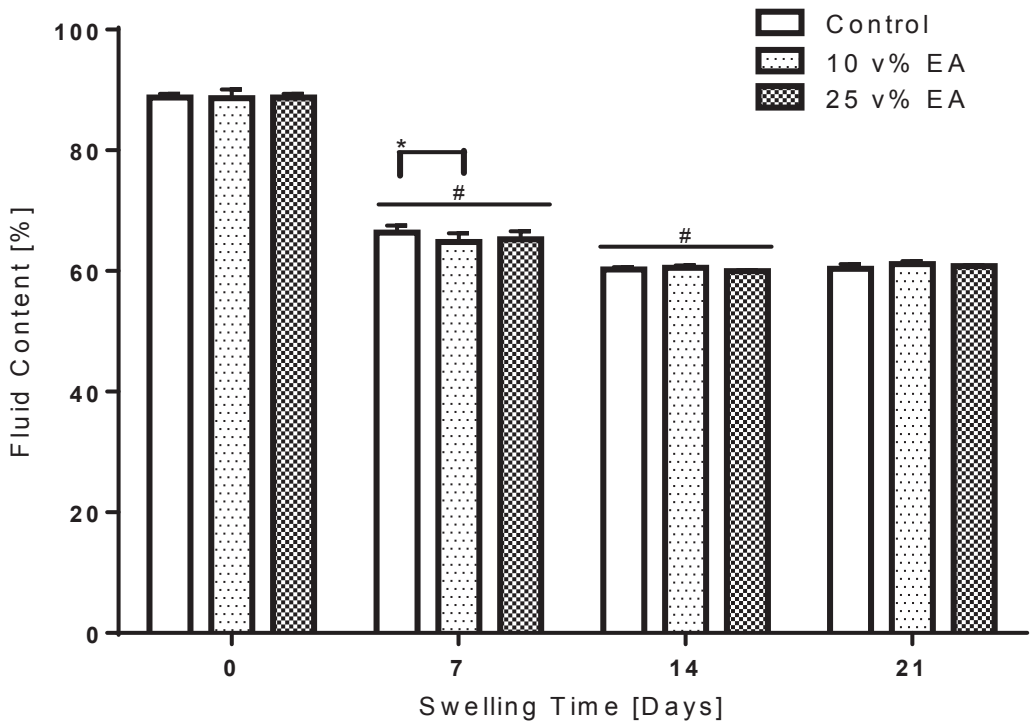

Figure 5.2: FC versus swelling time for 0 (control), 10 and 25 v% EA formulations.

As shown in Figures 5.1 and 5.2, the osmotic pressure results in a change in amount of liquid present in the cryogel. The liquid consists of water and any retained organic solvent not evaporated during synthesis. Cryogel controls synthesized without the presence of DCM as shown in Figure 5.1, exhibit a 25% loss of the liquid phase after seven days of osmotic conditioning. A further statistically significant reduction of the liquid phase is seen at 14 days, which then remains constant up to 21 days. After seven days of osmotic conditioning, the liquid content in DCM-synthesized cryogels exhibits the same trend as controls, with liquid phase content decreasing throughout the 14 days of swelling then remaining consistent from 14 to 21 days. At the 7-day time point there is a greater loss of fluid from the DCM-synthesized cryogels compared to the control.

There continues to be greater loss in fluid for 10 v% DCM cryogels at 14 and 21-day time points compared to controls but 25 v% DCM cryogels resulted in fluid content levels on par with controls at 14 and 21 days. The same effect of osmotic pressure on fluid loss with respect to swelling time of EA-synthesized cryogels is shown in Figure 5.2, where both 10 and 25 v% EA cryogels exhibit a reduction in liquid content up to 14 days. Unlike DCM cryogels, the only difference in fluid content when comparing the three formulations at each time point was seen between the control and 10 v% EA at seven days of swelling.

The pore microstructure studies were conducted using EA due to poor controllability with DCM synthesized cryogels. It was observed that DCM cryogels had macroscopic void areas at the bottom of the crosslinked cryogels, which was not seen in EA synthesized cryogels. This is likely due to the higher density of DCM compared to EA causing settling of DCM prior to freezing temperatures being reached during the freeze-thaw process. While this settling behavior may not have impacted *in vitro* analysis of the cryogel, its potential for pore sample uniformity and reproducibility is a concern for future *in vivo* studies. Consequently, EA was selected for further testing.

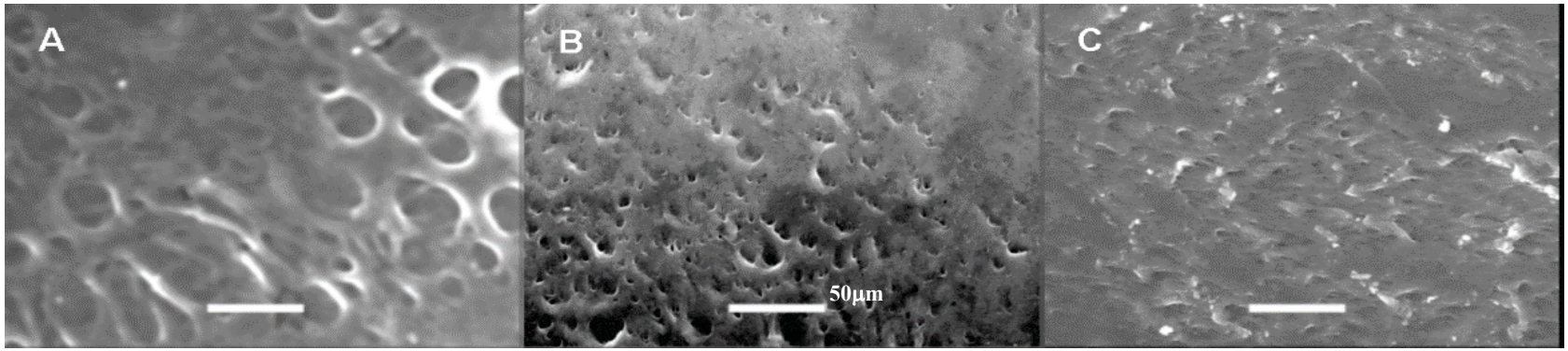

Figure 5.3: ESEM micrographs displaying influence of swelling time on porosity. (A) 25 v% EA at 0-week swelling. (B) 25 v% EA at 2-week swelling. (C) 25 v% EA at 4-week swelling.

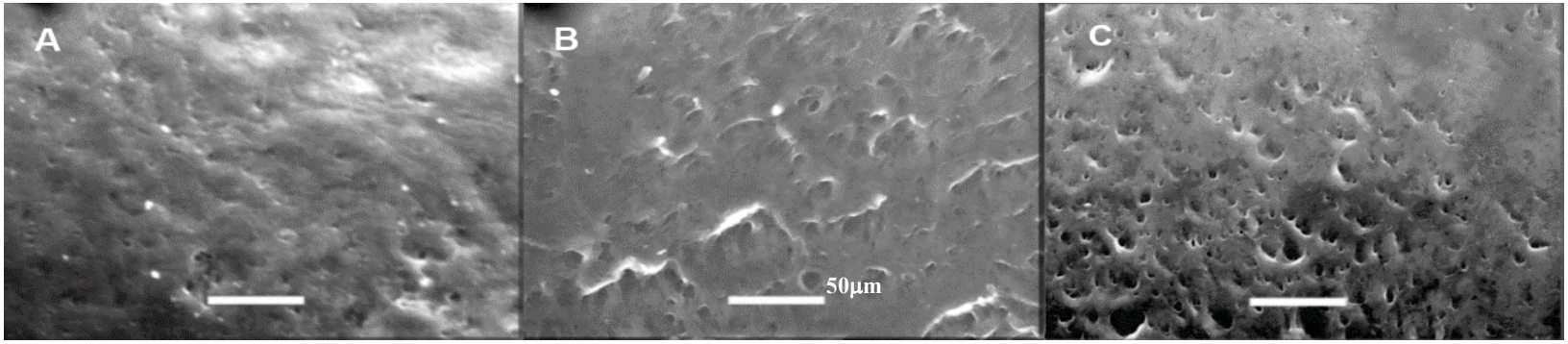

Figure 5.4: ESEM micrographs displaying influence of solvent volume on porosity after osmotic conditioning. (A) 0 v% EA at 2-week swelling. (B) 10 v% EA at 2-week swelling. (C) 25 v% EA at 2-week swelling.

The % porosity is determined from the ESEM micrographs using ImageJ to calculate the void surface area versus the total imaged area. Figures 5.3 and 5.4 shows representative ESEM images highlighting the change in pore network due to swelling time and solvent volume, respectively. The mixing of DCM or EA within the PVA solution creates interspersed spherical organic solvent droplets. Freezing temperature-induced PVA chain crosslinking is prohibited where the organic solvent droplets are present. This liquid-liquid phase separation yields a porous network that is highly dependent on the synthesis parameters. In figure 5.3, it is seen qualitatively that the pore size decreases over the 4-week period while the overall porosity is relatively consistent. Focusing on the 2-week time point in Figure 5.4, the addition of EA increases both the overall porosity and pore size over the control samples. However, the solvent volume (10 and 25 v%) has a proportional influence on porosity but minimal impact on pore diameter. This qualitative trend observed through ESEM was consistent at each swelling time point.

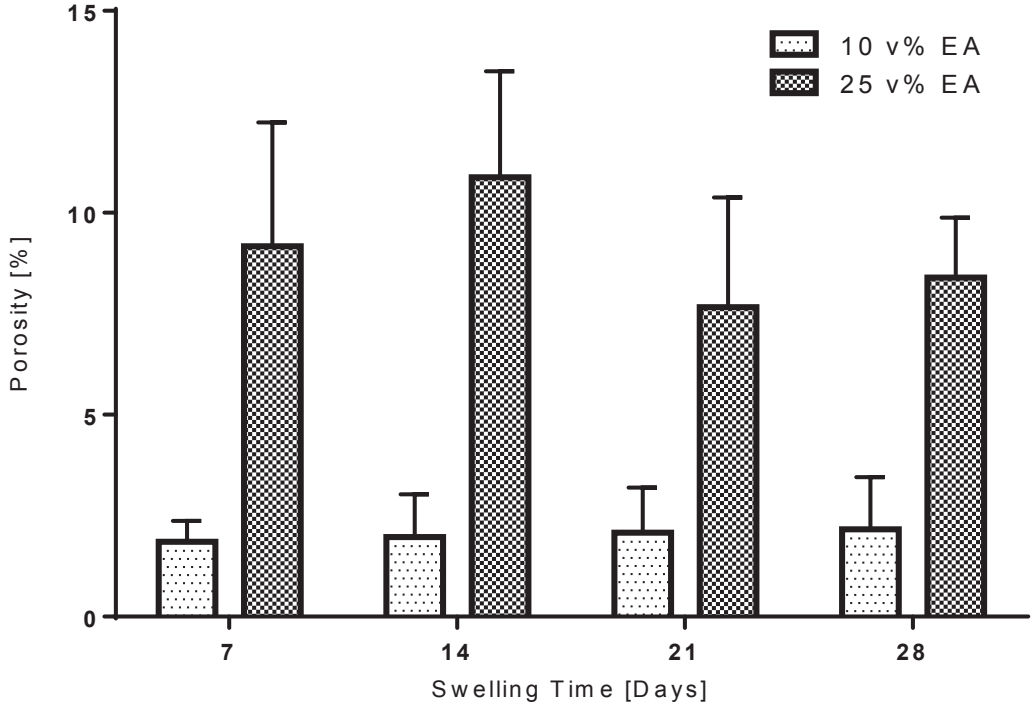

Figure 5.5: Porosity versus swelling time for 10 EA and 25 v% EA formulations.

Figure 5.5 highlights the impact of solvent volume on the porosity over 28 days of swelling. At both EA concentrations the porosity remains consistent throughout the swelling study. A clear effect of solvent concentration is seen at each time point, where the larger EA concentration yields significantly larger void volume.

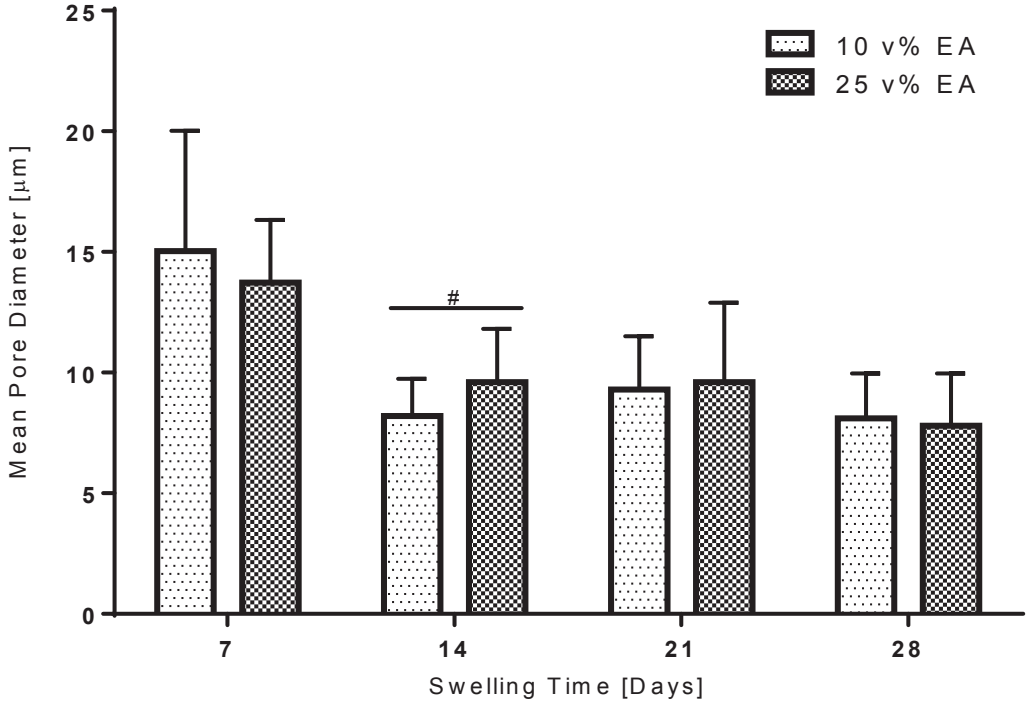

Figure 5.6: MPD versus swelling time for 10 and 25 v% EA formulations.

After seven days of swelling, the MPD ranged from 10.4 to 25.7 μm, with an average of 15.0 μm for 10 v% EA. At day seven, the higher EA content of 25 v%, yielded a statistically equivalent MPD to 10 v%, having a range of 10.0 to 18.3 and mean of 13.7 μm (Figure 5.6). Further significant decrease in MPD was seen at day 14, with 10 and 25 v% EA displaying 8.2 and 9.6 μm mean diameter respectively. From day 14 to day 28 there is no significant change in MPD for either formulation. At each time point, there is overlap of the MPD range for both formulations, supporting the lack of statistical significance in the different diameters.

Due to the large impact of swelling pressure on porosity of EA cryogels, alternative components for the liquid-liquid phase separation were explored. Oil and ESBO was evaluated as lipid-based porogens and were expected to have greater phase separation and improve the porosity. Furthermore, the presence of epoxides on ESBO are potentially capable reacting with free hydroxyl groups on PVA under the presence of an acid catalyst and increase the stability of the dispersed phase during freeze-thawing. Formulations were selected for swelling study based on preliminary porosity and compression testing results. Due to emulsion viscosity, phase separation and phase inversion not all PVA w%- Porogen v% combinations produced stable cryogels (Table 5.2).

Table 5.2: Lipid-based porogens formulations attempted for cryogel synthesis.

Porogen Type	Porogen v%	PVA w%	Mixing Speed [rpm]	Stable and Uniform Cryogel?	Adequate Porosity and Modulus?
Oil	10	10	300	Y	Y
Oil	10	10	1000	Y	Y
Oil	25	10	300	Y	Y
Oil	25	10	1000	Y	Y
Oil	10	20	300	Y	N
Oil	10	20	1000	N	-
Oil	25	20	300	Y	N
Oil	25	20	1000	N	-
Oil	10	30	300	N	-
Oil	25	30	300	N	-
Oil	25	30	1000	N	-
ESBOc	10	10	300	Y	Y
ESBOc	10	10	1000	Y	Y
ESBOc	25	10	300	Y	Y
ESBOc	25	10	1000	Y	Y
ESBOr	10	10	300	Y	Y
ESBOr	10	10	1000	Y	Y
ESBOr	25	10	300	Y	Y
ESBOr	25	10	1000	N	-
ESBOr	10	20	300	Y	Y
ESBOr	10	20	1000	N	-
ESBOr	25	20	300	Y	N
ESBOr	25	20	1000	N	-
ESBOr	10	30	300	N	-
ESBOr	25	30	300	N	-

Porosity analysis and compressive moduli values were used to select from stable formulations for further testing. The benefit of lipid-based porogens was contrasted to control formulations that represent PVA mixed without added porogens with respect to porosity. Figure 5.7 demonstrates the effect of PVA w% and mixing speed on the cryogel pore network.

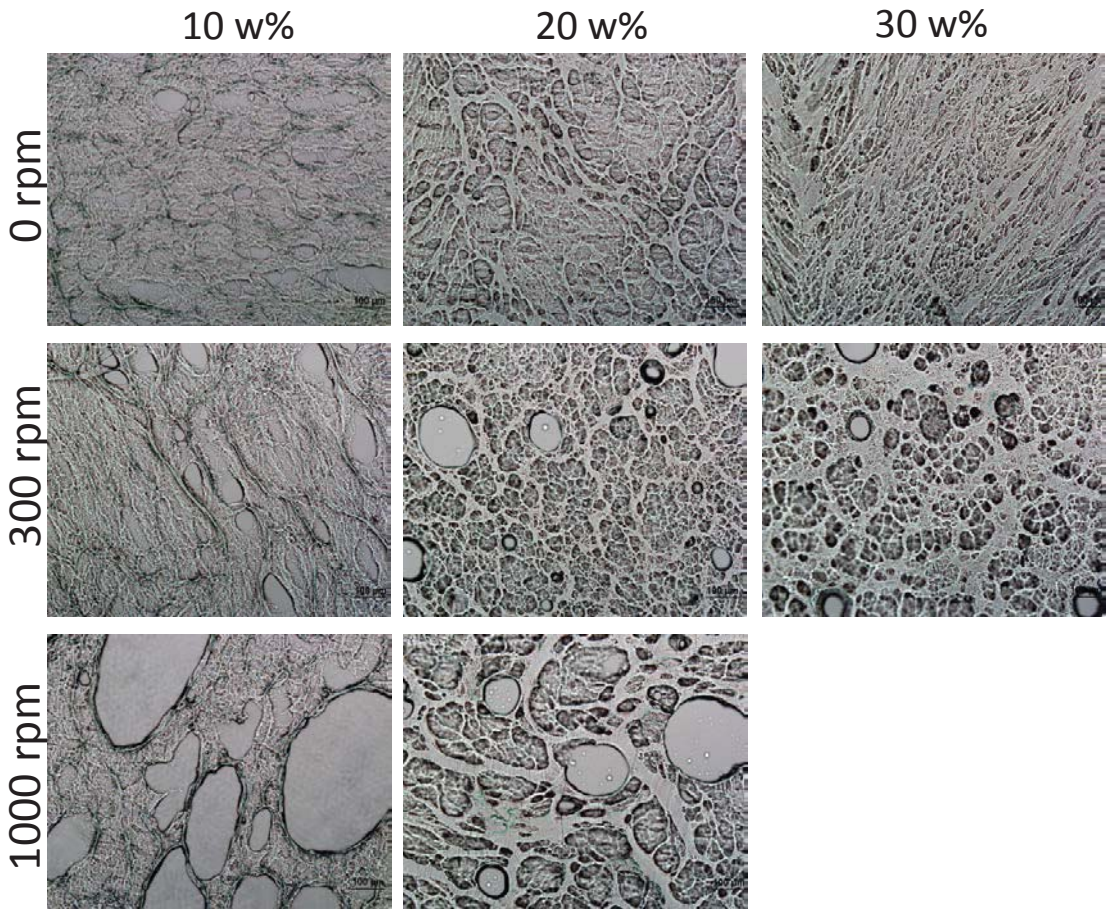

Figure 5.7: 0 v% porogen PVA cryogel porosity with respect to PVA w% and mixing speed.

The innate porosity of PVA cryogels is evident from the 0 rpm cryogel images. Increasing PVA w% leads to thicker polymer septum separate isolated pores and less dense polymer regions. Through mixing, air is entrapped within the polymer, with the degree of entrapment proportional to the viscosity of the polymer. This leads to small, highly distributed pores by low speed mixing and large pores from high speed mixing. The change in pore network when oil is used as a porogens is shown in Figure 5.8

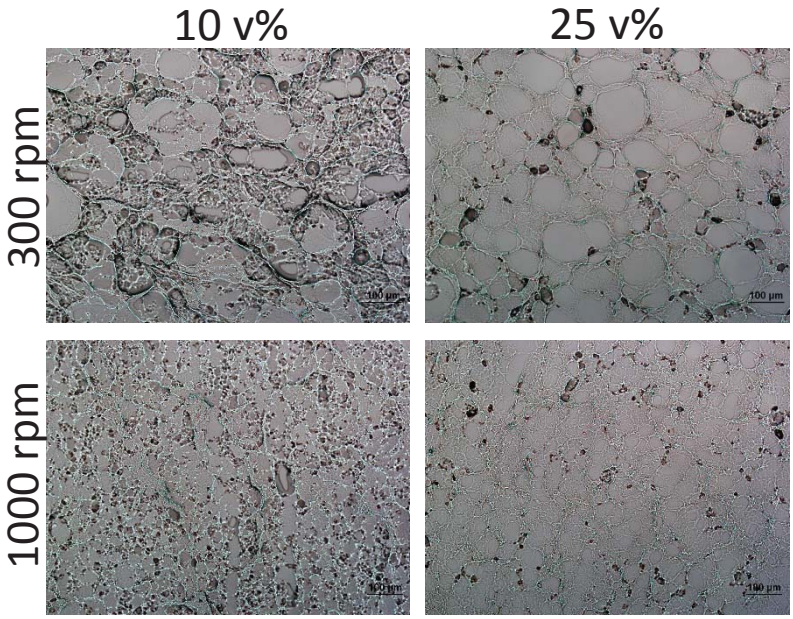

Figure 5.8: Oil in 10 w% PVA porosity with respect to oil v% and mixing speed.

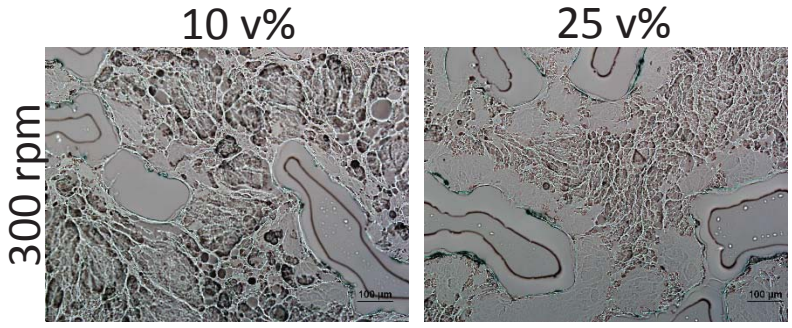

Figure 5.9: Oil in 20 w% PVA porosity with respect to oil v% and mixing speed.

Figure 5.8 and 5.9 shows the porosity obtained from oil porogens in 10 and 20 w% PVA respectively. Due to the low viscosity of 10 w% PVA both the continuous phase (PVA) and the dilute phase (oil) are well mixed resulting in a well distributed pore network. The effect of mixing speed is evident at both v%, where there is a decrease in average pore size with increased mixing speed. There is a decrease in the thickness of the polymer septum with increased v% and increased mixing speed. With 20 w% PVA large polymer septums are present, interspersed with islands of oil. In Figure 5.10, it is seen that there is a significant decrease in modulus at 10 v% when the mixing speed is increased. However this affect is not seen at 25 v% oil.

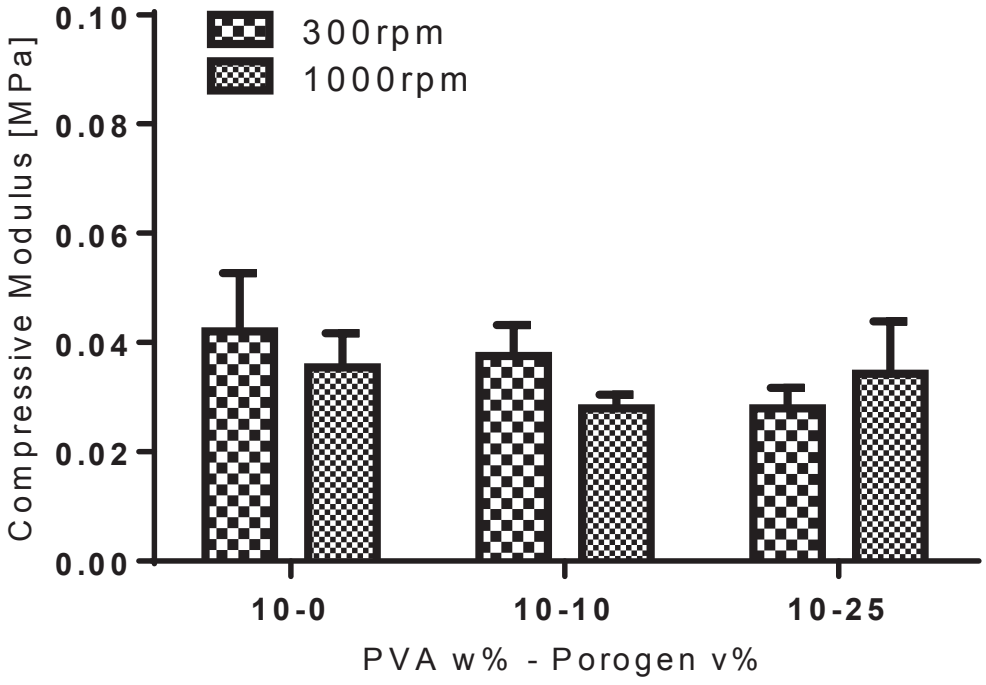

Figure 5.10: Compressive moduli of cryogels at various oil v% and mixing speeds.

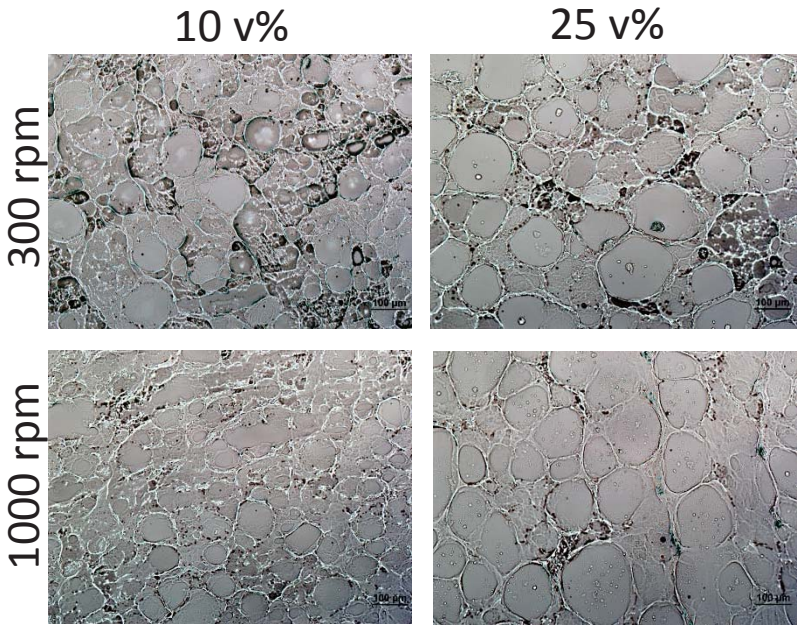

Figure 5.11: ESBOc in 10 w% PVA porosity with respect to ESBOc v% and mixing speed.

Figure 5.11 shows the porosity obtained from ESBOc porogens in 10 w% PVA. Due to the low viscosity of 10 w% PVA both the continuous phase (PVA) and the dilute phase (oil) are well mixed resulting in a well distributed pore network. There is minimal effect of mixing speed evident at both v%, where there average pore size is similar at low and high mixing speeds. Increasing the ESBOc volume at a constant mixing speed leads to slightly larger pore diameter. Figure 5.12 shows that ESBOc produces statistically equivalent moduli for each formulation tested.

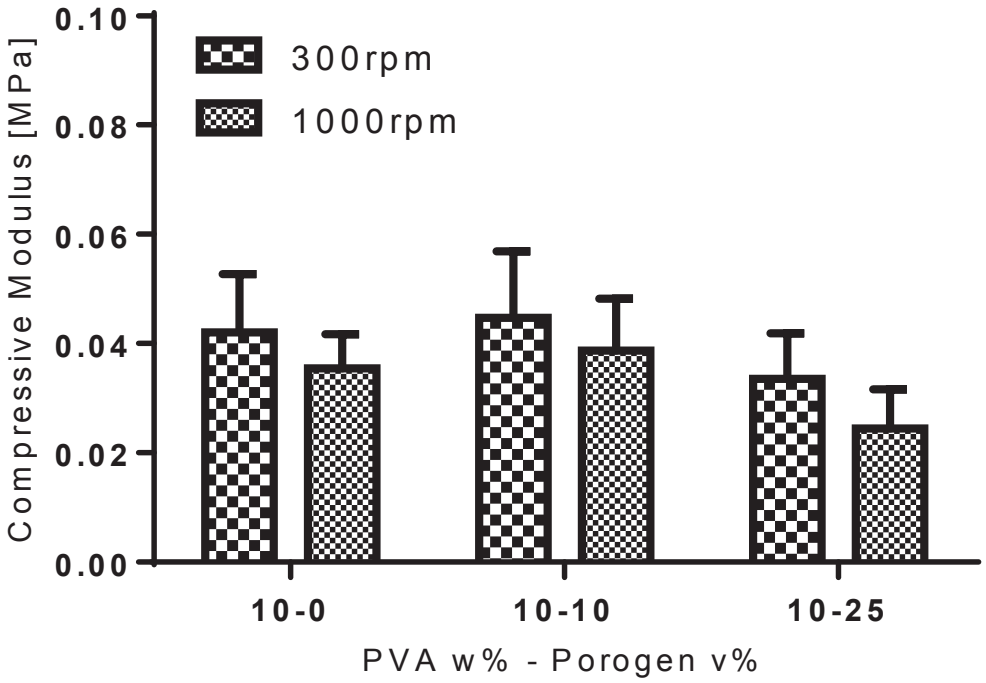

Figure 5.12: Compressive moduli of cryogels at various ESBOc v% and mixing speeds.

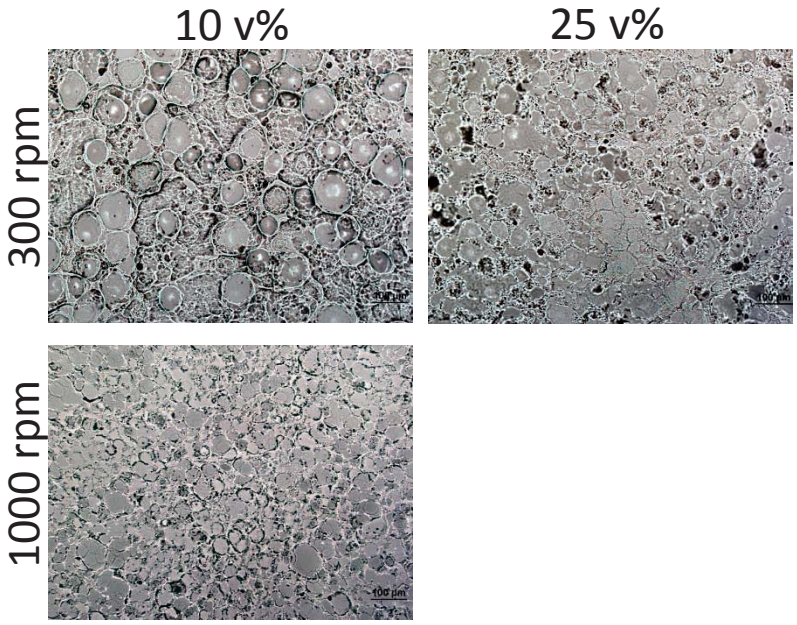

Figure 5.13: ESBO reacted in 10 w% PVA porosity with respect to v% and mixing speed.

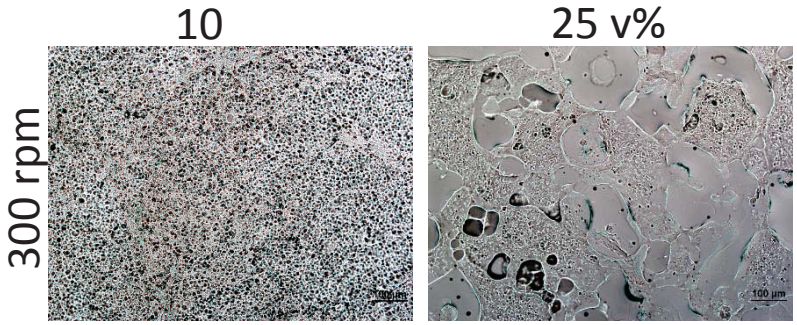

Figure 5.14: ESBOr in 20 w% PVA porosity with respect to ESBOr v% and mixing speed.

Figure 5.13 and 5.14 shows the porosity obtained from ESBOr porogens in 10 and 20 w% PVA respectively. Low v% and low mixing speed produces a highly variable pore diameter network with thick PVA septum. Increasing either the mixing speed or the ESBOr volume drastically decreases the average pore diameter and increases the pore uniformity while decreasing the thickness of the PVA septum. With 20 w% PVA two very distinct pore morphologies are formed. With low v%, a highly uniform, small diameter pore network is obtained. Increasing the volume leads to thick PVA septum with islands of ESBOr. Figure 5.15 shows that increasing the solvent volume at 10 w% PVA significantly reduces the moduli, while no effect is seen from changing the mixing speed. At 20 w% PVA, the low v% ESBOr is on par with the control moduli, while high v% ESBOr has a significantly reduced moduli.

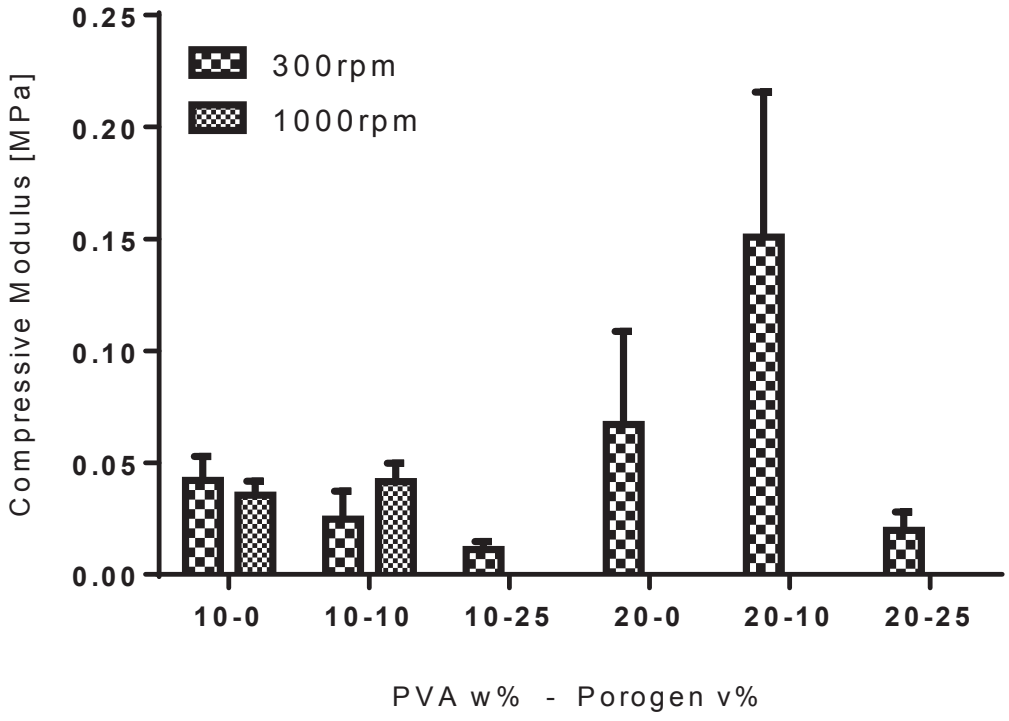

Figure 5.15: Compressive moduli of cryogels at various ESBOr v% and mixing speeds.

Of the stable cryogel formulations synthesized, those cryogels with porosity with adequate potential for cellular ingrowth were considered for further testing. Six formulations were selected for their potential for *in vivo* success and for the range in structural and functional properties they represent. The formulations selected are listed in Table 5.3 and the swelling ratio, compressive modulus and pore network was determined for each formulation over 14 days of swelling as shown in Figures 5.16 to 5.30.

Table 5.3: Variation in solvent types, solvent volume, and PVA w% and mixing speed.

Porogen Type	Porogen v%	PVA w%	Mix Speed [rpm]
Oil	25	10	300
Oil	25	10	1000
ESBOc	10	10	1000
ESBOr	10	10	300
ESBOr	10	10	1000
ESBOr	10	20	300

Figures 5.16 through 5.30 show the swelling ratio, compressive modulus and porosity at 0 day and 14 day swelling for i) control formulations, ii) oil based formulation, iii) ESBO reacted and non-reacted formulations and iv) low and high concentration PVA formulations.

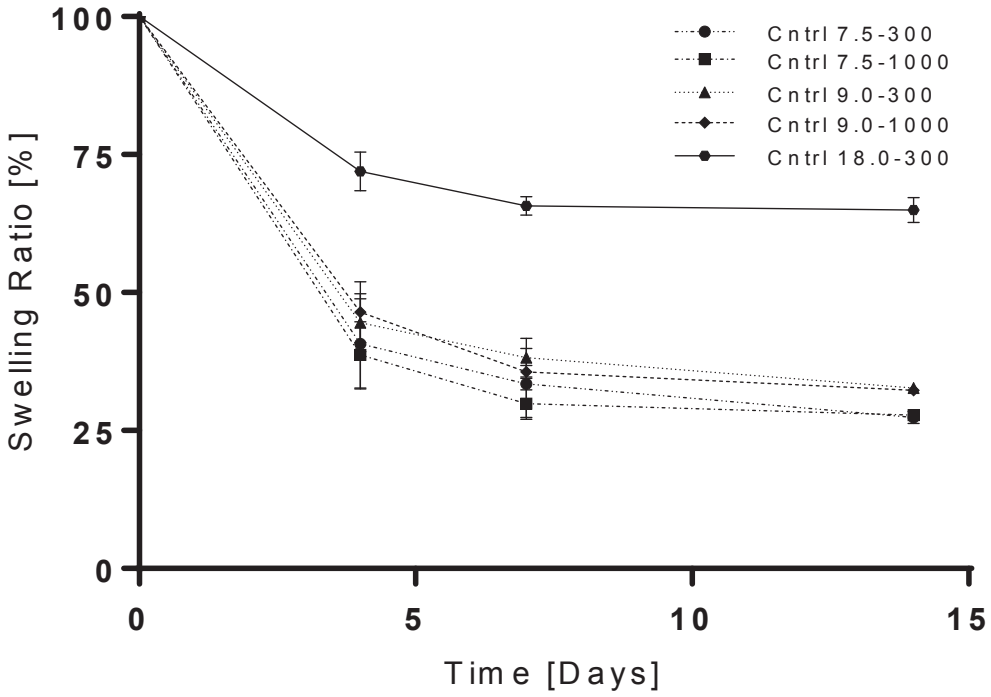

Figure 5.16: Control formulations swelling ratio versus swelling time. The legend indicates PVA w%-mixing speed

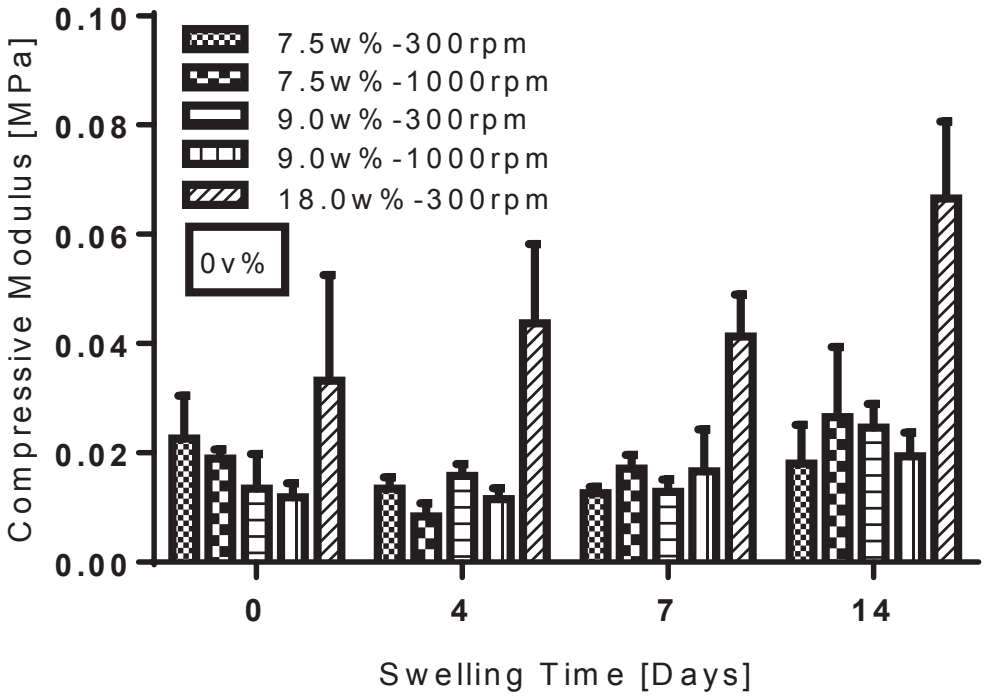

Figure 5.17: Control formulations modulus versus swelling time. The legend indicates PVA w%-mixing speed. Porogen volume is indicated in the box.

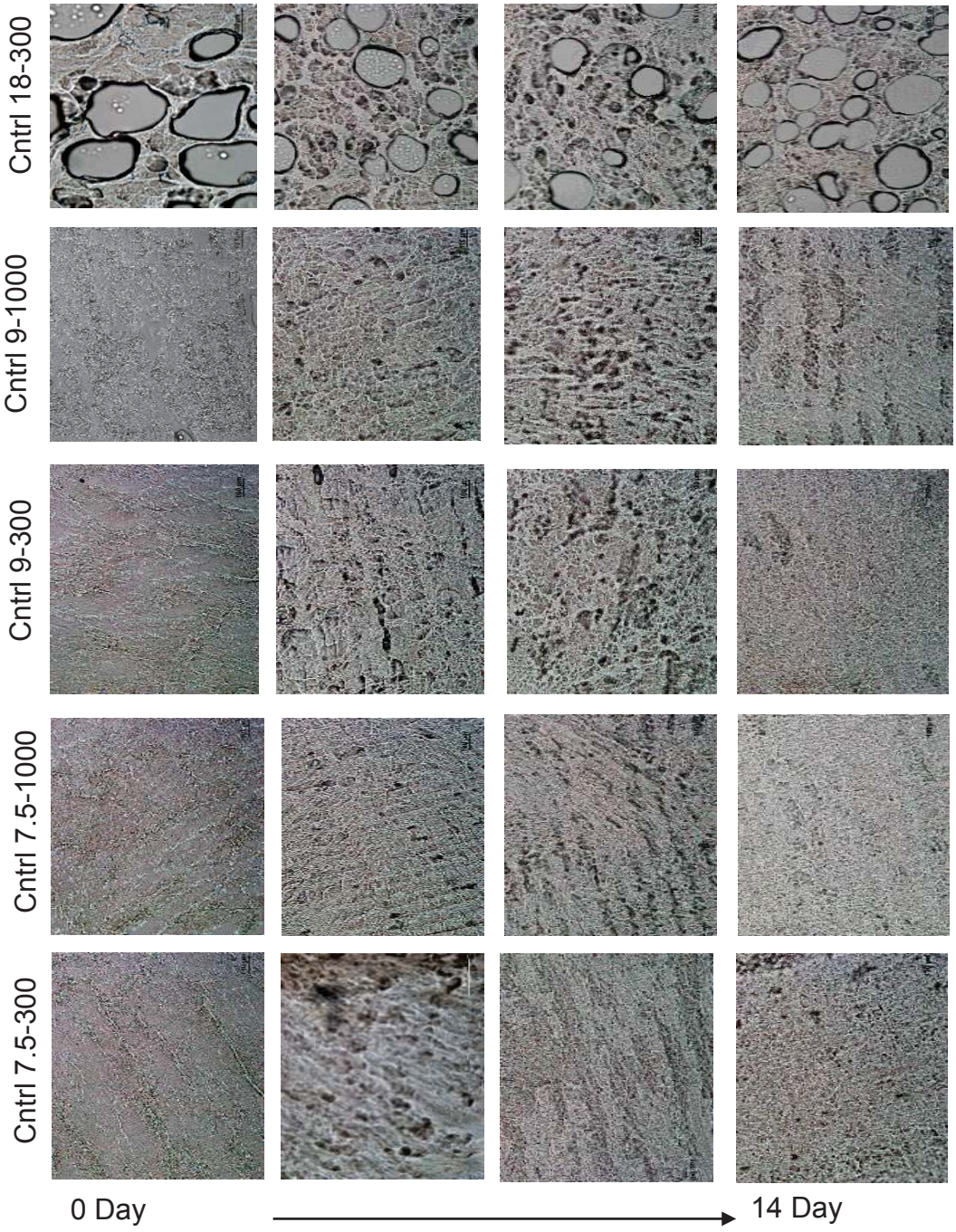

Figure 5.18: Control formulations pore structure versus swelling time. The rows are labeled as PVA w%-mixing speed rpm.

Figures 5.16-5.18 includes the swelling ratio, compressive modulus and pore microstructure for control formulations. These controls were selected to match the actual PVA content cryogel formulations factoring in both initial polymer concentration and solvent concentration. 18 w% PVA performed best in regards to modulus and minimal deswelling. It was also the only formulation to have large, interspersed pores. However, these pores are also separated by thick PVA septum and do not appear to have significant interconnectivity. Lower PVA concentrations have a more fibrous topography with irregularly shaped pores. The pore network for each concentration remains fairly constant over 14 days of swelling despite the significant deswelling over the sample evident by the decrease in swelling ratio.

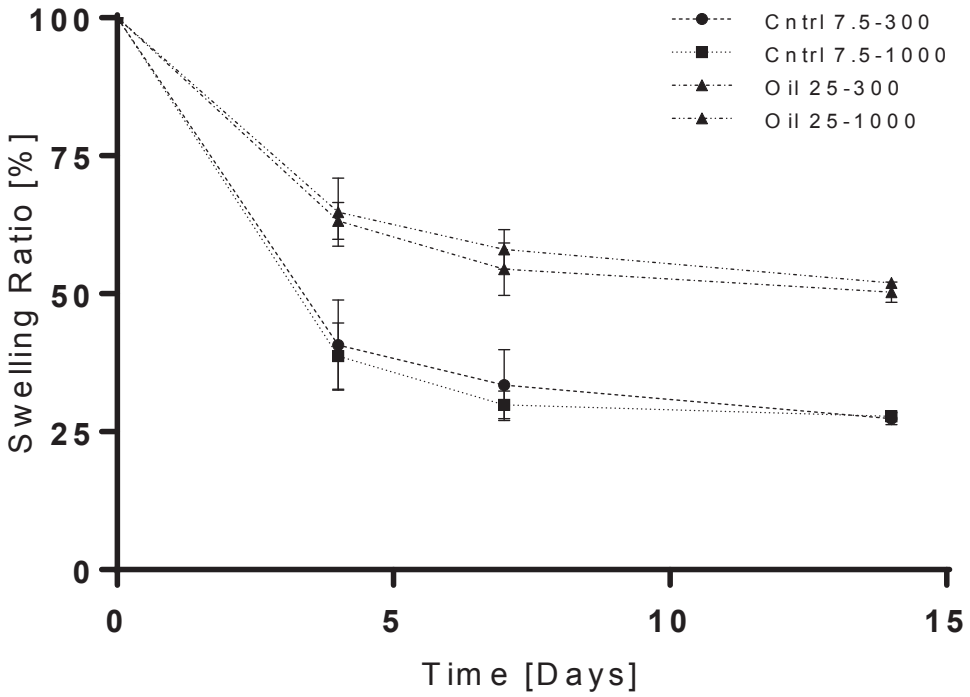

Figure 5.19: Oil at high and low mixing speed swelling ratio versus swelling time. The legend indicates porogen v%-mixing speed.

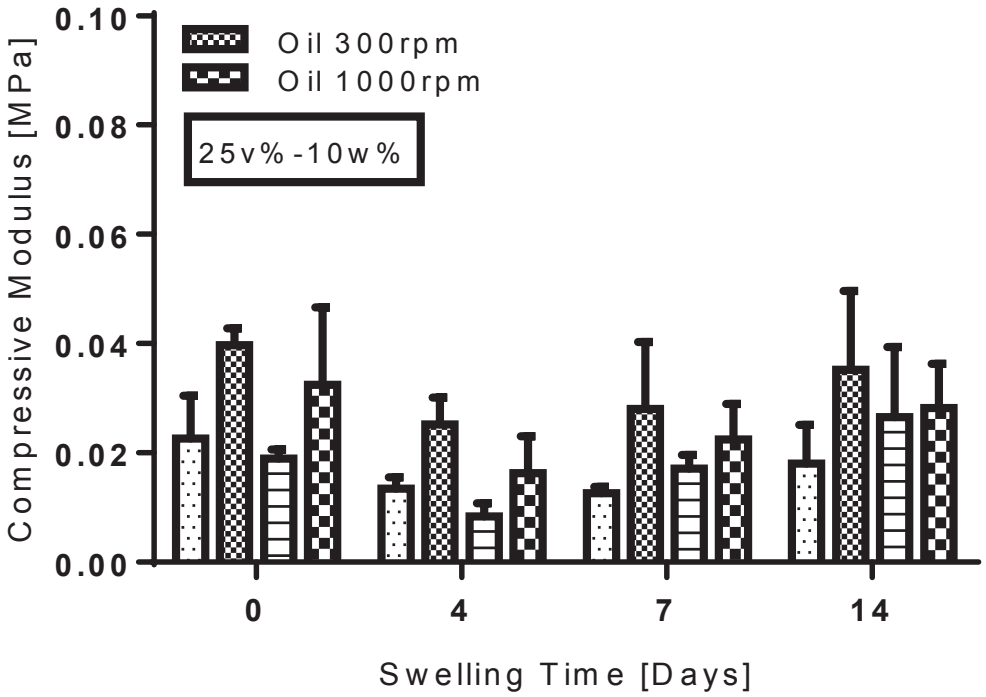

Figure 5.20: Oil at high and low mixing speed modulus versus swelling time. The legend indicates porogen mixing speed. Porogen volume and PVA w% is indicated in the box.

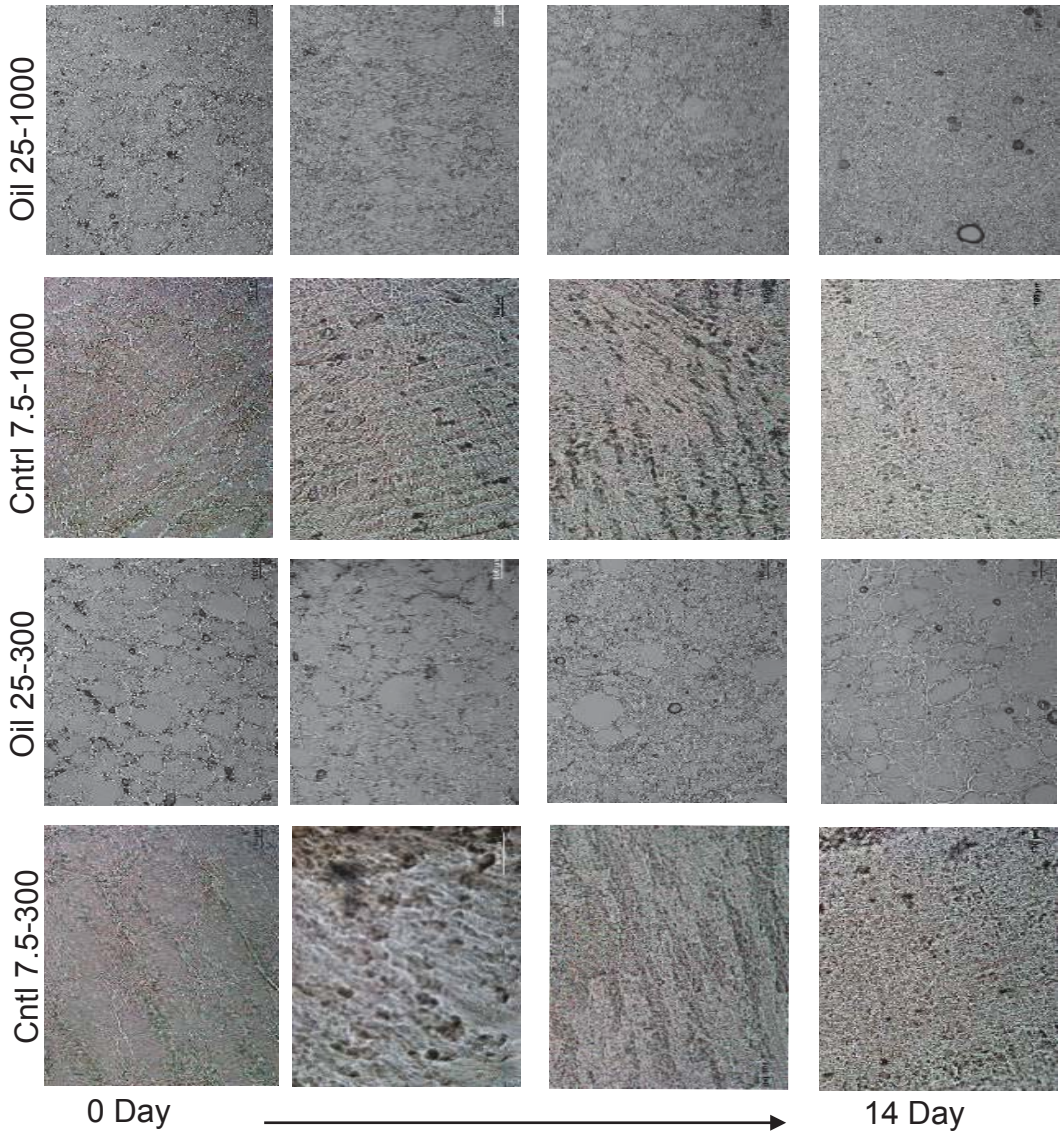

Figure 5.21: Oil at high and low mixing speed pore structure versus swelling time.

Figures 5.19-5.21 show the swelling ratio, compressive modulus and pore network throughout 14 days of swelling. Oil–synthesized cryogels show a slight protective effect with respect to fluid loss. This effect is independent of mixing speed. Fluid loss remains consistent between seven and 14 days. Despite the fluid loss there is no significant change in modulus for either formulation over 14 days. The pore networks remain visibly consistent over 14 days.

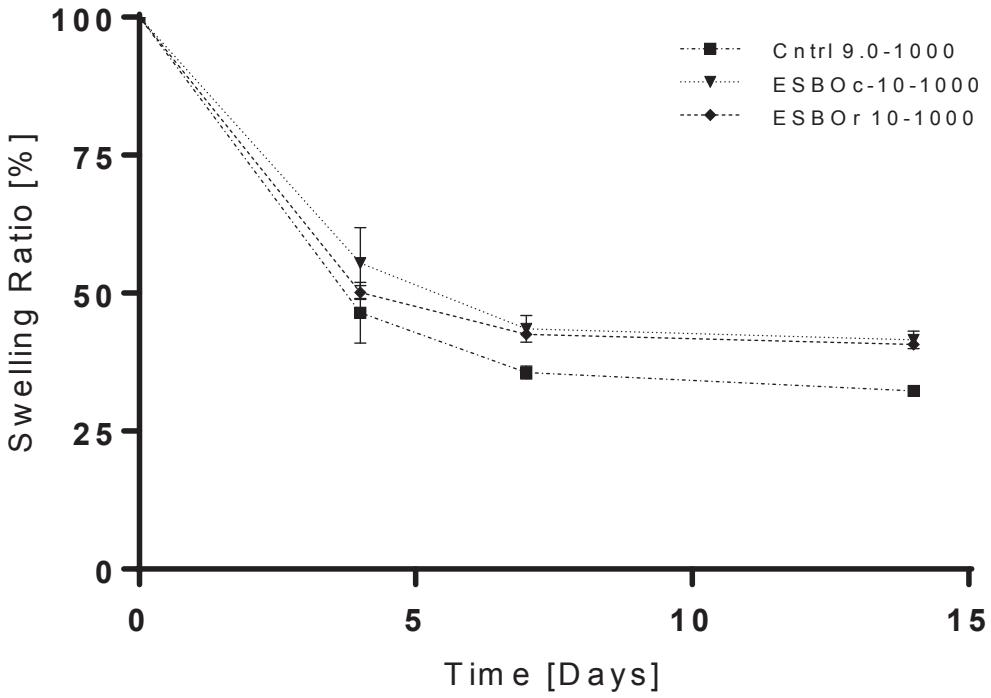

Figure 5.22: ESBO reacted and unreacted swelling ratio versus swelling time. The legend indicates porogen v%-mixing speed.

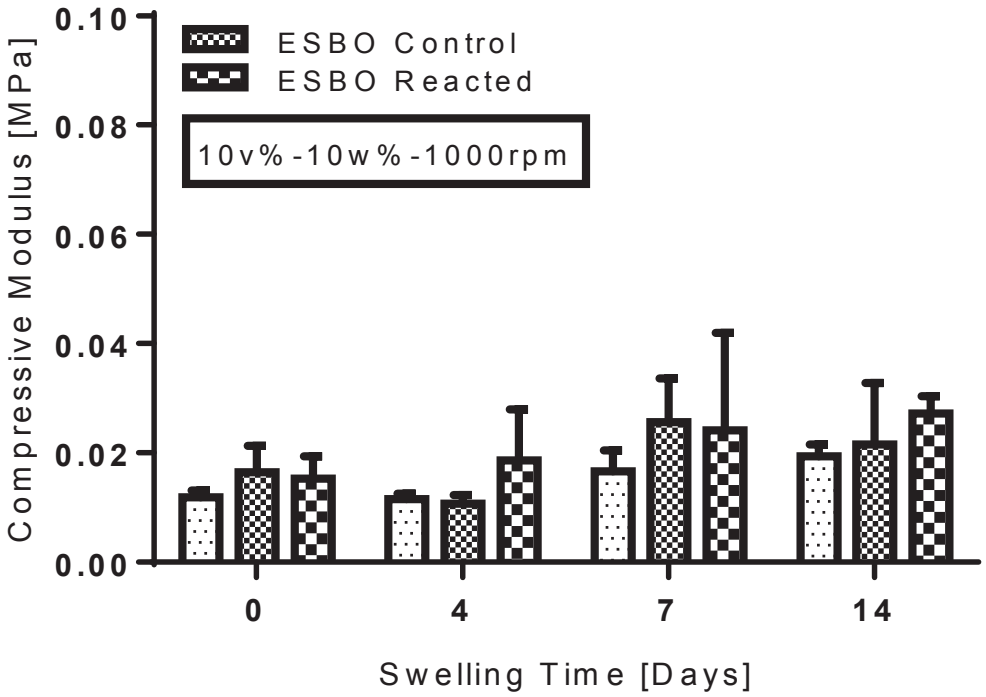

Figure 5.23: ESBO reacted and unreacted modulus versus swelling time. The legend indicates reaction conditions. Porogen v%-PVA w% and mixing speed is indicated in the box.

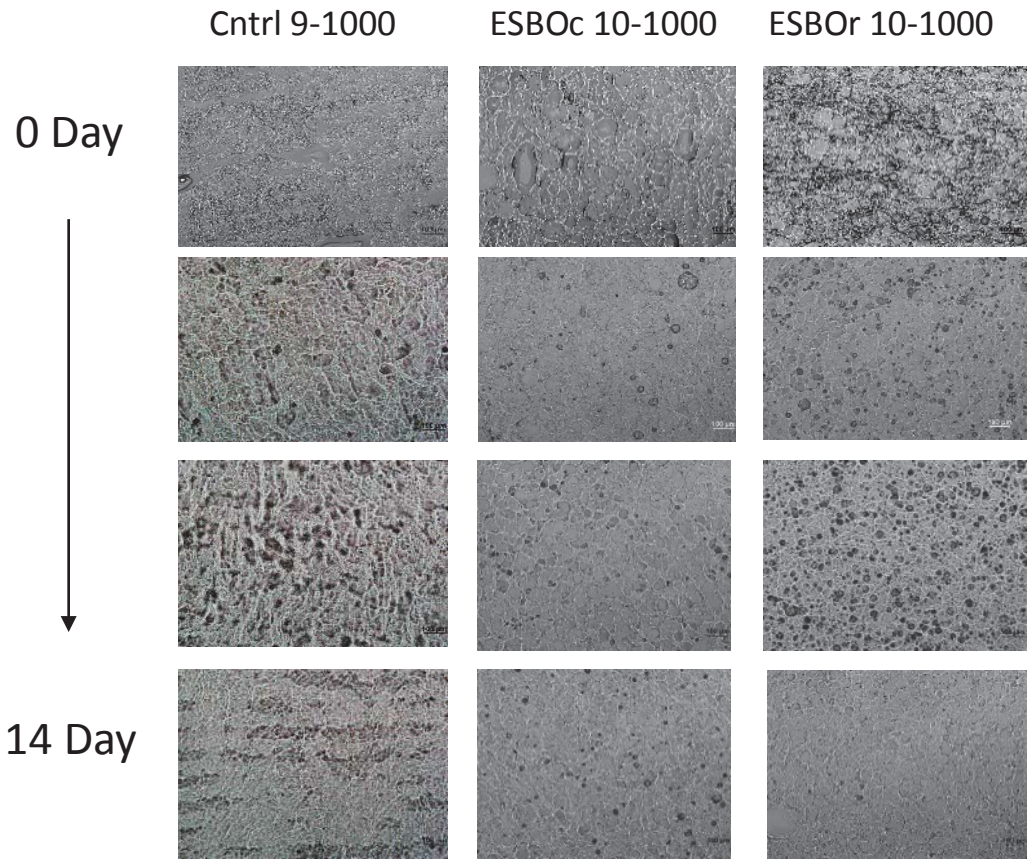

Figure 5.24: ESBO reacted and unreacted pore network versus swelling time. The columns indicate porogen v%-mixing speed.

Figures 5.22-5.24 show the swelling ratio, compressive modulus and pore network throughout 14 days of swelling for ESBO with and without the presence of an acid. Both ESBOc and ESBOr show a slight protective effect with respect to fluid loss over the control by the 14 day time point. Fluid loss remains consistent between seven and 14 days for both ESBOc and ESBOr. There is a small increase in modulus for ESBOc

between four and seven days swelling but not clear trend with respect to modulus for either formulation. There is greater definition of the pores for ESBOr after swelling, while ESBOc remains consistent with respect to pore network features.

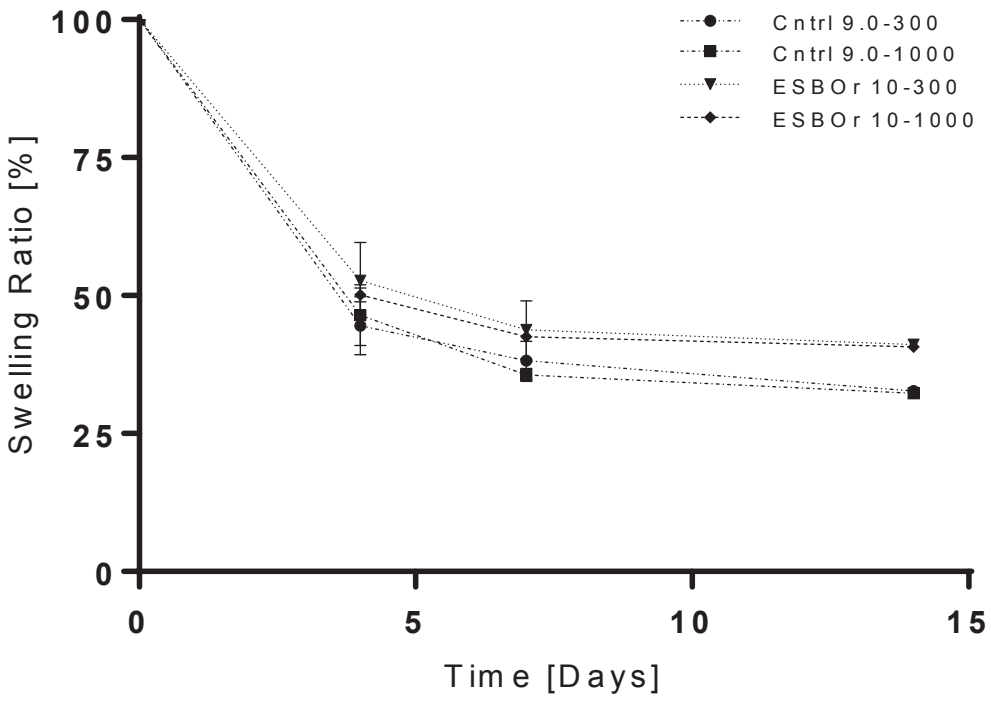

Figure 5.25: Reacted ESBO at high and low mixing speed swelling ratio versus swelling time. The legend indicates ESBOr v%-mixing speed.

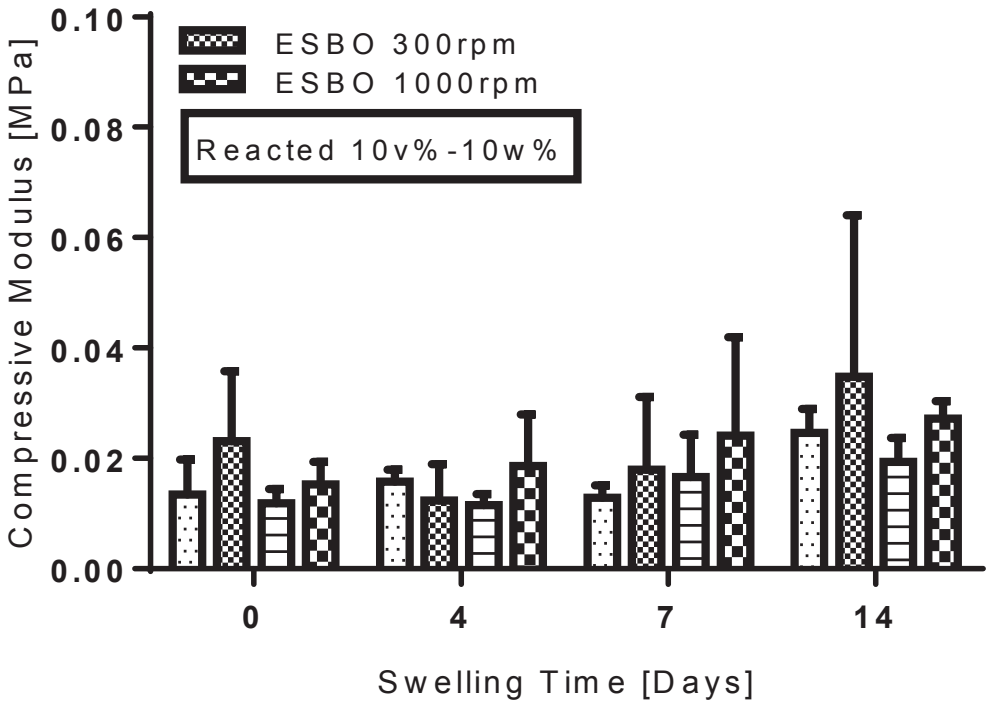

Figure 5.26: Reacted ESBO at high and low mixing speed modulus versus swelling time. Legend ESBO mixing speed. ESBOr v%-PVA w% is indicated in the box.

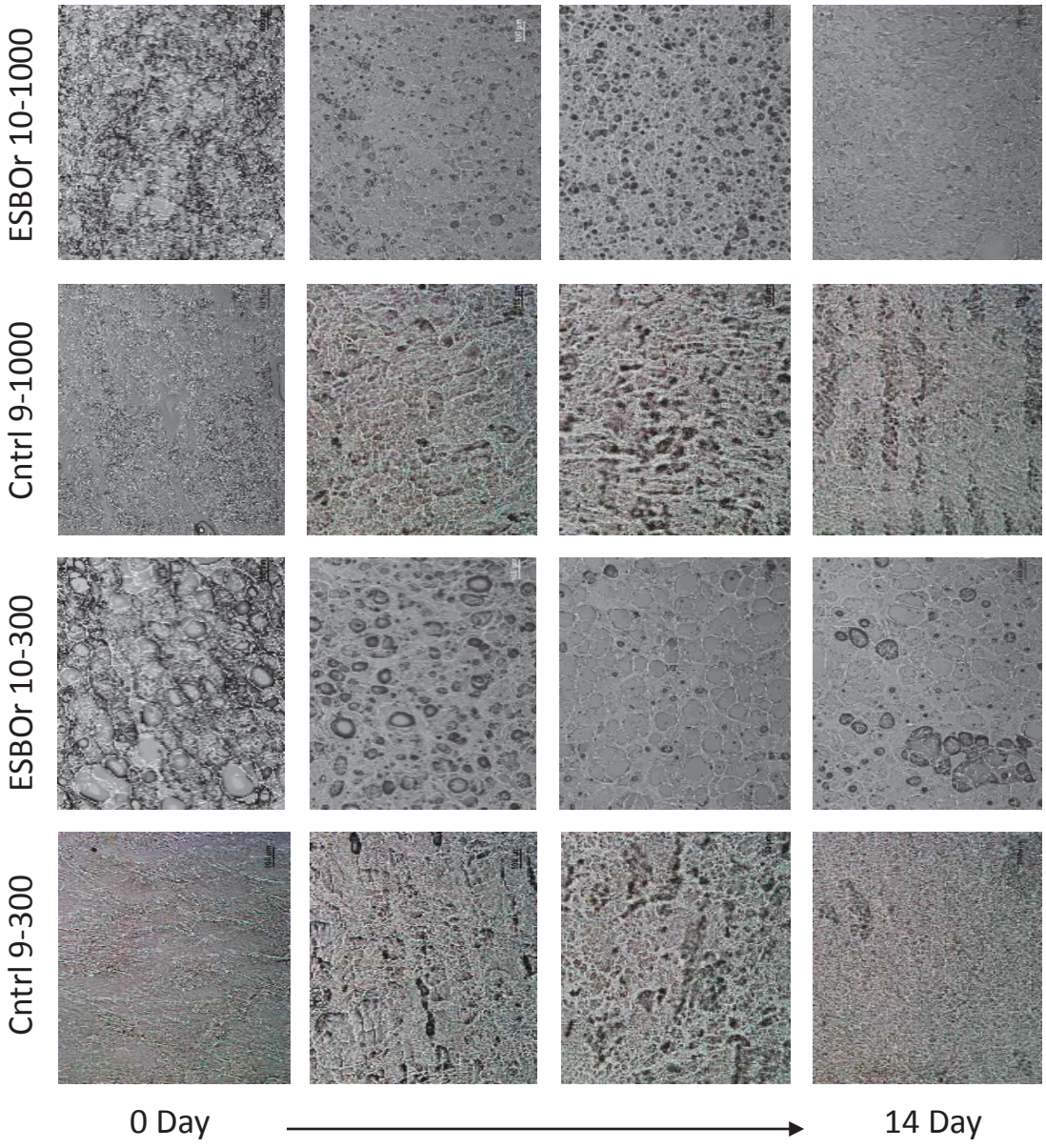

Figure 5.27: Reacted ESBO at high and low mixing speed swelling ratio versus swelling time. Columns represent ESBOr v%-mixing speed.

Figures 5.25-5.27 show the swelling ratio, compressive modulus and pore network throughout 14 days of swelling for ESBOr at high and low mixing speeds. Both high and low rpm formulations behave similarly with respect to fluid loss and both retain more

fluid than the controls. No trend is seen with respect to compressive modulus over 14 days of swelling. Higher mixing speed produces smaller average pores with both formulations showing more defined PVA septum over 14 days of swelling.

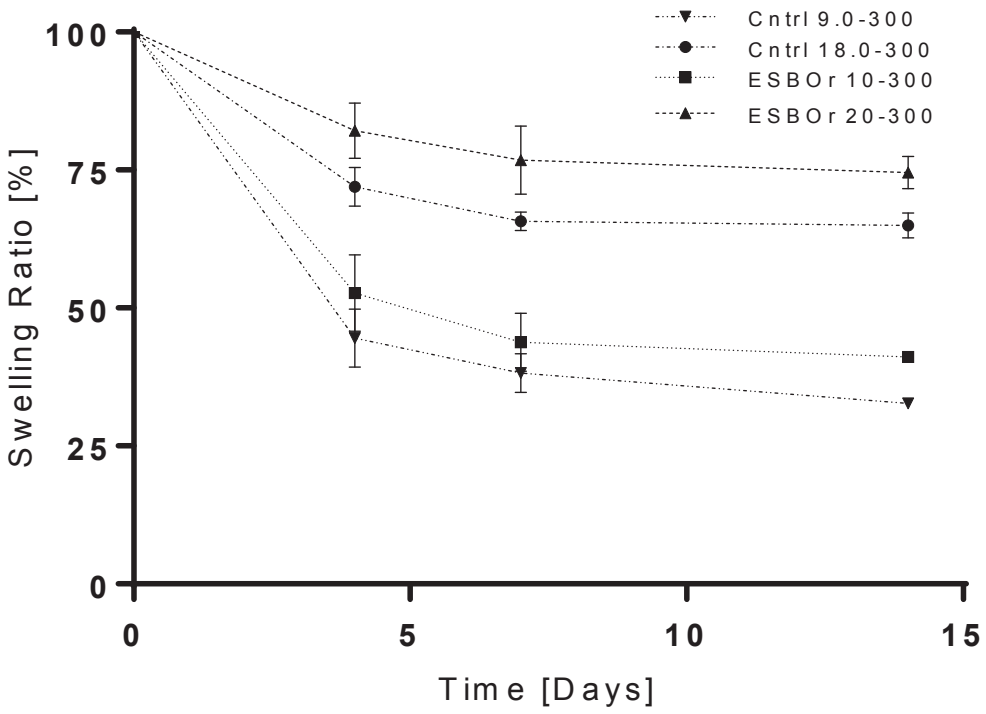

Figure 5.28: Low and high PVA concentration of reacted ESBO swelling ratio versus swelling time. Legend shows ESBOr PVA w%-mixing speed.

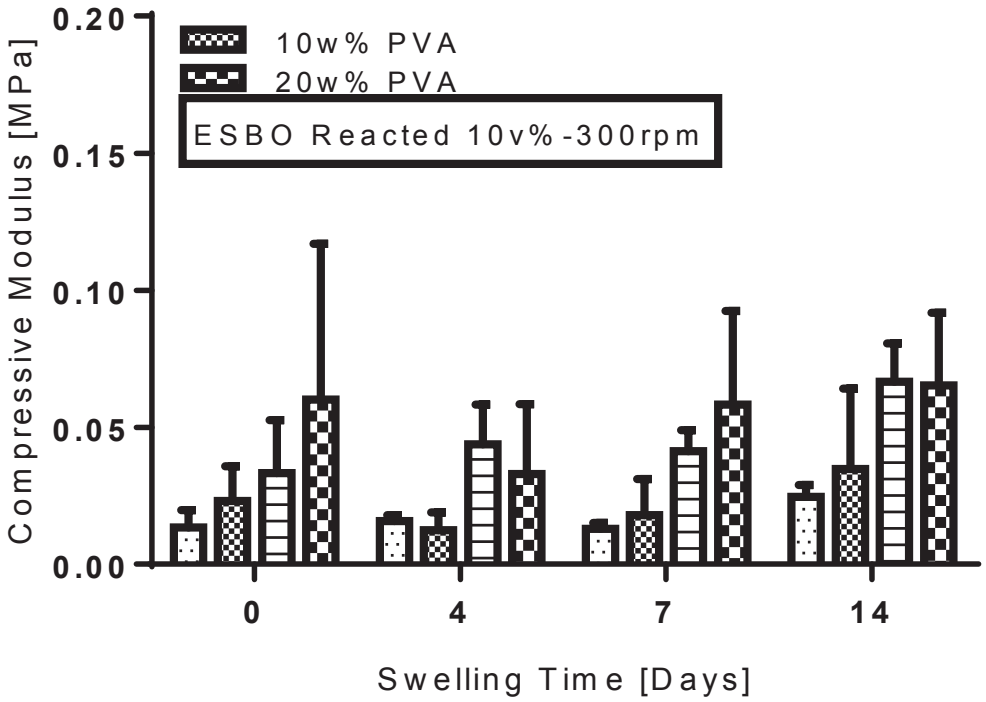

Figure 5.29: Low and high PVA concentration of reacted ESBO swelling ratio versus swelling time. Legend ESBOr PVA w%. ESBOr v%-mixing speed is indicated in the box.

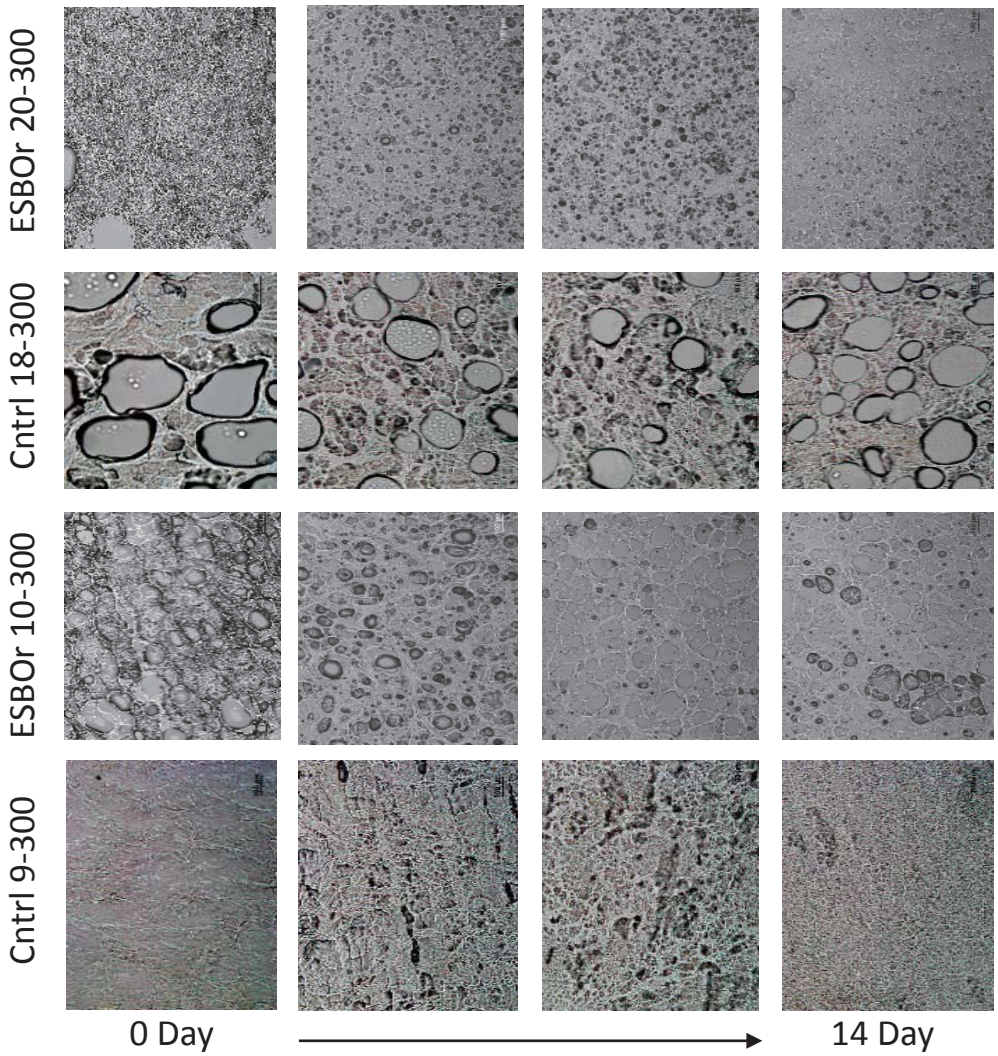

Figure 5.30: Low and high PVA concentration of reacted ESBO pore structure versus swelling time. Columns represent ESBOr PVA w%-mixing speed.

Figures 5.28-5.30 show the swelling ratio, compressive modulus and pore network throughout 14 days of swelling for ESBOr at high and low PVA concentration. A clear distinction is made for the different formulations with respect to fluid loss. ESBOr with 20 w% PVA retained the most fluid followed by the 18 w% PVA control. Both control

and non-control high PVA% demonstrated higher moduli than their respective lower PVA w% formulations. High w% PVA with ESBOr produces small uniform pores. Low w% PVA with ESBOr produces larger pores with greater variability. After swelling, there is greater definition of the pore network for both formulations. Both ESBOr formulations produce drastically different pore networks than their respective controls.

5.4 Discussion

Due to the biologically inert nature of PVA cryogels, integration with surrounding tissue is a challenge that must be addressed. Previous work has incorporated degradable microspheres to serve as chemotactic agents for cellular ingrowth for the goal of improved integration following cellular proliferation [17, 74, 75]. Other researchers have focused on functionalization of the cryogel surface through chemical incorporation of biomimetic compounds [21] . While these added features have shown value in cartilage tissue engineering applications, the importance for stable, adequately sized internal pore network for cryogel based systems cannot be over-stated. Additionally, the pore microstructure has influence over the fluid behavior throughout the cryogel, which can indirectly influence the ability to resist external loads.

The liquid-liquid phase separation method used in this research is advantageous due to: i) its simplicity from a polymer synthesis standpoint and ii) its controllability, showing a synthesis-structure-function relationship. DCM and EA were chosen as organic solvents due to their varied physical properties (i.e.: boiling point) and due to their potential for solvent extraction following cryogel crosslinking. Both DCM and EA are cytotoxic, thus

adequate extraction of the solvent is essential for *in vivo* applications. It is also expected that lipid-based porogens would negatively impact cell viability, thus adequate extraction of oil or ESBO would be needed for *in vivo* studies. A lipid extraction process utilizing repeated washes with ethanol followed by water was used prior to sample testing but no studies were done to quantify the amount of oil or ESBO remaining in the cryogel. The minimum amount of any porogen needed for optimized pore microstructure and modulus is important to determine, as amounts higher could unnecessarily complicate post-synthesis solvent extraction.

Physically crosslinked PVA-based cryogels have inherent mechanical strength even at a relatively low polymer concentration of 10 w%. Repeated freeze-thawing causes condensation of PVA-rich domains and expels water into the formed pores [58]. The larger volume of organic solvent is expected to produce greater solvent-rich, and conversely polymer-light, regions. Reducing the PVA-rich areas reduces the cryogel load baring capability due to the reduced solid matrix that primarily resists the external stress. There is a general trend of decreased modulus with increased porogen volume. This further supports the use of the minimum amount of porogen needed for optimal structural properties.

The fluid-filled pores are expected to act as incompressible fluids and contribute to the compressive modulus, improving the mechanical capabilities over the inherent mechanical strength. The ability for the fluid phase to support resistance of compressive load is dependent on multiple factors, primary of which is the pore network features

including pore diameter and pore interconnectivity. Small pores that have a low interconnectivity or highly tortuous path are expected to exhibit reduced ability for solvent flow within the deforming matrix, thus increased ability to resist the external load. Conversely, large pores with high interconnectivity and low tortuosity should have less difficulty for solvent flow through the matrix and are thus less able to resist external loads. Both of these affects are strain-rate dependent, where high strain rates, during running for example, would not allow large polymer matrix deformation during loading, thus greater entrapment of fluid can be expected with greater load resistance capabilities.

Traditionally, *in vitro* studies for biomaterials used PBS or similar solutions for material testing. PBS replicates body osmolarity and ion concentration but fails to fully recreate *in vivo* conditions. Charged macromolecules such as proteoglycans create an osmotic pressure in the knee joint, which has important implications for tissue replacement particularly when utilizing cryogels because their equilibrium fluid content and overall volume is influenced by external forces. The influence of osmotic pressure on the cryogels is reflected by a loss of fluid content. All formulations evaluated loss fluid over 14 days of swelling. Interestingly, only PVA w% impacted fluid loss to a significant degree, where a greater initial polymer content led to less fluid loss. Since fluid loss is accompanied by a macroscopic decrease in cryogel volume, implantation of this PVA-based cryogel into the knee joint prior to equilibrium could potentially cause a significant reduction of the cryogel volume. For bulk superporous cryogel applications, such as the case of cryogels for articular cartilage focal defect filling, the large volume reduction can lead to lessening of the cryogel and implant failure. For a two-phase cryogel system

where the superporous phase is solely occupies a small thickness of the periphery, the volume loss may be inconsequential. However, the actual thickness needed would may become significant if a larger superporous region is required to permit adequate cell migration and enhance implant stability. In vivo studies with superporous cryogel rims of variable thickness could be done to determine the minimal thickness needed. Alternatively, knowing the time point of *in vitro* cryogel equilibrium, shown to be between 7 and 14 days, allows for the cryogel to be conditioned *in vitro* and implanted at a time at which no further change in cryogel volume is expected.

The viscoelastic nature of the cryogel is due to the elastic strength of the polymer matrix in addition to the interaction between polymer and fluid phase during loading. It can be expected that the osmotic pressure decreases the overall fluid content in the cryogel and causes bulk condensation of the polymer phase, macroscopically seen as reduction in the cryogel volume, would also cause a change in the compressive modulus of the cryogel. However, osmotic conditioning did not consistently impart a significant change in modulus for the formulations tested. The consistent moduli can be explained by the ability for both organic solvents and lipids to act as external plasticizers when interacting with PVA chains and reduce the polymer stiffness [78]. This impact however does not

Figures 5.30 and 5.27 display an increased definition of pore network during the swelling study. This may be explained by the difference in water phases present within the cryogel. Cryogels have two phases of water: bulk and bound [58]. The bulk water- with or without lipid- is present within the porous cryogel network and is more susceptible to

external forces driving its flow, such as osmotic pressure. Bound water has non-covalent interaction with the polymer side chains and is less susceptible to movement. The presence of epoxides in ESBOc and ESBOr may promote more movement of the bound water compared to oil formulations causing condensation of the regions and more defined pore network after deswelling.

Since fluid loss alone does not appear to completely explain the lack of change in modulus during osmotic conditioning, it is important to evaluate how the pore microstructure is affected by osmotic pressure to explore its potential to influence fluid-polymer matrix interaction under loading. Figures 5.3 and 5.4 provided qualitative insight into the pore features and ImageJ analysis of the cross-sectional images allow for quantification of the porosity and pore diameter with EA. There is a significant effect of organic solvent volume on the porosity of the cryogel with 25 v% EA having approximately 7.32% increase in porosity over 10 v% EA cryogels. This highlights how simply changing the organic solvent volume in the liquid-liquid phase separation approach can be used to control the cryogel porosity. However, optical images of lipid-based formulations show a general constant pore network throughout the swelling study. The difference is likely due to the increased propensity for phase separation with lipid-based formulations compared to EA. The change in MPD for EA is in line with the trend for fluid loss where no change is seen after 14 days of swelling. It is likely that condensation of the polymer matrix causes decrease in the MPD resulting in efflux of bulk water from the pores in response to the osmotic pressure. It is important to note that the changing pore diameter does not affect the overall porosity since the smaller MPD is

matched to increased number of pores within each imaged area, which is in line with the decrease in overall cryogel volume due to deswelling. The pore diameters remain generally consistent for lipid-based formulations, further highlighting the stability of the pore network using oil or ESBO.

There are various limitations to the work presented. The compressive modulus is an important biomaterial parameter to determine for meniscal replacement suitability but it does not fully explore the various mechanical forces the biomaterial would be subjected to *in vivo*. More robust mechanical testing is needed to determine how the cryogel may perform under these dynamic conditions. The importance of pore network features and its impact of fluid dynamics and functional performance was discussed. Of these features, the pore interconnectivity is expected to have significant impact on the fluid flow under loading and in response to osmotic pressure. Significant preliminary work was conducted exploring various techniques to quantify void volume and degree of interconnectivity, however the ability to determine these parameters of cryogels in their native, hydrated state remains a challenge. Of the pore network features studied- MPD and porosity- ImageJ analysis of ESEM images remains one of the best, nondestructive methods to evaluate the pore network, despite the fact that imaging single, or even multiple two-dimensional cross-sections only approximates the overall pore network structure.

5.0 Conclusion

Clear understanding of the synthesis-structure-function relationship of potential materials is vital to identify opportunities for optimization of the properties needed to promote restoration of joint function and successful implant integration for this potential two-phase cryogel. Through this work, the impact of PVA cryogel pore network and compressive moduli on synthesis parameters was established. Pore diameter larger than stem cell size is expected to be required for cell migration *in vivo*, which is evident in each of the lipid-based cryogels studied.

Chapter 6: Characterize the transport properties of superporous and non-superporous cryogels

6.1 Introduction

Most research in biomaterials for meniscal replacement focuses on mechanical capabilities, biocompatibility, cellular ingrowth and chondroprotective ability. One area that has not received significant focus is the transport properties of meniscal replacements. Menisci are unique compared to other cartilaginous tissues, such as articular cartilage, due to their partial vascularity. This feature allows to the direct delivery of cell sustaining nutrients to the tissue [2]. From the periphery, these nutrients rely on diffusion to the remaining avascular regions of the meniscus. In addition, the meniscus further provides the delivery of nutrients to the avascular articular cartilage in the knee joint. While not the sole source of nutrients to chondrocytes, the meniscus does provide a pivotal role in regards to nutrient transport within the knee joint. Poor nutritional supply and inadequate removal of waste are believed to contribute to cartilaginous tissue degradation [79]. The diffusion coefficient through articular cartilage has been established for many solutes including glucose ($D=1.4\text{-}2.3 \times 10^{-10}$ m^2/s) and serum albumin ($D=0.2 \times 10^{-10}$ m^2/s) [80].

Much research has been devoted to transport properties of cryogels [81]. Cryogels themselves are often investigated for use as drug delivery devices, with many commercially available options present on the market [44, 82]. Transport through cryogels are a function of various controllable synthesis parameters including molecular weight between crosslinks, polymer weight fraction and pore size [83, 84]. Hydrogels can

be modified to further influence transport properties for a specific application. Similarly, cartilaginous tissue composition have influence over transport properties [80]. The water content of the tissue has significant influence over the transport [85].

For meniscal replacement applications the diffusion capabilities of the potential cryogel should be established. Since there is a clear synthesis-structure-function relationship for cryogels as established in Aim 2, an understanding of the diffusion requirements in the knee joint would guide the synthesis parameters for the cryogel. The superporous cryogels determined from Aim 2 to be suitable for use as a peripheral rim in meniscal replacement was evaluated for differences in protein transport. This is contrasted to the transport of a potential bulk phase cryogel formulation for meniscal replacement, in this case 18 w% PVA. An understanding of the transport capabilities through different hydrogel formulations can impact selection of synthesis parameters.

6.2 Materials and Methods

6.2.1 Materials

PVA, PVP, PBS, oil, and ESBO was obtained from previously described sources. Bovine serum albumin was obtained from Sigma Aldrich. Pierce BSA Protein Assay Kit was purchased from Thermo Scientific.

6.2.2 Cryogel Synthesis

Cryogels formulations were synthesized through previously described methods. The formulations selected for transport studies is summarized in Table 6.1. They represent a range of water content and pore network features.

Table 6.1: Cryogel formulations selected for transport studies.

Porogen Type	Porogen v%	PVA w%	Mixing Speed [rpm]	Osmotically Conditioned?
None	0	18	0	N
None	0	18	300	N
ESBOr	10	10	300	N
ESBOr	10	20	300	N
ESBOr	10	20	300	Y

6.2.3 Diffusion Apparatus

A customs designed, six chamber diffusion apparatus was used to control transport through the cryogels (Figure 6.1). Cryogels were cut to 1 mm thickness by hand using a razor blade. Each glass chamber consisted of a separate upper and lower well. The cryogel was secured between the two chambers in slight compression using an external adjustable manual control. Each well had an opening of 9.33 mm diameter that interfaced both sides of the cryogel. The inner section of each well held 3 ml of fluid and the outer well permitted the flow of deionized H_20 at a temperature of 32 ^oC to equilibrate with the inner section contents and represent knee joint intra-articular temperature. The flow through the outer section was maintained through the use of a temperature controlled water bath.

Figure 6.1: Custom six-chamber diffusion system.

The upstream (with respect to outer chamber fluid flow direction) well contained 4 mg/ml bovine serum albumin (BSA) that was used as a representative protein for diffusivity calculations. The downstream well contained PBS. 25 μl samples were taken from the downstream well at various time points until steady state was reached.

6.2.4 Ultraviolet-visible Spectroscopy

A Tecan (Morrisville, NC) Infinite Pro 200 ultraviolet-visible spectrometer was used for BSA protein concentration determination. Diffusion samples and standards were subjected to steps outlined in the BSA protein assay kit. The samples were reacted with the assay kit reagents for 30 min at 37 ^{o}C then allowed to cool to room temperature. The solutions were measured for absorbance at 562 nm. The standard BSA solutions were used to create a protein concentration standards curve by fitting a fourth order polynomial, through which unknown concentrations could be interpolated.

6.2.5 Diffusion Calculation

Diffusion calculations are modified from previous studies with similar experimental set-up [82, 86, 87]. The diffusion system is represented by the schematic in Figure 6.2 with the associated boundary conditions. C_1, C_2, and C_c represent the protein concentrations in the upstream well, downstream well, and cryogel respectively. The diffusion is considered to be one-dimensional in the z direction through a cryogel of thickness h_1.

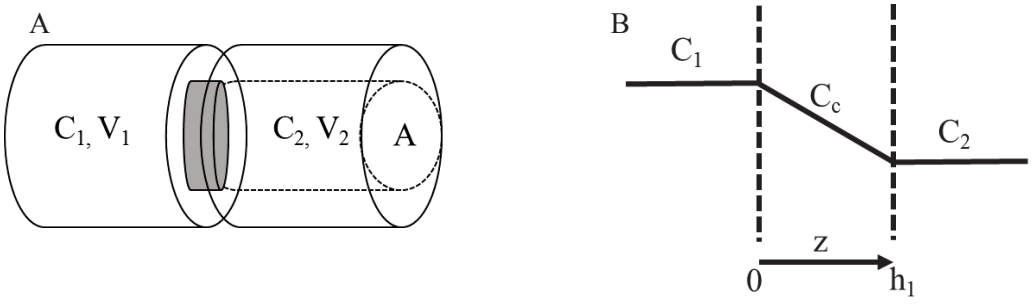

Figure 6.2: Diffusion study (A) schematic and (B) boundary conditions.

Boundary Conditions:

1) $t=t^0$: $C_c=C_1^0$ at $z=0$ and $C_c=0$ at $0<z\leq h_1$
2) $t>t^0$: $C_c=C_1$ at $z=0$ and $C_c=C_2$ at $z=h_1$
3) $C=C_1$ at $z<0$ and $C=C_2$ at $z>h_1$
4) $N=C_1^0V_1$ at $t=t^0$ where N is the number of moles of solute in the system

Assumptions:

1) Well mixed solution in both wells
2) No concentration gradient in either well
3) Total sample loss of 5% is negligible
4) t C_c to stabilize to linear profile << t diffusion (quasi-steady state)

To assume the solutions remain well mixed during the course of the experiment, the settling velocity can be used to establish the length of time before the effect of gravity on the BSA would be important. The settling velocity is based on Stokes Law:

$$v_s = \left[\frac{(\rho_s - \rho_f) r_s^2 g}{\mu_f}\right]$$

where ρ_s and ρ_f are the densities of the solute and fluid respectively, r_s is the solute radius, and μ_f is the fluid viscosity. This leads to a υ_s value on the order of 10^{-3} cm/h. For a 1 cm high chamber this indicates a settling time over 900 h, which is less than the 72 h over which the diffusion was measured.

A one-dimensional steady-state diffusion is based on Fick's Law:

$$J = -D_1 \frac{dC}{dz}$$

where J is the flux and D_1 is the diffusion coefficient. Since diffusion is only in the z direction and independent of concentration, flux can be written as:

$$J = -D_1 \frac{dC}{dz} = -D_1 \left(\frac{C_2 - C_1}{h_1}\right)$$

The concentration in the downstream well can be written as:

$$C_2 = \frac{N}{V} - \left(\frac{N}{V} - C_2^0\right) \exp\left[-\frac{(t - t^0)}{\tau}\left(\frac{D_1}{h_1}\right)\right]$$

where N is the number of moles of solute in the system, V is expressed as:

$$V = V_1 + Ah_1 + V_2$$

and τ is expressed as:

$$\tau = \frac{(V_1 + Ah_1/2)(V_2 + Ah_1/2)}{AV}$$

C_2 can be changed to the form:

$$-\ln\left(\frac{N/V - C_2}{N/V - C_2^0}\right) = \frac{D_1}{h_1}\left(\frac{t - t^0}{\tau}\right)$$

where the slope of the curve in the form Y = mX can be used to calculate D_1.

6.3 Results

6.3.1 Standards curve

Through the use of the BSA protein assay kit the following standards curve was obtained. The fourth order polynomial has good fit to the data with $r^2 = 0.9999$.

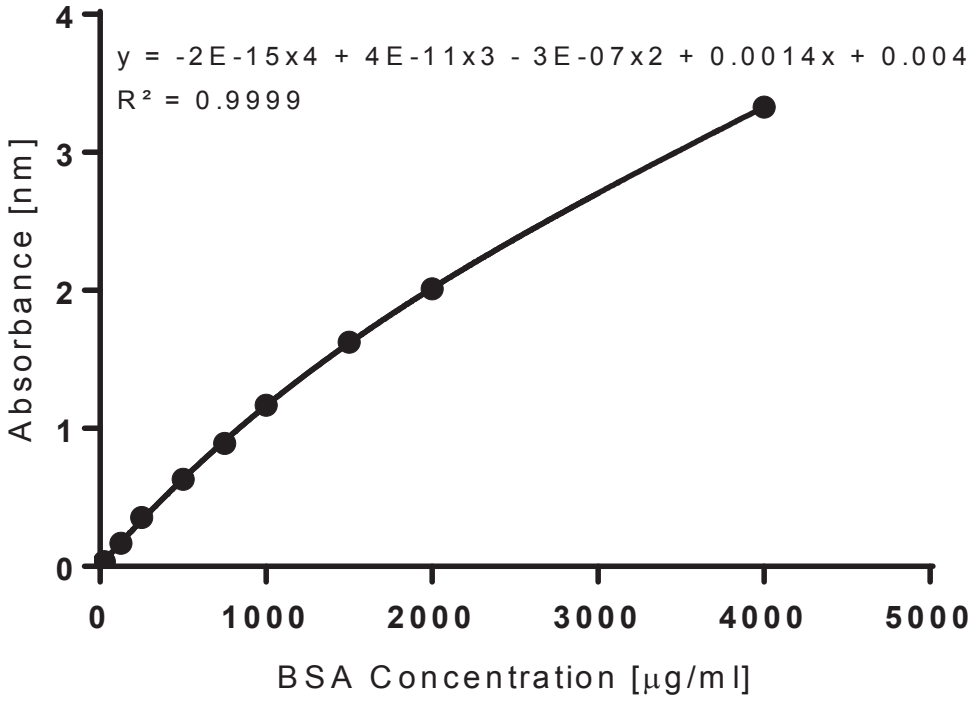

Figure 6.3: BSA standards curve.

6.3.2 Diffusion Coefficient

Table 6.2 shows the diffusion coefficient for various cryogel formulations.

Table 6.2: Diffusion coefficient values.

Porogen Type	Porogen v%	PVA w%	Mixing Speed [rpm]	Osmotically Conditioned?	D1 [cm^2/s]
None	0	18	0	N	4.00E-09
None	0	18	300	N	3.00E-09
ESBOr	10	10	300	N	3.00E-08
ESBOr	10	20	300	N	1.00E-09
ESBOr	10	20	300	Y	1.00E-09

The diffusion coefficient for each formulation evaluated is shown in Table 6.2. Both control formulations have similar D_1 values. A large increase in D_1 is seen in the ESBOr 10 v%-10 w%-300 rpm formulation. Both ESBOr with 20 w% with and without osmotic condition to equilibrium fluid content have equivalent D_1 values.

6.4 Discussion

Diffusion of molecules through native menisci is essential to support cell viability of surrounding articular cartilage. In addition, the bulk of the meniscus relies on diffusion of nutrients. Limited research has been done to evaluate the diffusive capabilities of biomaterials for meniscal replacement. For cryogel-based meniscal replacements, the synthesis parameters can have significant impact on the diffusive capabilities. This aim

explored the impact of cryogel compositional and structural features on the diffusion coefficient using BSA as a model protein.

The control formulations tested have equivalent water content but different pore network features. The large isolated pores in 18 w% PVA- 300 rpm mixed formulation does not significantly impact the diffusion coefficient. This would support previous research that has demonstrated the close relationship between water content and diffusion coefficient. ESBOr with 20 w% PVA has a similar fluid content to both control formulations but a drastically different pore network. The smaller pores seen with ESBOr decrease D_1 slightly but the values are still within the same order of magnitude. ESBOr with 10 w% has very large, well dispersed and likely highly interconnected pores. In addition, it also has a larger fluid content than all other formulations tested. It is likely that the fluid content led to the large increase in D_1. Cryogels under osmotic conditions found in the knee joint lose significant fluid as demonstrated by Aim 2. A conditioned ESBOr cryogel however, has equivalent D_1 to a non-osmotically conditioned cryogel. This is likely due to the fact that 20 w% PVA formulations were shown to have mild fluid loss during a swelling study compared to lower w% PVA formulations. It is possible that the loss of fluid that would normally drive D_1 down is matched by the highly porous nature (which remains consistent during deswelling) of these formulations resulting in equivalent diffusive capabilities. While the main purpose of this study was to explore the correlation between cryogel features and diffusivity, it is interesting to note that the diffusion coefficient of BSA through articular cartilage is 200×10^{-9} cm^2/s, which highlights the great ability of cartilaginous tissues to permit diffusion of nutrients to the cells within.

One limitation of the data presented is that the cryogels likely were not in a relaxed state throughout the experiment. Furthermore, is likely they were each under varied level of stress. The diffusion chamber requires manual tightening of the two wells to secure the sample in place. Cryogels under pressure can readily deform and extrude from their position, thus a significant amount of pressure was required to keep them in place. Care was taken to apply the same amount of external pressure on each chamber but it is likely there would be some variability in the actual amount each formulation experienced. Joint loading has significant impact on meniscal transport properties and evaluation of transport through cryogels under various loading conditions would be valuable to study. However the impact of joint loading on transport is outside the scope of this Aim.

6.5 Conclusions

This Aim demonstrated highlighted the importance of determining diffusive capabilities of synthetic meniscal replacements. The results suggest that fluid content, as opposed to porosity, have a significant influence on the diffusion coefficient. This can aid in the selection of synthesis parameters for cryogel-based cartilaginous tissue replacement if future research suggests that a certain range for diffusion coefficient is needed for optimal implant performance.

Chapter 7: Synthesize a meniscus dimension-matched fiber-reinforced cryogel with integrated superporous rim

7.1 Introduction

Tissue engineering of a native tissue requires extensive research into the components, synthesis parameters, structural features and functional capabilities of the engineered construct. This process typically entails first a strong comprehension of the theoretical and engineering principles of relevance for the material and for its application. A typical process entails material design, then synthesis, followed by relevant testing *in vitro* at various levels of scale. A recent paradigm shift has led researchers to understand the importance of translational research. Historically, the translational aspect of a biomaterial or similar construct was considered after repeated cycles of design, synthesis, and testing. It is widely recognized now that the successful development of a material for clinical applications is benefited from consideration of the translational challenges early in the developmental process [88].

The overall goal for this research project is to provide a foundation of knowledge to lead to the development of a clinically translatable meniscal replacement. The purpose of this aim is to provide a proof of concept that a superporous rim of optimal porosity and strength can be incorporated into the periphery of a mechanical-performance optimized, fiber-reinforced cryogel with the dimensions of a native meniscus. An understanding of the scale-up challenges may lead to novel design and engineering questions that may otherwise have been overlooked at this stage of the scientific investigation.

7.2 Materials and Methods

7.2.1 Materials

Optimized fiber-reinforced cryogels based on results from Aim 1 and optimized superporous cryogels based on results from Aims 2 and 3 will be selected for use in the development of a meniscal construct. Meniscal molds with bovine medical meniscus dimensions manufactured by the Hospital for Special Surgery will be used (Figure 7.1).

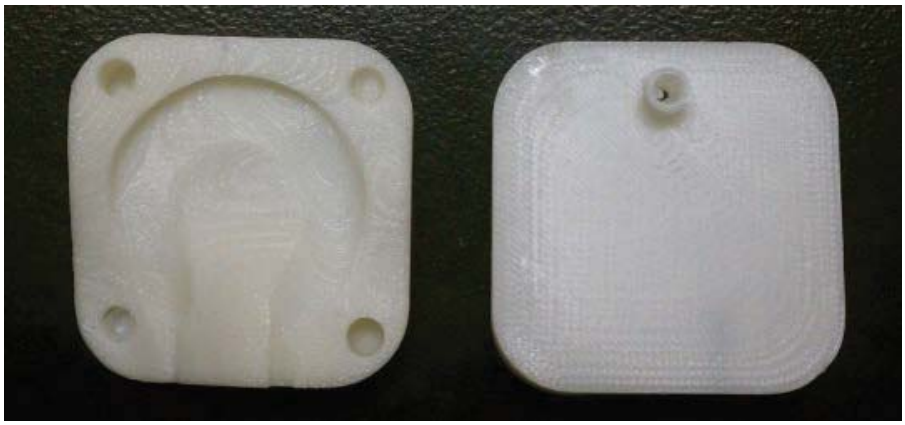

Figure 7.1: Bovine medical meniscal mold bottom (left) and top (right).

7.2.2 Fiber arrangement stability and scalability

To replicate the anisotripicity of the native meniscus, complex fiber arrangements were created and their scalability was explored. To aid in the retention of their shape during incorporation into meniscal molds, PVA was used as a tackifying agent.

The ability for PVA to serve as a tackifying agent was established though single fiber deformation studies. Multiple BFBs of equal length were coated with 10 w% PVA. The fibers were held in a U-shape representing 0^0 with respect to the long BFB axis while under atmospheric temperature and pressure. At various time points the fibers were held against gravity at one end and the opposite end was allowed to move freely. The resultant angle with respect to time was determined. The time required for $<10^o$ movement was considered a reference point for the time PVA would be needed to coat fibers in a complex arrangement prior to incorporating them into the meniscal mold.

7.2.3 Tri-composite cryogel synthesis

Meniscal molds are modified to permit the incorporation of two liquid phases and one solid phase: bulk fiber-reinforced cryogel and superporous cryogel. Glutaraldehyde treated FTs will be incorporated into the bulk cryogel making up approximately two-thirds of the total construct, with the superporous rim making up the remaining one-third. FTs will extend from the anterior and posterior horns of the device for use in anchoring to the tibial plateau. Care will be taken to prevent the exposure of FTs through the surface of the cryogel. The mold will be subjected to cryogel synthesis steps previously described.

Qualitative assessment of surface roughness and mechanical integrity will be made through handling of the scaffold. Particular attention will be made in assessing the stability of the superporous cryogel-bulk cryogel interface.

7.3 Results

7.3.1 Fiber stability with a PVA tackifying agent

The ability for PVA to coat a single BFB and lead to shape retention is shown in Figure 7.2. At ambient temperature and pressure, PVA lead to <10^{o} of BFB deformation by 300 min.

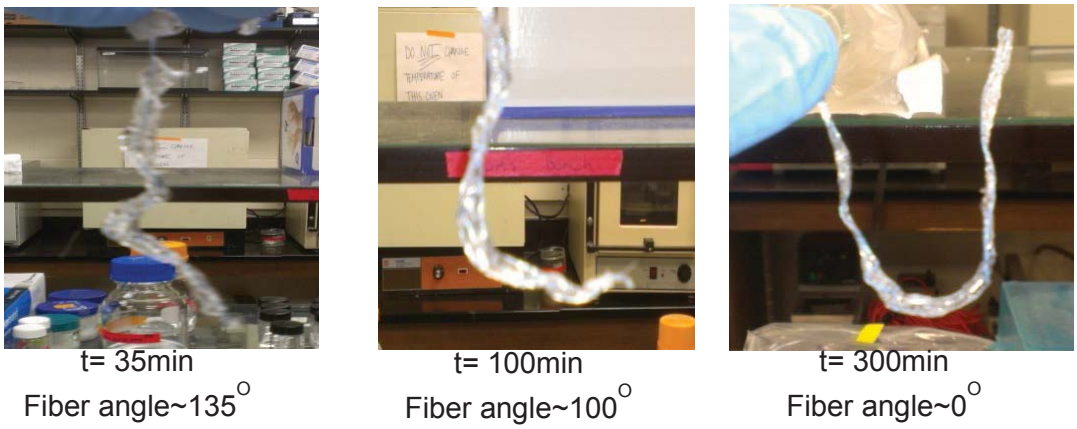

Figure 7.2: Proof of concept of PVA as a tackifying agent.

7.3.2 Fiber Arrangement Scalability

Previous work has provided a proof of concept that complex fiber arrangements can be incorporated into a cryogel and yield a mechanically sound scaffold. Figure 7.3 shows the complex arrangement using BFB to recreate the arrangement of collagen fibrils in the native meniscus. A protocol was developed to create the construct in a reproducible fashion.

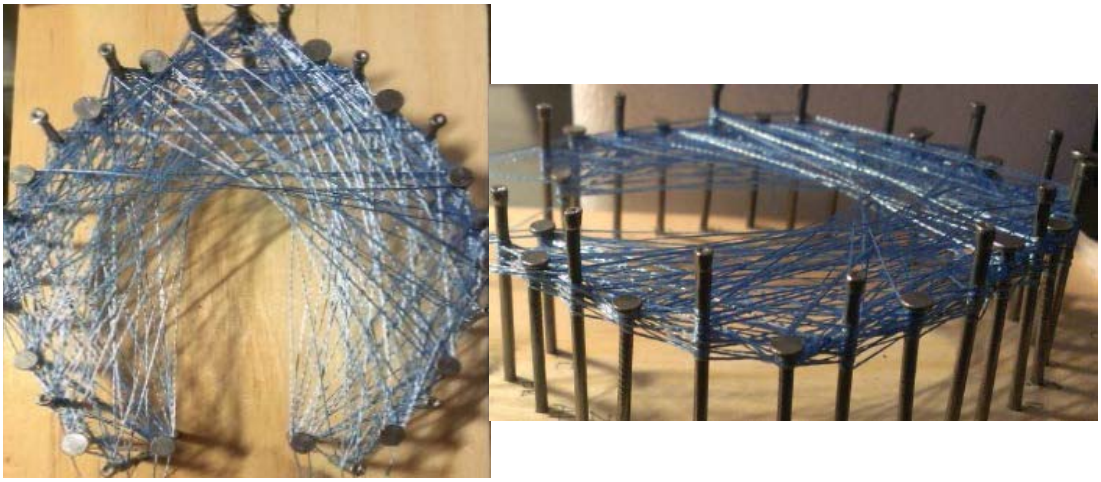

Figure 7.3:BFB complex anisotropic arrangement (two views).

The arrangement was recreated to scale to match the dimensions of bovine meniscus for use in the medial meniscus mold as shown in Figure 7.1. PVA was used as a tackifying agent to maintain the three dimensional orientation of the BFB arrangement (Figure 7.4). The BFB was incorporated into the mold to produce a stable fiber-reinforced cryogel without exposed BFB on the cryogel surface as seen in Figure 7.5.

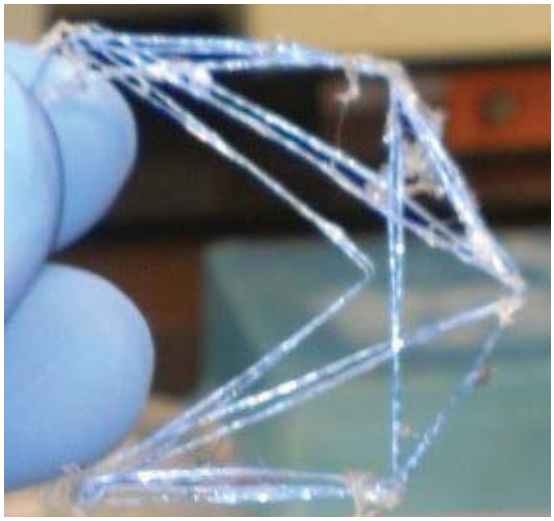

Figure 7.4: Scaled BFB arrangement.

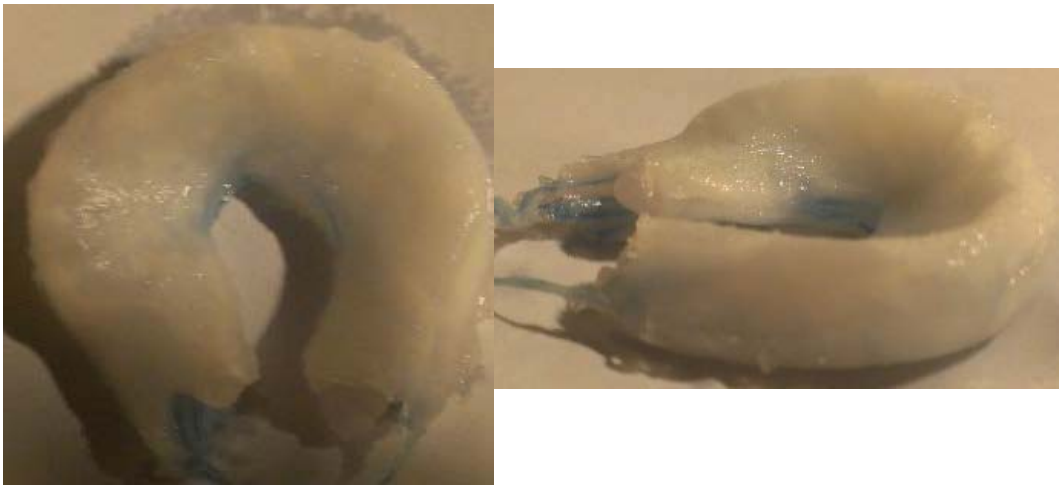

Figure 7.5: PVA cryogel with UHMWPE fibers matched to the shape of the meniscus (two views).

FTs were prepared for PVA tackifying and meniscal shape retention as shown in Figure 7.6.

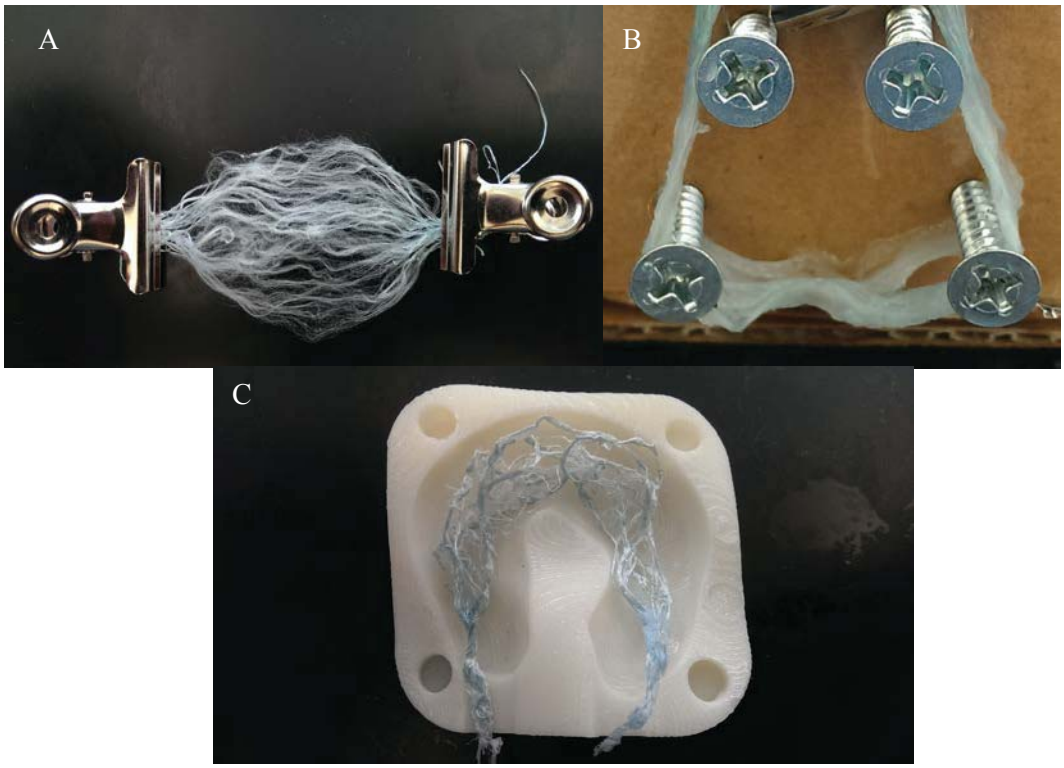

Figure 7.6: FT expanded from BFB (A) then set with PVA as a tackifying agent (B) and retained shape in meniscal mold (C).

Following injection of PVA into the mold containing glutaraldehyde-treat, PVA-coated FT, the PVA was allowed to cool for 4 hours producing the fiber-reinforced cryogel. Cooling and not complete freezing was done to add the peripheral PVA phase while adequate polymer chain mobility remained. A 2 mm thick peripheral rim was excised from the bulk cryogel and 10 v% ESBOr-20 w% PVA-300 rpm mixed cryogel was injected into the mold with the bulk cryogel in place. Food coloring was added to the superporous cryogel emulsion to better elucidate the demarcation between superporous

and bulk cryogel phases. Following freeze-thaw cycling, the tri-composite cryogel was removed from the mold as shown in Figure 7.7. The synthesis steps employed produced a stable and mechanically sound tri-composite cryogel with smooth surface topography indicated no FT extrusion onto the surface.

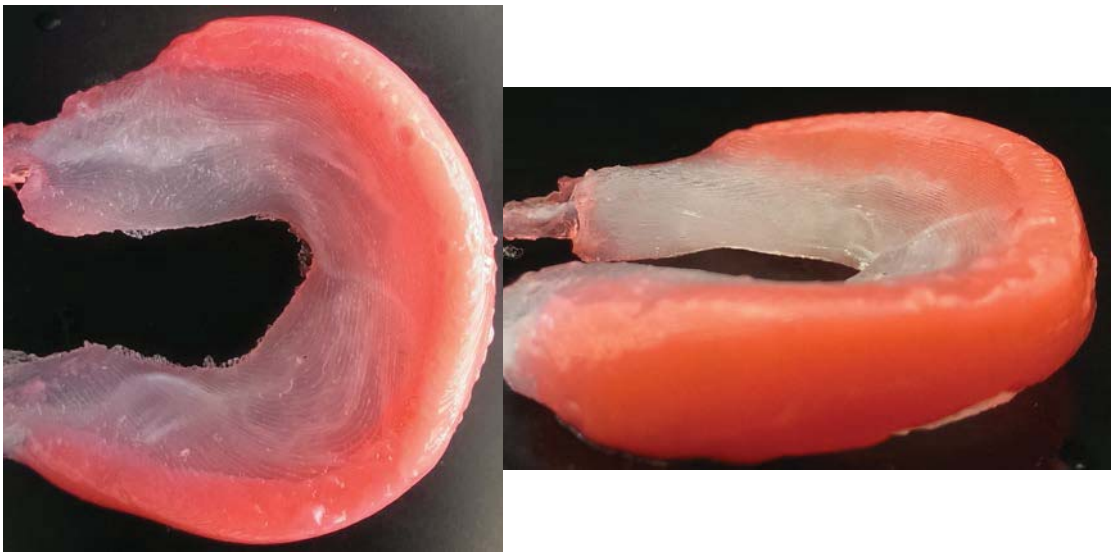

Figure 7.7: Tri-composite cryogel with superporous rim (two views).

7.4 Discussion

Based on the results from Aims 1, 2, and 3 optimized cryogel formulations were determined for tri-composite cryogel synthesis. PVA was successfully used as a tackifying agent for FT although difficulty experienced in recreating the full SF separation seen with uncoated FT. Machine processing equipment specialized in handling of small diameter coated fibers would be advantageous for future processing of FT for incorporation into the PVA bulk phase. The addition of a superporous periphery was

successful, with a clear demarcation between superporous and bulk phases seen. The benefit of the use of FT as opposed to fibers with necessary orientation and linearity, is that reproducibility of composite properties is easier to obtain. The ability to combine to components in a controlled fashion and obtain reproducible composite properties is tantamount to a successfully translatable meniscal replacement.

7.5 Conclusion

This Aim was successful in combining the optimal material synthesis parameters determined in Aims 1, 2 and 3. Complex fiber arrangements, including the preferred FT, high dispersion arrangement was successfully scaled to meniscal dimensions of an ovine animal model. This proof of concept demonstrates to potential of a tri-composite, fiber-reinforced cryogel with a superporous rim, to be successfully used as a novel meniscal replacement.

Chapter 8: Conclusions and Recommendations for Future Work

The work completed in Aim 1 successfully explored the ability for UHMWPE fibers to make a PVA cryogel anisotropic with respect to tensile and compressive forces. The successful development of a coupon system created composite specimens in a controlled and reproducible fashion. Inter-fiber spacing and fiber volume was shown the affect both tensile and compressive modulus. The role of glutaraldehyde surface treatment and increases fiber dispersion on IFSS was established. Furthermore, the benefit of highly dispersed fibers to resist tear propagation was demonstrated. Aim 1 concludes with the selection of optimal synthesis parameters for use in Aim 4.

The research conducted in this Aim 2 has explored to use of various solvents in the liquid-liquid phase separation synthesis of superporous cryogels. The synthesis-structure-function relationship has been established for this material. High PVA concentration, over 20 w%, appears to be needed to obtain modulus values on par with the compressive moduli of human meniscus.

Aim 3 demonstrated that protein can be transported through a superporous and non-superporous cryogel. The rate of transport is influenced primarily by cryogel water content. It was established that an osmotically conditioned cryogel synthesized with 20 w% PVA maintains its transport properties to that of a non-osmotically conditioning cryogel.

In Aim 4, the work completed has demonstrated the feasibility of incorporating fibers into cryogels matching the dimensions of the meniscus. Completion of Aims 1, 2 and 3 provided the needed information to synthesize each of the tri-composite components to produce a biomaterial that is suitable as a meniscal replacement device.

Future work should focus on further exploring the mechanical performance of highly dispersed, fiber-reinforced, glutaraldehyde-functionalized cryogels with higher fiber volume fractions using a redesigned coupon system and tested in dynamic loading conditions using a knee-simulator. It is also recommended that tests be conducted using type I collagen to functionalize the superporous cryogel phase and assess *in vitro* and *in vivo* cellular migration and proliferation.

The proposed cryogel synthesis method and selected materials employ an ***innovative*** approach that is aimed to be clinically translatable and allow for controllable material properties. The development of a fiber-reinforced, anisotropic superporous cryogel will provide a ***positive impact*** by bringing the field of tissue engineering closer to providing a viable treatment option for individuals suffering from debilitating meniscal tears.

List of References

[1] Makris EA, Hadidi P, Athanasiou KA. The knee meniscus: structure-function, pathophysiology, current repair techniques, and prospects for regeneration. Biomaterials 2011;32:7411-31.

[2] Beaufils PaV, R. The Meniscus. First ed. Berlin Heidelberg: Springer-Verlag; 2010. p. 407.

[3] Wang H, Chen T, Torzilli P, Warren R, Maher S. Dynamic contact stress patterns on the tibial plateaus during simulated gait: a novel application of normalized cross correlation. Journal of biomechanics 2014;47:568-74.

[4] Gilbert S, Chen T, Hutchinson ID, Choi D, Voigt C, Warren RF, et al. Dynamic contact mechanics on the tibial plateau of the human knee during activities of daily living. Journal of biomechanics 2014;47:2006-12.

[5] Chia HN, Hull ML. Compressive moduli of the human medial meniscus in the axial and radial directions at equilibrium and at a physiological strain rate. J Orthop Res 2008;26:951-6.

[6] Joshi MD, Suh JK, Marui T, Woo SL. Interspecies variation of compressive biomechanical properties of the meniscus. J Biomed Mater Res 1995;29:823-8.

[7] Hannink G, van Tienen TG, Schouten AJ, Buma P. Changes in articular cartilage after meniscectomy and meniscus replacement using a biodegradable porous polymer implant. Knee surgery, sports traumatology, arthroscopy : official journal of the ESSKA 2011;19:441-51.

[8] Bedi A, Kelly N, Baad M, Fox AJ, Ma Y, Warren RF, et al. Dynamic contact mechanics of radial tears of the lateral meniscus: implications for treatment. Arthroscopy : the journal of arthroscopic & related surgery : official publication of the Arthroscopy Association of North America and the International Arthroscopy Association 2012;28:372-81.

[9] Rath E, Richmond JC. The menisci: basic science and advances in treatment. Br J Sports Med 2000;34:252-7.

[10] Wang H, Chen T, Gee AO, Hutchinson ID, Stoner K, Warren RF, et al. Altered regional loading patterns on articular cartilage following meniscectomy are not fully restored by autograft meniscal transplantation. Osteoarthritis and cartilage / OARS, Osteoarthritis Research Society 2015;23:462-8.

[11] Cook JL. The current status of treatment for large meniscal defects. Clin Orthop Relat Res 2005:88-95.

[12] Sohn DH, Toth AP. Meniscus transplantation: current concepts. The journal of knee surgery 2008;21:163-72.

[13] Wang H, Gee AO, Hutchinson ID, Stoner K, Warren RF, Chen TO, et al. Bone Plug Versus Suture-Only Fixation of Meniscal Grafts: Effect on Joint Contact Mechanics During Simulated Gait. Am J Sports Med 2014;42:1682-9.

[14] Pereira H, Frias AM, Oliveira JM, Espregueira-Mendes J, Reis RL. Tissue engineering and regenerative medicine strategies in meniscus lesions. Arthroscopy : the journal of arthroscopic & related surgery : official publication of the Arthroscopy Association of North America and the International Arthroscopy Association 2011;27:1706-19.

[15] Maher SA, Rodeo SA, Doty SB, Brophy R, Potter H, Foo LF, et al. Evaluation of a porous polyurethane scaffold in a partial meniscal defect ovine model. Arthroscopy : the journal of arthroscopic & related surgery : official publication of the Arthroscopy Association of North America and the International Arthroscopy Association 2010;26:1510-9.

[16] Kobayashi M, Chang YS, Oka M. A two year in vivo study of polyvinyl alcohol-hydrogel (PVA-H) artificial meniscus. Biomaterials 2005;26:3243-8.

[17] Spiller KL, Laurencin SJ, Charlton D, Maher SA, Lowman AM. Superporous hydrogels for cartilage repair: Evaluation of the morphological and mechanical properties. Acta biomaterialia 2008;4:17-25.

[18] Elbert DL. Liquid-liquid two-phase systems for the production of porous hydrogels and hydrogel microspheres for biomedical applications: A tutorial review. Acta biomaterialia 2011;7:31-56.

[19] Baker MI, Walsh SP, Schwartz Z, Boyan BD. A review of polyvinyl alcohol and its uses in cartilage and orthopedic applications. Journal of biomedical materials research Part B, Applied biomaterials 2012;100:1451-7.

[20] Jiang S, Liu S, Feng W. PVA hydrogel properties for biomedical application. Journal of the mechanical behavior of biomedical materials 2011;4:1228-33.

[21] Kyburz KA, Anseth KS. Three-dimensional hMSC motility within peptide-functionalized PEG-based hydrogels of varying adhesivity and crosslinking density. Acta biomaterialia 2013;9:6381-92.

[22] Desai ES, Tang MY, Ross AE, Gemeinhart RA. Critical factors affecting cell encapsulation in superporous hydrogels. Biomedical materials (Bristol, England) 2012;7:024108.

[23] Yamaoka H, Asato H, Ogasawara T, Nishizawa S, Takahashi T, Nakatsuka T, et al. Cartilage tissue engineering using human auricular chondrocytes embedded in different hydrogel materials. Journal of biomedical materials research Part A 2006;78:1-11.

[24] Holloway JL, Lowman AM, Palmese GR. Mechanical evaluation of poly(vinyl alcohol)-based fibrous composites as biomaterials for meniscal tissue replacement. Acta biomaterialia 2010;6:4716-24.

[25] Musumeci G, Castrogiovanni P, Leonardi R, Trovato FM, Szychlinska MA, Di Giunta A, et al. New perspectives for articular cartilage repair treatment through tissue engineering: A contemporary review. World journal of orthopedics 2014;5:80-8.

[26] Hasan J, Fisher J, Ingham E. Current strategies in meniscal regeneration. Journal of biomedical materials research Part B, Applied biomaterials 2014;102:619-34.

[27] Buma P, Ramrattan NN, van Tienen TG, Veth RP. Tissue engineering of the meniscus. Biomaterials 2004;25:1523-32.

[28] http://www.nucleuscatalog.com/. Knee Joint. 2009.

[29] Englund M, Guermazi A, Lohmander LS. The meniscus in knee osteoarthritis. Rheum Dis Clin North Am 2009;35:579-90.

[30] Bhattacharyya T, Gale D, Dewire P, Totterman S, Gale ME, McLaughlin S, et al. The clinical importance of meniscal tears demonstrated by magnetic resonance imaging in osteoarthritis of the knee. J Bone Joint Surg Am 2003;85-A:4-9.

[31] Kambic HE, Futani H, McDevitt CA. Cell, matrix changes and alpha-smooth muscle actin expression in repair of the canine meniscus. Wound Repair Regen 2000;8:554-61.

[32] Jang SH, Ha JK, Lee DW, Kim JG. Fibrin Clot Delivery System for Meniscal Repair. Knee Surg Relat Res 2011;23:180-3.

[33] Myers P, Tudor F. Meniscal Allograft Transplantation: How Should We Be Doing It? A Systematic Review. Arthroscopy : the journal of arthroscopic & related surgery : official publication of the Arthroscopy Association of North America and the International Arthroscopy Association 2015;31:911-25.

[34] Raghunath J, Salacinski HJ, Sales KM, Butler PE, Seifalian AM. Advancing cartilage tissue engineering: the application of stem cell technology. Current opinion in biotechnology 2005;16:503-9.

[35] Beris AE, Lykissas MG, Papageorgiou CD, Georgoulis AD. Advances in articular cartilage repair. Injury 2005;36 Suppl 4:S14-23.

[36] Lin Z, Willers C, Xu J, Zheng MH. The chondrocyte: biology and clinical application. Tissue engineering 2006;12:1971-84.

[37] Li WJ, Tuli R, Okafor C, Derfoul A, Danielson KG, Hall DJ, et al. A three-dimensional nanofibrous scaffold for cartilage tissue engineering using human mesenchymal stem cells. Biomaterials 2005;26:599-609.

[38] Hui JH, Ouyang HW, Hutmacher DW, Goh JC, Lee EH. Mesenchymal stem cells in musculoskeletal tissue engineering: a review of recent advances in National University of Singapore. Annals of the Academy of Medicine, Singapore 2005;34:206-12.

[39] James SL, Connell DA, Saifuddin A, Skinner JA, Briggs TW. MR imaging of autologous chondrocyte implantation of the knee. European radiology 2006;16:1022-30.

[40] Hwang NS, Varghese S, Puleo C, Zhang Z, Elisseeff J. Morphogenetic signals from chondrocytes promote chondrogenic and osteogenic differentiation of mesenchymal stem cells. Journal of cellular physiology 2007;212:281-4.

[41] Karande TS, Ong JL, Agrawal CM. Diffusion in musculoskeletal tissue engineering scaffolds: design issues related to porosity, permeability, architecture, and nutrient mixing. Annals of biomedical engineering 2004;32:1728-43.

[42] Lu Y, Dhanaraj S, Wang Z, Bradley DM, Bowman SM, Cole BJ, et al. Minced cartilage without cell culture serves as an effective intraoperative cell source for cartilage repair. J Orthop Res 2006;24:1261-70.

[43] Myers KR, Sgaglione NA, Goodwillie AD. Meniscal scaffolds. The journal of knee surgery 2014;27:435-42.

[44] Peppas NA, Hilt JZ, Khademhosseini A, Langer R. Hydrogels in Biology and Medicine: From Molecular Principles to Bionanotechnology. Advanced Materials 2006;18:1345-60.

[45] Vernengo J, Fussell GW, Smith NG, Lowman AM. Evaluation of novel injectable hydrogels for nucleus pulposus replacement. Journal of biomedical materials research Part B, Applied biomaterials 2007.

[46] Hans ML, Maxwell C, Ehrlichman RS, Metzger K, Liang Y, Siegel SJ, et al. Evaluation of in vitro release and in vivo efficacy of mPEG-PLA-haloperidol conjugate micelle-like structures. Journal of biomedical materials research Part B, Applied biomaterials 2007.

[47] Bakshi A, Fisher O, Dagci T, Himes BT, Fischer I, Lowman A. Mechanically engineered hydrogel scaffolds for axonal growth and angiogenesis after transplantation in spinal cord injury. Journal of neurosurgery 2004;1:322-9.

[48] Dziubla TD, Lowman AM. Vascularization of PEG-grafted macroporous hydrogel sponges: a three-dimensional in vitro angiogenesis model using human microvascular endothelial cells. Journal of biomedical materials research Part A 2004;68:603-14.

[49] Peppas CHaN. Structure and Applications of Poly(vinyl alcohol) Hydrogels Produced by Conventional Crosslinking or by Freezing/Thawing Methods. In: Dusek K, editor. Advances in Polymer Science2000. p. 38-65.

[50] Oka M, Ushio K, Kumar P, Ikeuchi K, Hyon SH, Nakamura T, et al. Development of artificial articular cartilage. Proceedings of the Institution of Mechanical Engineers 2000;214:59-68.

[51] Katta JK, Marcolongo M, Lowman A, Mansmann KA. Friction and wear behavior of poly(vinyl alcohol)/poly(vinyl pyrrolidone) hydrogels for articular cartilage replacement. Journal of biomedical materials research Part A 2007.

[52] Thomas J, Lowman A, Marcolongo M. Novel associated hydrogels for nucleus pulposus replacement. Journal of biomedical materials research Part A 2003;67:1329-37.

[53] Thomas J, Gomes K, Lowman A, Marcolongo M. The effect of dehydration history on PVA/PVP hydrogels for nucleus pulposus replacement. Journal of biomedical materials research Part B, Applied biomaterials 2004;69:135-40.

[54] Joshi A, Fussell G, Thomas J, Hsuan A, Lowman A, Karduna A, et al. Functional compressive mechanics of a PVA/PVP nucleus pulposus replacement. Biomaterials 2006;27:176-84.

[55] Maher SA, Doty SB, Torzilli PA, Thornton S, Lowman AM, Thomas JD, et al. Nondegradable hydrogels for the treatment of focal cartilage defects. Journal of biomedical materials research Part A 2007.

[56] Kelly BT, Robertson W, Potter HG, Deng XH, Turner AS, Lyman S, et al. Hydrogel meniscal replacement in the sheep knee: preliminary evaluation of chondroprotective effects. Am J Sports Med 2007;35:43-52.

[57] Holloway JL, Lowman AM, Palmese GR. Aging behavior of PVA hydrogels for soft tissue applications after in vitro swelling using osmotic pressure solutions. Acta biomaterialia 2013;9:5013-21.

[58] Holloway JL, Spiller KL, Lowman AM, Palmese GR. Analysis of the in vitro swelling behavior of poly(vinyl alcohol) hydrogels in osmotic pressure solution for soft tissue replacement. Acta biomaterialia 2011;7:2477-82.

[59] Spiller KL, Laurencin SJ, Lowman AM. Characterization of the behavior of porous hydrogels in model osmotically-conditioned articular cartilage systems. Journal of biomedical materials research Part B, Applied biomaterials 2009;90:752-9.

[60] Spiller KL, Maher SA, Lowman AM. Hydrogels for the repair of articular cartilage defects. Tissue engineering Part B, Reviews 2011;17:281-99.

[61] Tissakht M, Ahmed AM. Tensile stress-strain characteristics of the human meniscal material. Journal of biomechanics 1995;28:411-22.

[62] Fithian DC, Kelly MA, Mow VC. Material properties and structure-function relationships in the menisci. Clin Orthop Relat Res 1990:19-31.

[63] Holloway JL, Lowman AM, VanLandingham MR, Palmese GR. Interfacial optimization of fiber-reinforced hydrogel composites for soft fibrous tissue applications. Acta biomaterialia 2014;10:3581-9.

[64] Yim JH, Ayan H, Pappas D, Vasilets VN, Fridman A, Palmese GR. Functionalization of polymers using n 2 pulsed dielectric barrier discharge. Pulsed Power Conference, 2007 16th IEEE International2007. p. 582-6.

[65] Korhonen RK, Laasanen MS, Toyras J, Rieppo J, Hirvonen J, Helminen HJ, et al. Comparison of the equilibrium response of articular cartilage in unconfined compression, confined compression and indentation. Journal of biomechanics 2002;35:903-9.

[66] Wu J, Ding Q, Dutta A, Wang Y, Huang YH, Weng H, et al. An injectable extracellular matrix derived hydrogel for meniscus repair and regeneration. Acta biomaterialia 2015;16:49-59.

[67] Kon E, Filardo G, Tschon M, Fini M, Giavaresi G, Marchesini Reggiani L, et al. Tissue engineering for total meniscal substitution: animal study in sheep model--results at 12 months. Tissue engineering Part A 2012;18:1573-82.

[68] Atesok K, Doral MN, Bilge O, Sekiya I. Synovial stem cells in musculoskeletal regeneration. J Am Acad Orthop Surg 2013;21:258-9.

[69] Gadjanski I, Spiller K, Vunjak-Novakovic G. Time-dependent processes in stem cell-based tissue engineering of articular cartilage. Stem cell reviews 2012;8:863-81.

[70] Spiteri CG, Pilliar RM, Kandel RA. Substrate porosity enhances chondrocyte attachment, spreading, and cartilage tissue formation in vitro. Journal of Biomedical Materials Research Part A 2006;78A:676-83.

[71] Spiller KL, Liu Y, Holloway JL, Maher SA, Cao Y, Liu W, et al. A novel method for the direct fabrication of growth factor-loaded microspheres within porous nondegradable hydrogels: controlled release for cartilage tissue engineering. Journal of controlled release : official journal of the Controlled Release Society 2012;157:39-45.

[72] Lozinsky VI, Galaev IY, Plieva FM, Savina IN, Jungvid H, Mattiasson B. Polymeric cryogels as promising materials of biotechnological interest. Trends in biotechnology 2003;21:445-51.

[73] Martens P, Anseth KS. Characterization of hydrogels formed from acrylate modified poly(vinyl alcohol) macromers. Polymer 2000;41:7715-22.

[74] Charlton DC, Peterson MG, Spiller K, Lowman A, Torzilli PA, Maher SA. Semi-degradable scaffold for articular cartilage replacement. Tissue engineering Part A 2008;14:207-13.

[75] Scholten PM, Ng KW, Joh K, Serino LP, Warren RF, Torzilli PA, et al. A semi-degradable composite scaffold for articular cartilage defects. Journal of biomedical materials research Part A 2011;97:8-15.

[76] Urban JP, Maroudas A, Bayliss MT, Dillon J. Swelling pressures of proteoglycans at the concentrations found in cartilaginous tissues. Biorheology 1979;16:447-64.

[77] Schneider CA, Rasband WS, Eliceiri KW. NIH Image to ImageJ: 25 years of image analysis. Nat Meth 2012;9:671-5.

[78] Edmund H I, Herman F M. Principles of Plasticization. Plasticization and plasticizer processes: American chemical society; 1965. p. 1-26.

[79] Horner HA, Urban JP. 2001 Volvo Award Winner in Basic Science Studies: Effect of nutrient supply on the viability of cells from the nucleus pulposus of the intervertebral disc. Spine (Phila Pa 1976) 2001;26:2543-9.

[80] Jackson A, Gu W. TRANSPORT PROPERTIES OF CARTILAGINOUS TISSUES. Curr Rheumatol Rev 2009;5:40.

[81] Hassan CM, Stewart JE, Peppas NA. Diffusional characteristics of freeze/thawed poly(vinyl alcohol) hydrogels: applications to protein controlled release from multilaminate devices. Eur J Pharm Biopharm 2000;49:161-5.

[82] Engberg K, Frank CW. Protein diffusion in photopolymerized poly(ethylene glycol) hydrogel networks. Biomedical materials (Bristol, England) 2011;6:055006.

[83] Cascone MG, Sim B, Downes S. Blends of synthetic and natural polymers as drug delivery systems for growth hormone. Biomaterials 1995;16:569-74.

[84] Burczak K, Fujisato T, Hatada M, Ikada Y. Protein permeation through poly(vinyl alcohol) hydrogel membranes. Biomaterials 1994;15:231-8.

[85] Travascio F, Jackson AR, Brown MD, Gu WY. Relationship between solute transport properties and tissue morphology in human annulus fibrosus. J Orthop Res 2009;27:1625-30.

[86] Jackson AR, Yuan TY, Huang CY, Travascio F, Yong Gu W. Effect of compression and anisotropy on the diffusion of glucose in annulus fibrosus. Spine (Phila Pa 1976) 2008;33:1-7.

[87] Lee CJ, Vroom JA, Fishman HA, Bent SF. Determination of human lens capsule permeability and its feasibility as a replacement for Bruch's membrane. Biomaterials 2006;27:1670-8.

[88] Holzapfel BM, Reichert JC, Schantz JT, Gbureck U, Rackwitz L, Noth U, et al. How smart do biomaterials need to be? A translational science and clinical point of view. Adv Drug Deliv Rev 2013;65:581-603.

Vita

Samuel James Laurencin
Place of Birth: Philadelphia, PA, USA
Date of Birth: February 6, 1983

Education:
Drexel University; Philadelphia, PA
7/2007 – 5/2015: Doctor of Medicine, Specializing in Orthopaedic Surgery
7/2005 – 6/2007: Master of Science in Chemical Engineering
9/2000 – 6/2005: Bachelor of Science in Chemical Engineering

Research and Professional Experience:
9/2013 – 5/2015: Research Fellow, Polymers and Composites Laboratory, Drexel University
10/2011 – 9/2013: Visiting Research Scholar, Biomaterials and Drug Delivery Group, Temple University
1/2005 – 8/2009: Research Fellow, Biomaterials and Drug Delivery Group, Drexel University
9/2000 – 8/2003: Research Specialist, Center for Advanced Biomaterials and Tissue Engineering, Drexel University
5/2001 – 8/2001: Research Assistant, National Science Foundation (NSF) Research Experience for Undergraduates, Rensselaer Polytechnic Institute

Honors and Recognition:
1st Place Oral Presentation Competition, Drexel University College of Medicine Research Day, 2015
UNCF / Merck Graduate Research Fellowship, 2013
Drexel University College of Medicine Scholarship Recipient, 2007
National Medical Fellowships / MetLife Foundation Award for Academic Excellence in Medicine, 2008
2nd Place Poster Presentation Competition, American Institute of Chemical Engineers Centennial Meeting, 2008
Alpha Kappa Alpha Sorority Educational Advancement Foundation Scholarship, 2007
Drexel University College of Engineering Dean's Fellowship, 2007
Drexel University Research Excellence Award, 2007
NSF Bridge to Doctorate Fellowship, 2005
University of Delaware Research Symposium Excellence in Research Award, 2005
Kappa Alpha Psi Fraternity Student of the Year, 2005
American Chemical Society Scholarship, 2000
National Action Council for Minorities in Engineering Vanguard Scholarship, 2000
Alpha Phi Alpha Fraternity, Incorporated Scholarship Recipient, 2000
G. W. Carver H.S. for Engineering and Science Alumni Association Award, 2000